MASTERARBEIT | MASTER'S THESIS

Titel | Title

Community dynamics of Symbiodiniaceae and Bacteria in reef-building corals

verfasst von | submitted by

Linn Ødegaard Yttrelid MA BSc

angestrebter akademischer Grad | in partial fulfilment of the requirements for the degree of

Master of Science (MSc)

Wien | Vienna, 2025

Studienkennzahl lt. Studienblatt | Degree programme code as it appears on the student record sheet:	UA 066 833
Studienrichtung lt. Studienblatt | Degree programme as it appears on the student record sheet:	Masterstudium Ecology and Ecosystems
Betreut von | Supervisor:	Univ.-Prof. i.R. Dr. Gerhard Herndl

Contents

Abstract

Coral holobionts rely on dynamic microbial partnerships to maintain homeostasis and ecological resilience under environmental stress. Yet, the extent to which interdependent microbial communities, such as Symbiodiniaceae and Bacteria, exhibit distinct or coordinated responses to external stressors remains poorly understood. This thesis investigates microbial responses in three *Madracis* coral species exposed to mild (irradiance changes) and acute (a positive thermal anomaly) stress on reefs in Curaçao, integrating Symbiodiniaceae and bacterial community data across host species and environmental gradients.

This thesis characterized shifts in community composition, diversity, and cross-domain co-occurrence across 137 coral samples using high-throughput ITS2 (Illumina MiSeq) and full-length 16S rRNA gene sequencing (Oxford Nanopore MinION). Host species emerged as the dominant driver of both Symbiodiniaceae and bacterial community structure. Although Symbiodiniaceae identity influenced bacterial composition in bivariate analyses, multivariate models revealed host identity as the overriding factor. During bleaching, *Madracis pharensis* colonies dominated by B15 Symbiodiniaceae types were more frequently bleached than those with B7, suggesting increased susceptibility linked to B15 dominance.

In the transplantation experiment, *Madracis mirabilis* and *Madracis decactis* exhibited divergent microbial responses despite identical environmental conditions. *M. mirabilis* showed an increase in Symbiodiniaceae diversity and moderate restructuring of its bacterial community, including increased richness over time. In contrast, *M. decactis* experienced a decline in Symbiodiniaceae diversity and maintained a comparatively stable bacterial community. These contrasting patterns highlight species-specific differences in microbial flexibility and constraint.

Together, these findings support a hierarchical model of holobiont organization, where host identity exerts dominant control over both Symbiodiniaceae and bacterial community composition, while environmental stressors act as modulators, and symbiont identity may influence bacterial communities but remains secondary to host effects. This thesis highlights the importance of cross-partner integration in coral microbiome research and underscores the need to consider host-specific dynamics when assessing coral resilience under climate change.

Zusammenfassung

Korallen-Holobionten sind auf dynamische mikrobielle Partnerschaften angewiesen, um Homöostase und ökologische Resilienz unter Umweltstress aufrechtzuerhalten. Dennoch ist bislang unzureichend verstanden, inwieweit voneinander abhängige mikrobielle Gemeinschaften wie Symbiodiniaceae und Bakterien unterschiedlich oder koordiniert auf äußere Stressfaktoren reagieren. Diese Arbeit untersucht die mikrobiellen Reaktionen bei drei *Madracis*-Korallenarten, die mildem (Lichtveränderungen) und akutem Stress (eine positive thermische Anomalie) an Riffen von Curaçao ausgesetzt waren. Dabei wurden Symbiodiniaceae- und Bakteriengemeinschaften in Abhängigkeit von Wirtsart und Umweltgradienten analysiert.

Mittels Hochdurchsatz-Sequenzierung der ITS2-Region (Illumina MiSeq) und Voll-Längen-Sequenzierung des 16S rRNA-Gens (Oxford Nanopore MinION) wurden Veränderungen in der Gemeinschaftszusammensetzung, Diversität und domänenübergreifenden Kookkurrenz in 137 Korallenproben charakterisiert. Die Wirtsart erwies sich als der stärkste Einflussfaktor auf die Zusammensetzung sowohl der Symbiodiniaceae- als auch der Bakteriengemeinschaften. Zwar beeinflusste die Symbiodiniaceae-Identität in bivariaten Analysen die bakterielle Zusammensetzung, multivariate Modelle zeigten jedoch, dass die Wirtsidentität den übergeordneten Einfluss hatte. Während der Bleiche waren Kolonien von *Madracis pharensis*, die von Symbiodiniaceae-Typ B15 dominiert wurden, häufiger gebleicht als solche mit Typ B7 – ein Hinweis auf eine erhöhte Anfälligkeit bei B15-Dominanz.

Im Transplantationsexperiment zeigten *Madracis mirabilis* und *Madracis decactis* trotz identischer Umweltbedingungen unterschiedliche mikrobielle Reaktionen. *M. mirabilis* wies eine Zunahme der Symbiodiniaceae-Diversität und eine moderate Umstrukturierung der bakteriellen Gemeinschaft auf, einschließlich eines Anstiegs der bakteriellen Diversität über die Zeit. *M. decactis* hingegen zeigte einen Rückgang der Symbiodiniaceae-Diversität bei gleichzeitig stabiler Bakteriengemeinschaft. Diese kontrastierenden Muster verdeutlichen artspezifische Unterschiede in mikrobieller Flexibilität und Begrenzung.

Insgesamt stützen die Ergebnisse ein hierarchisches Modell der Holobiontenorganisation, in dem die Wirtsidentität die dominante Kontrolle über die Zusammensetzung sowohl der Symbiodiniaceae- als auch der Bakteriengemeinschaften ausübt. Umweltstressoren wirken als Modulatoren, während die Symbiontenidentität bakterielle Gemeinschaften beeinflussen kann, jedoch dem Wirtseinfluss untergeordnet bleibt. Diese Arbeit betont die Bedeutung der Integration domänenübergreifender Partnerschaften in der Korallenmikrobiomforschung und unterstreicht die Notwendigkeit, wirtsartspezifische Dynamiken bei der Bewertung der Korallenresilienz im Klimawandel zu berücksichtigen.

Acknowledgements

First, I would like to thank my primary supervisor, Dr. Pedro Frade, for his continuous support, insightful feedback, and guidance throughout this project. His expertise has been essential in shaping this research.

I also appreciate the support of my official supervisor, Prof. Dr. Gerhard Herndl, for his guidance during the formal stages of the thesis and for providing valuable input to ensure the academic quality of this work.

A special thanks to Dr. Chloé Stévenne for helping me specifically with the raw processing of the 16S sequences, and in general for support during bioinformatic analyses and help with organization.

The project would not have been possible without the samples collected and processed by Giulia Marchioro and Helena Silberhumer, during their fieldtrip to Curaçao in 2023. An additional thanks for the collaboration on processing the samples, also including Ferdinand Meiss.

Thank you, Manuela Quiroga, my fellow student, for good conversations during the process on how to solve certain aspects and how to proceed.

I would like to express my gratitude to Restore Seas for funding this project, including sequencing of my samples at the University of Ghent and the University of Liège. This generous support made this research possible and was crucial to its success.

I would like to thank the Natural History Museum Vienna, particularly the Molecular Systematics Laboratory, for their support throughout this project. Access to collections, laboratory facilities, and training in key techniques provided an important foundation for this research.

Lastly, I would like to give a personal thank you to my partner, my family, and my closest friends for always believing in me, offering unwavering encouragement, and providing emotional support throughout this journey.

1 General introduction

1.1 Coral reefs

Despite occupying less than 0.2% of the ocean floor, coral reefs support over 25% of marine life, making them among the most diverse ecosystems on Earth (Fisher et al., 2015; Knowlton, 2010; Roberts et al., 2002). Reef-building corals act as ecosystem engineers by constructing complex three-dimensional reef structures that provide shelter, feeding grounds, and breeding habitats for numerous marine species (Kerry & Bellwood, 2012; Wang et al., 2021). These reefs also play a vital role in nutrient cycling and primary productivity by maintaining symbiotic relationships that enable nutrient recycling in oligotrophic waters (Rädecker et al., 2015). Beyond their ecological value, coral reefs offer coastal protection, fisheries support, and significant ecosystem services, including shoreline stabilization and tourism (economy) (Hoegh-Guldberg et al., 2019).

1.2 Reef-building corals

Reef-building corals, or hermatypic corals, are animals in the phylum Cnidaria, class Anthozoa, subclass Hexacorallia, and order Scleractinia (Kayal et al., 2013). Most reef-building corals are colonial, composed of genetically identical polyps functioning as a modular organism (Hughes & Jackson, 1985; Jackson, 1977). Each polyp contains an outer ectoderm and an inner endoderm, separated by a mesoglea (Furla et al., 2005). The endoderm houses intracellular dinoflagellate algae from the family Symbiodiniaceae (Furla et al., 2005; Muscatine & Cernichiari, 1969). These symbiotic algae contribute significantly to the coral's energy needs through photosynthesis, supplying the host with organic carbon (Muscatine, 1990; Quigley et al., 2020). This relationship enables reef-building corals to thrive in nutrient-poor (oligotrophic) tropical waters, where external food sources are often limited (Rädecker et al., 2015) The calicoblastic ectoderm forms the coral skeleton by depositing calcium carbonate, enabling the development of reef structures (Allemand et al., 2004; Furla et al., 2005).

1.3 The coral holobiont

Corals form meta-organisms, or holobionts, composed of the coral animal and a diverse assemblage of microorganisms, including Symbiodiniaceae, Bacteria, Archaea, Fungi, and viruses (Bourne et al., 2016; Voolstra et al., 2024) (Figure 1.1). These microbial communities contribute critically to coral health, development, and resilience (Glasl et al., 2016; Peixoto et al., 2017).

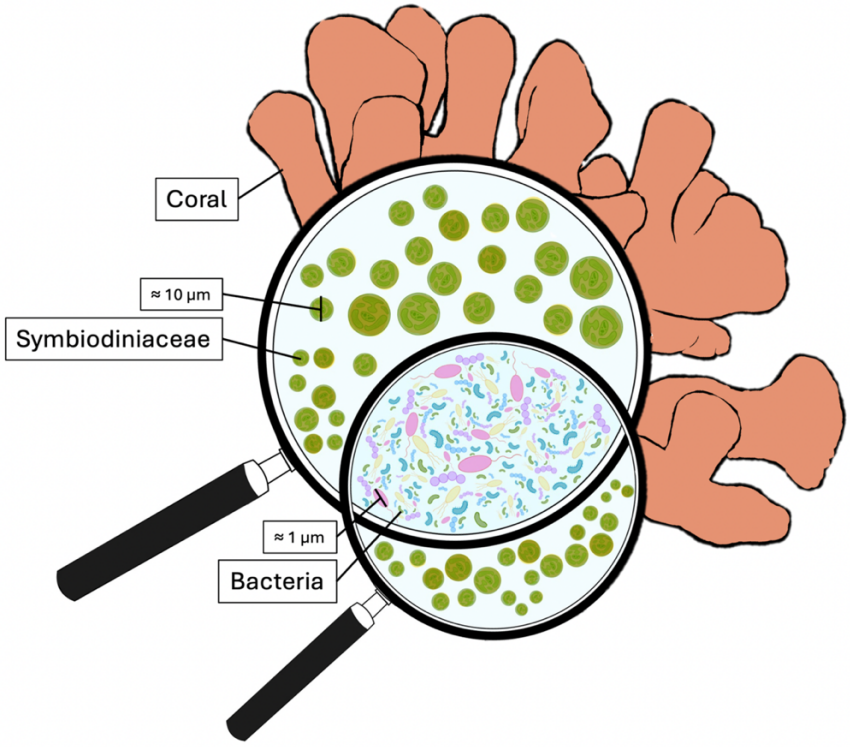

Figure 1.1 The coral holobiont is a complex association of the coral animal and diverse microbial partners. This includes Symbiodiniaceae (≈10 µm), which reside within host tissues, and Bacteria (≈1 µm), which inhabit the mucus, tissue, and skeleton. Other microbial groups include Archaea, Fungi and viruses, that together influence coral health and resilience. Illustration drawn in GoodNotes.

1.3.1 Symbiodiniaceae

Symbiodiniaceae are intracellular dinoflagellates that provide corals with most of their energy via photosynthesis, producing energy rich compounds in exchange for shelter and nutrients (Muscatine, 1990; Muscatine & Porter, 1977; Quigley et al., 2020). Through photosynthesis, these algae remove CO_2, elevating pH and carbonate ion concentration near the site of calcification, thereby facilitating calcium carbonate deposition, a process known as light-enhanced calcification (Allemand et al., 2004; Furla et al., 2005; Moya et al., 2008).

Previously classified into clades, Symbiodiniaceae are now organized into genera based on molecular and ecological traits (LaJeunesse et al., 2018). *Symbiodinium*, corresponding to Clade A, is a basal genus adapted to high or fluctuating light conditions. *Breviolum* (Clade B) includes both free-living and symbiotic forms, commonly inhabiting stable, shallow waters. *Cladocopium* (Clade C) stands out as the most diverse and widespread genus among coral hosts. In contrast, *Durusdinium* (Clade D) comprises extremophiles notable for their resilience to coral bleaching (Cunning et al., 2017; LaJeunesse et al., 2018).

1.3.2 Bacteria

Bacteria are a fundamental component of the coral holobiont, contributing to nutrient cycling, disease resistance, and the regulation of host homeostasis (Neave et al., 2016; Voolstra et al., 2024). Coral microbiomes span the mucus, tissue, and skeleton compartments and include numerous bacterial phyla, with Pseudomonadota, Bacteroidota, Bacillota, and Cyanobacteriota among the most frequently reported in tropical reef-building corals (Huggett & Apprill, 2019; Neave et al., 2017; Pollock et al., 2018; Voolstra et al., 2024). Core families such as Endozoicomonadaceae, Rhodobacteraceae, and Alteromonadaceae often dominate healthy corals and are thought to support key physiological processes, including carbon and nitrogen metabolism, sulfur cycling, and the production of vitamins and antibiotics (Neave et al., 2016; Pogoreutz et al., 2020; Raina et al., 2016).

Coral microbiomes are structured in part by host identity, with evidence for phylosymbiosis, where host phylogeny predicts microbial composition, although this does not necessarily imply co-evolution (O'Brien et al., 2020; Pollock et al., 2018). Beyond taxonomic structure, recent studies have also highlighted microbial functional potential, including genes involved in oxidative stress resistance, and nutrient acquisition (Matthews et al., 2020; Rädecker et al., 2015).

1.4 Studying Symbiodiniaceae and Bacteria in corals

Recent advances in molecular biology have revolutionized the study of coral microbiomes. Symbiodiniaceae, once considered a single species, are now recognized as a diverse family with distinct ecological traits (LaJeunesse et al., 2018). Their diversity

is typically assessed using the internal transcribed spacer 2 (ITS2) region of ribosomal DNA, a marker that provides high taxonomic resolution but presents challenges due to its multicopy nature and associated intra- and intergenomic variation (Cunning et al., 2017; Hume et al., 2019; Pochon et al., 2014). Early methods such as Denaturing Gradient Gel Electrophoresis (DGGE) or cloning offered limited resolution, but high throughput sequencing now enables detection of both dominant and background symbiont types at much greater depth (Apprill & Gates, 2007; Hume et al., 2019). The SymPortal framework has become a standard tool for ITS2 analysis, using defining intragenomic variants (DIVs) to better distinguish true biological patterns (Hume et al., 2019; Quigley et al., 2020).

Bacterial communities, traditionally classified by morphology and metabolic traits, were long studied using culture-based methods (Morata de Ambrosini et al., 2014). While these approaches remain standard in clinical microbiology, they are time-consuming and miss the vast majority of non-cultivable bacteria (Kai et al., 2019; Morata de Ambrosini et al., 2014). Molecular methods, especially sequencing of the 16S rRNA gene, have transformed the ability to identify bacteria across diverse taxa. The gene's combination of conserved and variable regions allows for both broad and specific taxonomic classification (Kai et al., 2019).

Second-generation platforms like Illumina have made high-throughput sequencing of short regions routine and are widely used in microbial ecology due to their scalability and accuracy (Hu et al., 2021). Illumina sequencing operates through a sequencing-by-synthesis approach, in which fluorescently labeled nucleotides are incorporated and detected one at a time during DNA polymerization (Hu et al., 2021). However, these platforms generate short reads, which can limit resolution across complex regions. Third-generation technologies such as Oxford Nanopore Technologies' MinION provide full-length 16S reads in real time, enabling improved resolution of bacterial taxa and better capturing of structural variation (Lu et al., 2016). MinION uses nanopores embedded in a membrane to detect changes in electrical current as DNA strands pass through, allowing direct sequencing of long fragments.

In this thesis, Symbiodiniaceae were characterized using Illumina sequencing of the ITS2 region, and bacterial communities were profiled using full-length 16S sequencing on the MinION platform. This dual strategy enables robust, high-resolution comparisons of microbial diversity, structure, and co-occurrence.

2 Introduction

The highly productive reef ecosystems are threatened by climate change and anthropogenic stressors that drive widespread coral reef degradation. As of April 2025, the ongoing global bleaching event has affected 83.7% of the world's coral reef area, making it the most extensive bleaching event on record (NOAA Coral Reef Watch, 2025).

Bleaching is primarily caused by heat stress and is often exacerbated by high irradiance, nutrient enrichment, hypoxia, and other co-stressors (Helgoe et al., 2024; Maynard et al., 2015; Pogoreutz et al., 2020; Suggett & Smith, 2019). It results in the dysfunction or loss of algal symbionts and/or chlorophyll and subsequent declines in coral health (Lesser, 1997; Venn et al., 2006). Ocean acidification, coastal pollution, sedimentation, and destructive fishing practices further compromise coral growth, reproduction, and disease resistance (Hughes et al., 2003; Voolstra et al., 2024). These stressors act synergistically to reduce coral resilience and threaten the long-term stability of reef ecosystems (Ban et al., 2014; Hoegh-Guldberg et al., 2019). Understanding how the coral holobiont respond to environmental stressors is key to finding ways to protect these important ecosystems.

2.1 Symbiodiniaceae exposed to environmental stressors

Genera of Symbiodiniaceae differ in their photo physiological responses, growth rates, and thermal tolerances, which in turn influence host performance under environmental stress (LaJeunesse et al., 2018). They can exhibit strong host specificity, although some coral species can shuffle or switch symbionts in response to environmental change (Ros et al., 2021). This symbiont flexibility has been observed during recovery from bleaching events or other disturbances, often involving a temporary dominance of more thermally tolerant genera like *Durusdinium* (Silverstein et al., 2015; Stat & Gates, 2011).

Environmental stressors such as elevated temperature, high irradiance, and nutrient enrichment impair Symbiodiniaceae physiology by disrupting photosynthesis and generating reactive oxygen species (ROS) that damage both algal and host cells (Suggett & Smith, 2019; Warner et al., 1999). These processes lead to photoinhibition, oxidative stress, and chloroplast degradation, which are central to the onset of coral bleaching (Lesser, 1997; Warner et al., 1999). In contrast, low-light conditions and shading can enhance thermal tolerance and reduce bleaching risk (Oakley & Davy, 2018;

Tagliafico et al., 2022). Under prolonged stress, community shifts may occur, with more thermally resilient genera such as *Durusdinium* becoming dominant, often accompanied by trade-offs in coral growth and reproduction (Cooper et al., 2011; Stat & Gates, 2011). Consequently, the structure and flexibility of Symbiodiniaceae communities play a pivotal role in determining coral vulnerability and resilience to environmental change.

2.2 Bacteria exposed to environmental stressors

Species-specific responses to environmental stressors have been observed across coral taxa. For instance, *Pocillopora* spp. often retain relatively stable bacterial communities under moderate stress, while *Acropora* spp. show rapid microbiome restructuring in response to even minor environmental fluctuations (Marchioro et al., 2020; McDevitt-Irwin et al., 2017; Ziegler et al., 2019). Such changes in microbiome composition can influence coral physiology, health, and resilience, underscoring the importance of understanding how microbial communities respond to disturbance.

Environmental disturbances often cause rapid and profound shifts in coral-associated bacterial communities (Glasl et al., 2016; McDevitt-Irwin et al., 2017; Ziegler et al., 2019). These changes can follow divergent trajectories, either toward dysbiosis or toward beneficial restructuring (Voolstra et al., 2024). Dysbiosis involves a breakdown in microbial regulation and reduced diversity (Bourne et al., 2008), along with the proliferation of opportunistic or potentially pathogenic taxa such as Vibrionaceae, Rhodobacteraceae, and Flavobacteriaceae (McDevitt-Irwin et al., 2017; Pogoreutz et al., 2018). These shifts are often accompanied by increased expression of virulence or stress-response genes and may reflect deteriorating holobiont health (van de Water et al., 2018).

Conversely, the coral probiotic hypothesis proposes that microbial communities can restructure in ways that enhance host resilience by enriching for bacterial taxa involved in antioxidant production, nitrogen fixation, or antimicrobial activity (Peixoto et al., 2017; Pogoreutz et al., 2020; Reshef et al., 2006). Such adaptive restructuring may involve increased abundance of Alphaproteobacteria such as Rhodospirillaceae (e.g., *Inquilinus*) and genera like Pseudoalteromonas, Erythrobacter, Roseobacter, Halomonas, and Cobetia, which are linked to thermal tolerance and antimicrobial function. These shifts may also include functional enrichment of stress-mitigating genes

such as ferredoxin (ROS scavenging), nifW (nitrogen fixation), and GroES (protein folding), as observed in heat-tolerant coral microbiomes (Peixoto et al., 2017; Ziegler et al., 2017).

2.3 Linking Symbiodiniaceae and Bacteria

Recent evidence suggests that Symbiodiniaceae and Bacteria interact more directly than previously recognized. Both ectosymbiotic and endosymbiotic bacterial taxa have been identified within or near algal cells, and several of these bacteria appear to influence algal stress tolerance (Lawson et al., 2017; Maire et al., 2021). For instance, Rhizobiales such as *Bradyrhizobium* and *Labrenzia* may facilitate nitrogen fixation and the production of antioxidant compounds like DMSP, while Myxococcales may help suppress pathogenic bacteria (Gardner et al., 2023; Maire et al., 2021). These interactions suggest that bacterial associates can modulate oxidative stress, contribute key nutrients, and support holobiont stability under environmental stress.

The bacterial community composition has also been shown to correlate with Symbiodiniaceae identity. Corals dominated by *Durusdinium* often exhibit lower bacterial diversity and distinct microbial assemblages compared to those dominated by *Cladocopium* (Quigley et al., 2020). For example, *Durusdinium*-dominated juveniles of *Acropora tenuis* harbored higher relative abundances of Alphaproteobacteria and Cyanobacteria, while shifts in Symbiodiniaceae types (e.g., from D1 to D1a) were linked to restructuring in bacterial taxa such as Planctomycetota and Bacteroidota. These patterns suggest that Symbiodiniaceae not only shape the microbial niche through metabolite production or signaling but may also exert fine-scale filtering effects on specific bacterial groups (Maire et al., 2021; Quigley et al., 2020). Such structuring could influence holobiont function and stress tolerance, especially in early life stages where microbial flexibility is critical (Voolstra et al., 2024).

These findings call for a shift in perspective: rather than viewing coral–Symbiodiniaceae and coral–Bacteria interactions in isolation, the coral holobiont should be considered as an integrated, multi-partner system (Matthews et al., 2020; Peixoto et al., 2017). Interactions among microbes may be critical for maintaining resilience, with specific bacterial taxa supporting the persistence and function of Symbiodiniaceae, though the mechanisms and stability of these associations remain poorly understood.

2.4 Study system: the genus *Madracis*

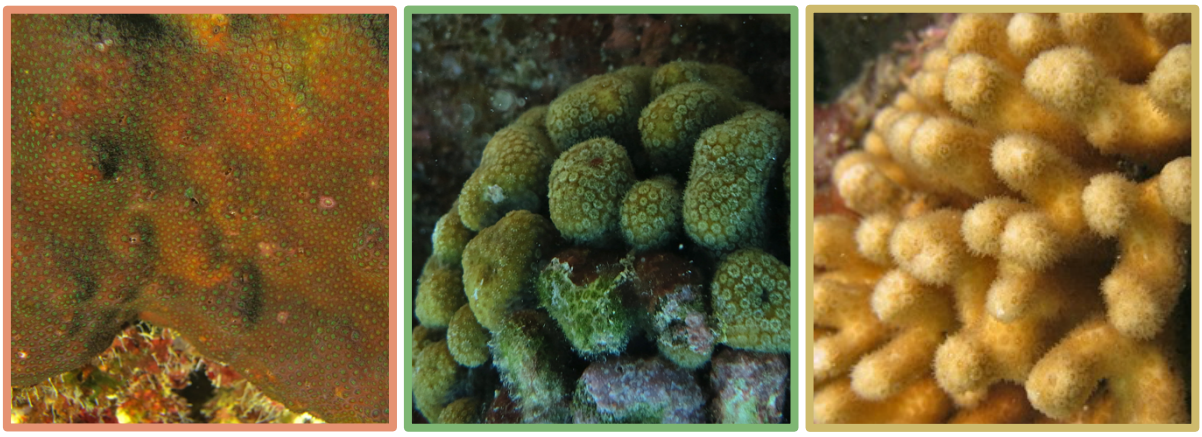

Figure 2.1 Three *Madracis* species: *M. pharensis* (pink frame), *M. decactis* (green frame), and *M. mirabilis* (yellow frame). Photographs of *M. pharensis* and *M. decactis* by Giulia Marchioro (used with permission). Photograph of *M. mirabilis* by Florida Fish and Wildlife Conservation Commission (2012), licensed under CC BY-NC-ND 2.0.

This thesis focuses on three Caribbean species of the genus *Madracis* (family Pocilloporidae): *Madracis pharensis*, *Madracis decactis*, and *Madracis mirabilis*. These species are common reef-builders across a wide depth range, with *M. pharensis* found at 5–60 m, *M. decactis* at 5–40 m, and *M. mirabilis* at 2–25 m (Frade et al., 2008b). Their contrasting depth distributions and environmental niches make them ideal candidates for studying microbial community dynamics across light and thermal gradients (Frade et al., 2010). Previous studies show that these species associate predominantly with *Breviolum* symbionts, though the dominant types differ among species and with depth, B7 being a generalist, B13 associated with shallow *M. mirabilis*, and B15 more common in deep *M. pharensis* (Frade et al., 2008a).

2.5 Aims, objectives, and hypotheses

While numerous studies have examined Symbiodiniaceae and bacterial communities separately, relatively few have directly compared their responses across host species and environmental gradients (Matthews et al., 2020). Furthermore, microbial community shifts remain understudied in corals dominated by *Breviolum*, particularly under simultaneous exposure to both mild (irradiance changes) and acute (a positive thermal anomaly) stressors.

To address this gap, this thesis investigates the structure and dynamics of Symbiodiniaceae and bacterial communities in *Madracis* corals subjected to depth transplantation and natural bleaching. High-throughput sequencing (Illumina for ITS2

and Oxford Nanopore for 16S rRNA) was used to characterize changes in microbial composition and diversity across host species and environmental conditions. By integrating algal and bacterial datasets, this thesis evaluates whether microbial responses to environmental stress are parallel, divergent, or independently modulated by host identity, symbiont composition, and/or environmental context.

Aim: To investigate how microbial communities in reef-building corals respond to mild and acute stressors, and how these responses are shaped by host identity, symbiont composition, and/or environmental change.

Objectives:

1. Characterize the Symbiodiniaceae and bacterial communities in reef-building corals during a depth-transplantation experiment.
2. Characterize the Symbiodiniaceae and bacterial communities in reef-building corals during a natural bleaching event.
3. Investigate the drivers of bacterial community variation and the interactions between bacterial and Symbiodiniaceae communities, focusing on the roles of host species, photosymbiont identity, and environmental conditions

Hypotheses:

1. It is expected that depth transplantation will lead to subtle shifts in Symbiodiniaceae composition, with increased prevalence of more thermally tolerant types in corals transplanted to shallower, higher-light environments. Concurrently, it is expected that bacterial communities will show moderate restructuring consistent with the probiotic hypothesis, potentially enriching for groups involved in stress mitigation.
2. It is expected that bleaching will be associated with a marked reduction in Symbiodiniaceae diversity and a shift toward more thermally tolerant symbionts. Bacterial communities in bleached corals will probably show signs of dysbiosis, including reduced diversity and increased relative abundance of opportunistic or stress-associated taxa reflecting impaired holobiont stability.
3. It is expected that bacterial community composition will correlate with both host species identity and Symbiodiniaceae type and that corals harboring more thermotolerant symbionts will exhibit distinct bacterial assemblages, possibly enriched in stress-adaptive functions.

3 Methods

3.1 Sample collection and processing

This thesis investigated how Symbiodiniaceae and bacterial communities in reef-building corals respond to both mild and acute environmental stressors, specifically, irradiance changes (transplantation) and a positive thermal anomaly (natural bleaching). The main fieldwork comprised a reciprocal depth-transplantation experiment alongside concurrent sampling of naturally bleached and non-bleached corals. Three coral species were included: *Madracis mirabilis* and *Madracis decactis* in the transplantation experiment, and *Madracis pharensis* in the bleaching observations.

A total of 139 *Madracis* coral samples were collected in 2023 from Snake Bay, Curaçao, in the southern Caribbean (during fieldwork by PhD candidate Giulia Marchioro). The reciprocal depth-transplantation experiment was conducted from the 16th of November to the 12th of December 2023 (as part of MSc research by Helena Silberhumer). Colonies of *M. mirabilis* and *M. decactis* were collected from depths of 10 m and 20 m and split into two fragments: one served as a control (retained at the native depth), and the other was transplanted to the opposite depth. Light availability at 10 m and 20 m was estimated using a model based on in situ measurements across multiple colonies (Frade et al., 2008a). According to this model, light intensity at 10 m was approximately 730 µmol m^{-2} s^{-1}, while at 20 m it was around 354 µmol m^{-2} s^{-1}, representing roughly a two-fold difference in irradiance between the two depths.

After a five-day acclimatization period, fragments were attached to underwater racks at the new depth. Each depth included both control (n = 6) and transplanted (n = 6) colonies per species. Samples were taken from each colony at two timepoints: the day of transplantation (T0) and 25 days later (T25), resulting in 48 samples per species. Temperature was continuously recorded at both depths throughout the experiment. At the beginning of the transplantation period, temperatures at both 10 m and 20 m were approximately 30 °C, decreasing to around 29 °C by the end of the experiment. Further details of the experimental setup are provided in Appendix B.

During the course of the experiment, a natural coral bleaching event occurred, affecting *M. pharensis*. In response, 43 additional *M. pharensis* samples were collected throughout the transplantation period, approximately 10 of which showed visible signs of

bleaching. Bleaching status in *M. pharensis* was determined based on a combination of visual assessment and symbiont cell density. Samples were categorized as bleached if they had a symbiont density below 1.15×10^6 cells cm^{-2}, and as non-bleached if they exceeded this threshold. Visual signs of bleaching corresponded well with this density-based classification. Chlorophyll content was also measured and tended to be lower in bleached samples, providing additional support, though it was not used as the primary criterion for categorization.

For all samples, small coral fragments were collected using bone cutters, placed into labeled zip-lock bags, and flash-frozen in liquid nitrogen in the field. Samples were then transported on dry ice to the Natural History Museum Vienna (NHM), where they were stored at -80 °C until further processing.

Tissue removal was performed using an airbrushing technique in 1× PBS buffer (Appendix C). The resulting tissue slurry was aliquoted for genetic analyses (16S and ITS2 metabarcoding), symbiont cell counts (via hemocytometer), and chlorophyll content measurements (via absorbance). The remaining skeletons were bleached, dried, and used to estimate surface area based on foil wrapping, allowing symbiont densities to be normalized to skeletal surface area (Appendix C).

3.2 DNA extractions, PCRs, and sequencing

DNA extractions were performed on 137 coral tissue samples and two negative controls using the ZymoBIOMICS™ DNA Miniprep Kit with an added washing step (Appendix D). DNA concentrations were quantified using the QuantiFluor® dsDNA System.

To confirm the presence of the target regions—the second internal transcribed spacer (ITS2) and the 16S ribosomal RNA gene—PCRs were performed using the primer pairs SymPochITS2F/SymPochITS2R (for ITS2) and 515F/806Rb (for 16S). PCR reactions were carried out using Qiagen Taq DNA polymerase, following a slightly modified version of the manufacturer's protocol (Appendix E). Amplicons were visualized on a 1.5% agarose gel. Following confirmation of amplification, DNA extracts were sent to Ghent University (Belgium) for 16S sequencing and to the GIGA-Genomics platform of the University of Liège (Belgium) for ITS2 sequencing.

16S rRNA gene sequencing was performed using Oxford Nanopore MinION technology, following the protocol by van der Loos et al. (2021). The primer pair 27_BCtail-

FW (TTTCTGTTGGTGCTGATATTGC_AGAGTTTGATCMTGGCTCAG) and 1492R_BCtail-RV (ACTTGCCTGTCGCTCTATCTTC_CGGTTACCTTGTTACGACTT) was used. PCRs were performed using Phire Tissue Direct PCR Master Mix with the following thermal profile: 98 °C for 3 minutes; 30 cycles of 98 °C for 8 seconds, 60 °C for 8 seconds, and 72 °C for 30 seconds; and a final extension at 72 °C for 3 minutes. Barcoding and library preparation followed the protocols for the PCR Barcoding Expansion Pack 1-96 and SQK-LSK109 kit. Sequencing was conducted on a MinION R9.4.1 flow cell over 48 hours.

ITS2 sequencing was performed using Illumina MiSeq technology and the primer pair SYM_VAR_5.8S2/ SYM_VAR_REV, as described in Hume et al. (2018). The forward and reverse primer sequences were TCGTCGGCAGCGTCAGATGTGTATAAGAGACAG-GAATTGCAGAACTCCGTGAACC and GTCTCGTGGGCTCGGAGATGTGTATAAGAGACAG-CGGGTTCWCTTGTYTGACTTCATGC, respectively. The underlined segments are Illumina adaptor overhangs, which precede the ITS2-specific primer sequences. The KAPA HiFi HotStart ReadyMix was used for PCR amplification, with the following cycling conditions: 3 minutes at 95°C, 25 cycles of 30 seconds at 95°C, 30 seconds at 55°C, and 30 seconds at 72°C, followed by a final 5-minute extension at 72°C. Sequencing was performed on an Illumina MiSeq platform using MiSeq Reagent Kit v3 for 2×250 bp paired-end reads.

3.3 Read processing and statistical analyses

2.3.1 Read processing and taxonomic assignment

2.3.1.1 16S rRNA gene sequences

Raw long-read 16S rRNA sequences (fastq.gz files) were quality-assessed using NanoPlot (v1.32.1) to evaluate read length distribution and overall quality. Filtering was performed with Chopper (v0.9.0) (De Coster & Rademakers, 2023), retaining only reads between 1300–1800 bp and with an average Phred quality score ≥12. Taxonomic classification was conducted using Emu (v3.4.6), which applies an expectation–maximization (EM) algorithm to classify full-length 16S sequences (Curry et al., 2022). A custom SILVA v138.2 reference database, optimized for DADA2 and formatted for Emu, was used to assign taxonomy based on the latest nomenclature. Throughout this thesis, the resulting taxonomic units are referred to as OTUs (Operational Taxonomic Units). In the context of Emu, these OTUs are not defined by sequence clustering or exact amplicon variants

(ASVs) but are instead probabilistically assigned to taxa based on full-length read alignment and iterative likelihood estimation.

Classified 16S taxonomic abundance profiles were imported into R (version 4.4.2). Mitochondrial and chloroplast sequences were excluded. Contaminants were identified using negative controls and filtered with the decontam package (v1.20.0) (Davis et al., 2018), applying the prevalence method with a threshold of 0.5. The resulting OTU table was rarefied to a standardized sequencing depth of 39,886 reads per sample, based on a trade-off between read depth and sample retention (Figure 3.1). Ten samples with insufficient sequencing depth were excluded.

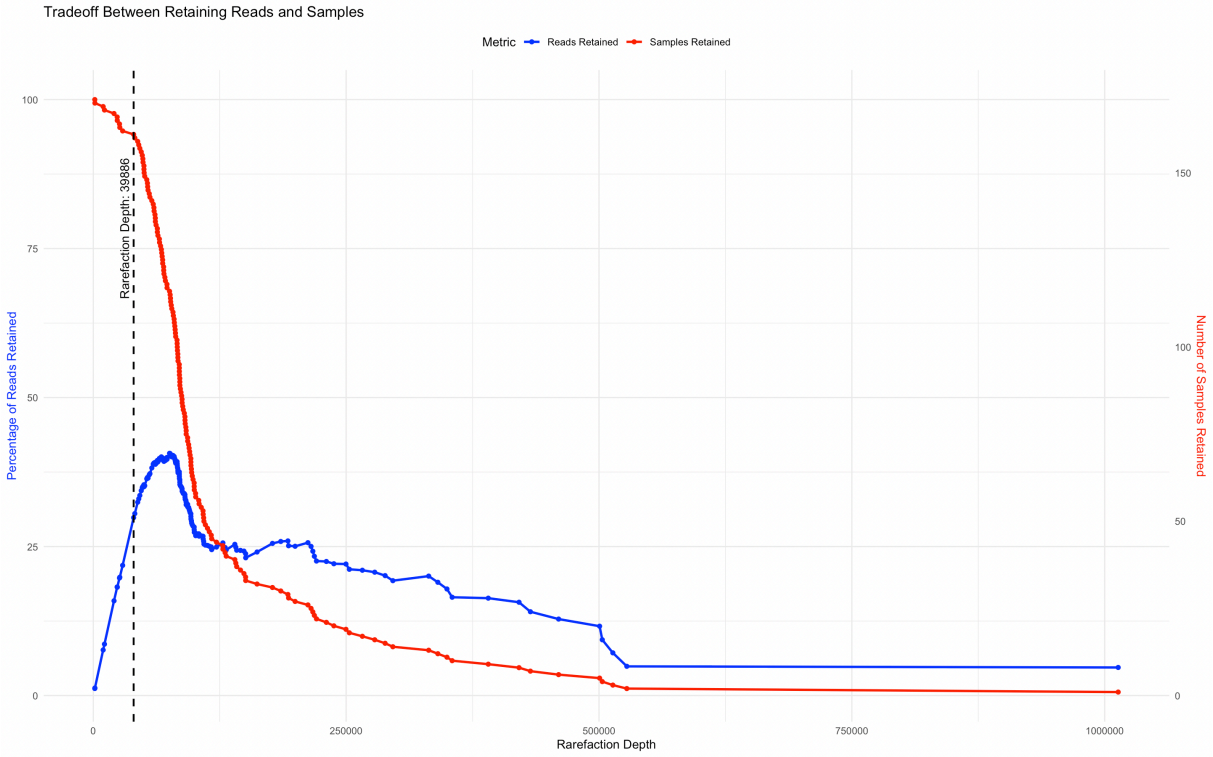

Figure 3.1 Tradeoff between rarefaction depth and sample/sequence retention for bacterial 16S data. The plot shows the percentage of reads retained (blue line, left y-axis) and the number of samples retained (red line, right y-axis) across a range of rarefaction depths. A rarefaction depth of 39,868 reads was selected (dashed line), balancing sufficient sequencing depth while retaining a high number of samples. This threshold ensured adequate coverage without substantial loss of sample size for downstream diversity analyses.

3.3.1.2 ITS2 sequences

Symbiodiniaceae ITS2 sequence processing was conducted using the SymPortal framework (Hume et al., 2019), which accounts for intragenomic variation by identifying diagnostic ITS2 variants (DIVs) and assembling them into ecologically meaningful ITS2-profiles. Quality filtering involved removal of non-Symbiodiniaceae sequences using mothur, BLAST+, and Minimum Entropy Decomposition (MED). To minimize the impact of

sequencing errors, only ITS2-profiles supported by more than 200 reads were retained for analysis. Abundance tables and ITS2-profiles were imported into R for downstream analyses.

3.3.2 Statistical analyses

All statistical analyses and visualizations were performed in R (version 4.4.2) using the following packages: *vegan* (Oksanen et al., 2024), *phyloseq* (McMurdie & Holmes, 2013), *ggplot2* (Wickham, 2025), *dplyr* (Wickham et al., 2023c), *tidyr* (Wickham, 2023a), *car* (Fox et al., 2019), *RColorBrewer* (Neuwirth, 2014), *ggrepel* (Slowikowski, 2021), *pairwiseAdonis* (Martinez Arbizu, 2020), *broom* (Hyndman, 2019), *indispecies* (De Cáceres & Legendre, 2022), *Deseq2* (Love et al., 2014), *pheatmap* (Kolde, 2019), *ggvegan* (Simpson, 2023), *decontam* (Davis et al., 2018), and *tidyverse* (Wickham, 2023b). Some figures were additionally created or finalized in Microsoft Excel (version 16.89, Microsoft Corporation, 2024).

Alpha diversity was calculated using observed richness and Shannon diversity indices. Levene's test was used to assess homogeneity of variances before selecting appropriate tests (parametric or non-parametric). Between-group comparisons were conducted using t-tests, ANOVA, Wilcoxon rank-sum, or Kruskal–Wallis tests as appropriate. Significant results across multiple groups were followed up with Tukey HSD or pairwise Wilcoxon post-hoc tests. Results were visualized with boxplots.

Beta diversity was assessed using Bray–Curtis dissimilarity matrices calculated from relative abundance data. Differences in community composition were tested with PERMANOVA (999 permutations), using explanatory variables as described above. Principal Coordinates Analysis (PCoA) was used to visualize differences in community structure.

Community-level differences in composition were evaluated across coral species, timepoint, transplant status, and bleaching condition. For Symbiodiniaceae (ITS2), dominant and main ITS2-profiles were extracted and visualized using pie charts. Relative abundance patterns of bacterial communities (16S) were examined using bubble plots to highlight dominant OTUs across groups. To identify bacterial OTUs differing significantly between groups, differential abundance testing was conducted using DESeq2. Likelihood Ratio Tests (LRT) were used to detect global differences across

species, Symbiodiniaceae main profiles, transplantation treatments, and bleaching conditions, while pairwise Wald tests were used to assess OTU-level differences within comparisons. Volcano plots were used to visualize the pairwise comparisons.

In addition, Indicator Species Analysis (IndVal) was used to identify bacterial OTUs specifically associated with Symbiodiniaceae main profiles (B7, B13, B15), with significance defined as IndVal > 0.7 and $p \leq 0.05$. To evaluate associations between bacterial and Symbiodiniaceae community structures, PERMANOVA tests were conducted at the OTU level to assess bacterial community differences among ITS2-profiles. Spearman's rank correlations were calculated between individual bacterial OTUs and ITS2-profiles across all samples, with significant associations defined as |rho| > 0.5 and Benjamini–Hochberg adjusted $p \leq 0.05$. These correlations were visualized using heatmaps. Furthermore, Mantel tests were used to assess global covariation between bacterial and Symbiodiniaceae community dissimilarity matrices (Bray–Curtis), with 999 permutations and Spearman's correlation, conducted both across all samples and within host species. Finally, Canonical Correspondence Analysis (CCA) was used to evaluate how bacterial community structure was influenced by explanatory variables. CCA was applied across the full dataset and for each host species individually. All statistical tests were considered significant at $p \leq 0.05$, with Benjamini-Hochberg correction applied for multiple testing where appropriate.

4 Results

4.1 Symbiodiniaceae community structure

A total of 137 coral samples from the three species *Madracis pharensis*, *Madracis mirabilis* and *Madracis decactis* were retained for Symbiodiniaceae community analysis. An initial average of 56,859 raw reads per sample underwent quality control, denoising, and taxonomic assignment within the SymPortal framework, yielding 59 distinct ITS2-profiles and 853 DIVs (Distinct Intragenomic Variants). On average, each sample harbored 2.9 ± 1.5 ITS2-profiles and 26.8 ± 16.2 DIVs. Except for one sample, each colony was dominated by one ITS2-profile (Supplementary figure A1). The ITS2 community was overwhelmingly dominated by *Breviolum* lineages, which accounted for 98.4% of total relative abundance across all samples. In contrast, *Symbiodinium* represented 1.05%, *Cladocopium* 0.25%, and *Durusdinium* less than 0.01%.

The five most abundant DIVs and ITS2-profiles in the dataset all belonged to the genus *Breviolum*. At the ITS2-profile level, the most abundant profile overall was B7-B7d-B7e, comprising 50.0% of all Symbiodiniaceae across samples, followed by B13/B7-B13a-B13b-B7d-B13c (26.7%) and B7.B7e (7.9%). Other frequently observed profiles included B13/B7-B13a-B7d-B13c (3.7%) and B15d-B15a-B15b-B19bi-B15c-B15e-B15f (3.6%). These profiles represent sets of ITS2 sequence variants co-occurring within samples, with the first variant indicating the most abundant (dominant) sequence in the profile. A similar pattern emerged at the DIV level: B7 alone represented 61.2% of all Symbiodiniaceae reads, followed by B13 (13.0%), B7d (3.8%), B13a (2.8%), and B15d (2.0%). Together, these five DIVs accounted for over 80% of the total Symbiodiniaceae abundance, highlighting the dominance of a small number of *Breviolum* lineages across the dataset.

4.1.1 Symbiodiniaceae communities are host species-specific

Symbiodiniaceae community structure differed significantly among the three *Madracis* species. *M. decactis* harbored the most diverse communities, whereas *M. mirabilis* exhibited the lowest diversity (Figure 4.1b, c). Both Shannon diversity (Kruskal–Wallis: $\chi^2 = 34.33$, df = 2, $p < 0.001$, n = 137) and observed richness ($\chi^2 = 16.25$, df = 2, $p < 0.001$)

varied significantly among species, with *M. decactis* showing significantly higher alpha diversity than the two other species.

Community composition also clustered distinctly by host species in the PCoA (Figure 4.1a), a pattern supported by PERMANOVA (pseudo-F = 19.31, df = 2, p = 0.001, n = 137). All pairwise comparisons were significant after Bonferroni correction (p = 0.003), indicating strong host-specificity.

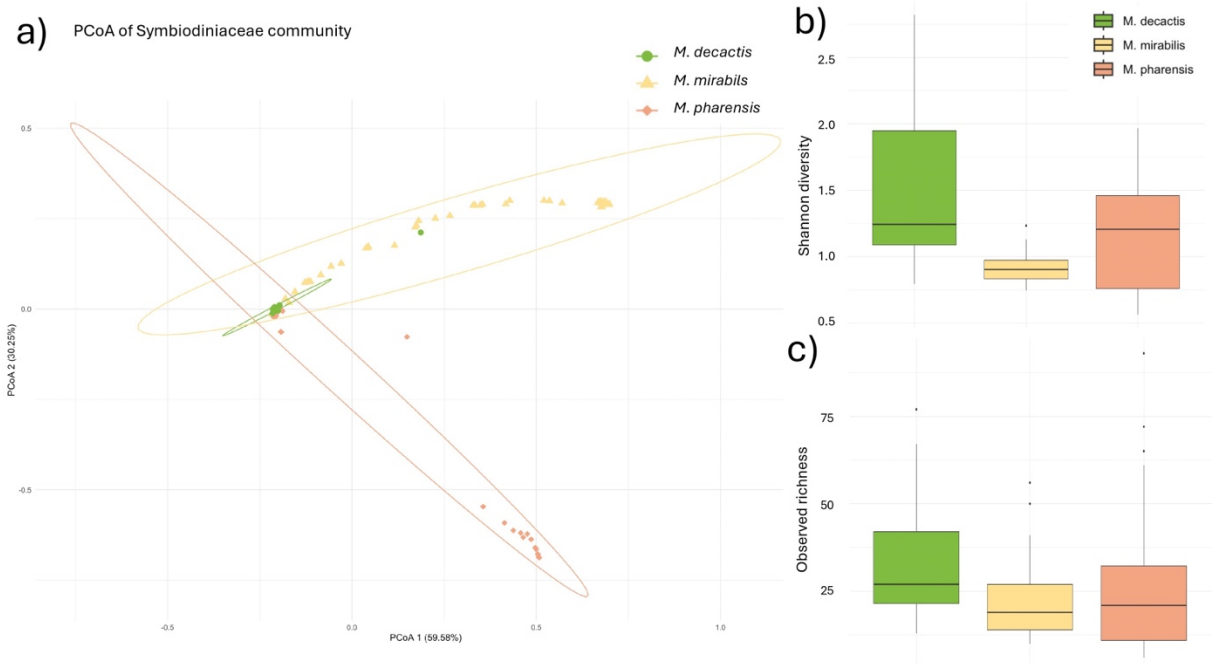

Figure 4.1 Symbiodiniaceae community structure differs among *Madracis* species. All analyses were performed at the DIV level. (a) Principal Coordinates Analysis (PCoA) based on Bray–Curtis dissimilarities of Symbiodiniaceae communities. Each point represents a coral sample from *M. decactis* (green, n = 47), *M. mirabilis* (yellow, n = 48), or *M. pharensis* (pink, n = 42). Ellipses represent 95% confidence intervals. Community composition differed significantly among species (PERMANOVA: pseudo-F = 19.31, df = 2, p = 0.001, n = 137); all pairwise comparisons were significant (Bonferroni-adjusted p = 0.003). (b) Shannon diversity index of Symbiodiniaceae communities. Diversity was significantly higher in *M. decactis* compared to *M. mirabilis* ($p < 0.001$) and *M. pharensis* ($p = 0.0022$); no difference was observed between *M. mirabilis* and *M. pharensis* ($p = 0.2273$). Kruskal–Wallis: $\chi^2 = 34.33$, df = 2, $p < 0.001$, n = 137. (c) Observed richness also differed significantly among species, with *M. decactis* exceeding both *M. mirabilis* ($p < 0.001$) and *M. pharensis* ($p = 0.00315$), while no difference was detected between *M. mirabilis* and *M. pharensis* ($p = 1.000$). Kruskal–Wallis: $\chi^2 = 16.25$, df = 2, $p < 0.001$, n = 137. All p-values are Bonferroni-adjusted.

4.1.2 Depth transplantation effects on Symbiodiniaceae communities

M. mirabilis colonies were consistently dominated by clade B13-associated ITS2-profiles, especially B13/B7-B13a-B13b-B7d-B13c. At T25, a slight increase in the diversity of ITS2-profiles was observed (Figure 4.2), though the dominant type remained unchanged (Figure 4.2a). In contrast, *M. decactis* colonies were almost exclusively dominated by clade B7-associated profiles (B7-B7d-B7e) at both T0 and T25, with only one colony dominated by B13/B7-B13a-B13b-B7d-B13c at T25 (Figure 4.3).

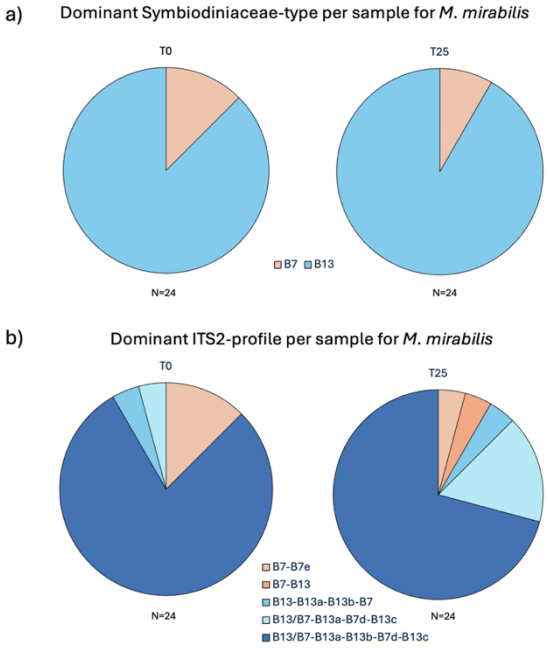

Figure 4.2 (a) Dominant Symbiodiniaceae type per sample at the start of the experiment (T0) and after 25 days (T25). Most colonies hosted B13 types, with a small proportion containing type B7. (b) Distribution of dominant ITS2-profiles per sample at T0 and T25. Most colonies were dominated by the B13/B7-B13a-B13b-B7d-B13c profile. (n = 24).

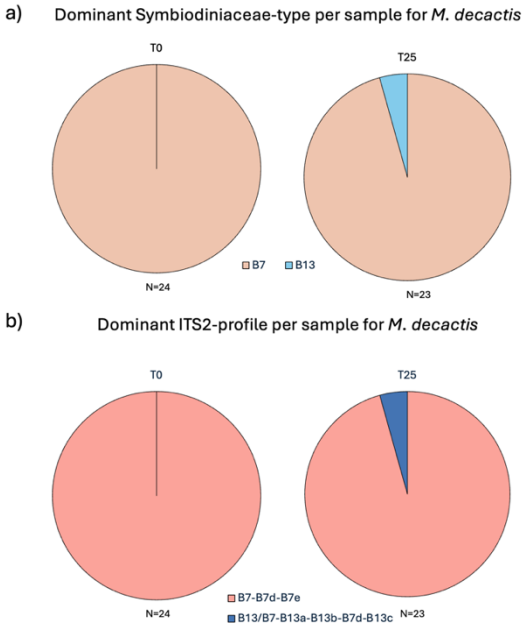

Figure 4.3 (a) Dominant Symbiodiniaceae type per sample, confirming dominance of type B7 at both T0 and T25. (b) Distribution of dominant ITS2-profiles per sample. All T0 samples were dominated by the B7-B7d-B7e profile, with one colony shifting to B13/B7-B13a-B13b-B7d-B13c at T25 (n = 24 (T0), n = 23 (T25)).

4.1.2.1 *M. mirabilis* (10 m origin)

In *M. mirabilis* colonies originating from 10 m – Symbiodiniaceae diversity and composition changed over time but showed no clear effect of transplantation (Figure 4.4a, 4.5a). Shannon diversity differed significantly across treatments (ANOVA: $F_{(2, 21)} = 14.7$, $p < 0.001$). Control colonies at T0 (n = 12) had significantly lower diversity than both

control T25 (Tukey HSD: n = 6; p = 0.050) and transplant T25 colonies (Tukey HSD: n = 6, p < 0.001). No significant difference was found between the two T25 groups. Observed richness did not differ significantly between groups (Kruskal–Wallis: χ^2 = 0.816, df = 2, p = 0.665, n = 24; Supplementary figure A2a).

PCoA showed overlapping clusters across treatments. However, a significant effect of treatment on community composition was detected (PERMANOVA: pseudo-F = 4.662, df = 2, p = 0.013, n = 24), with a significant difference between control T0 and control T25 (p = 0.039) (Figure 4.5a).

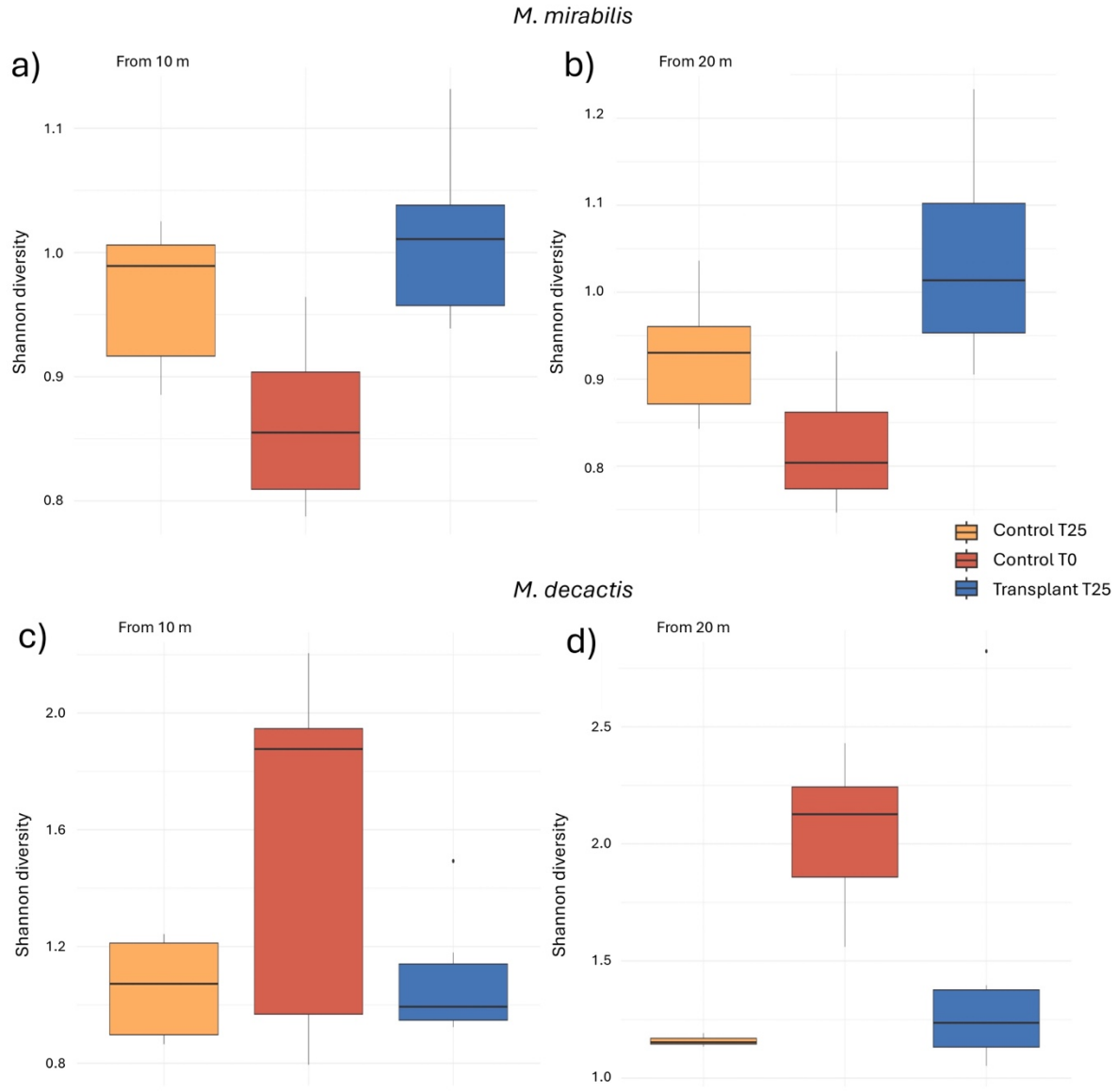

Figure 4.4 Shannon diversity of Symbiodiniaceae communities across transplant treatments. All analyses were performed at the DIV level. (a) *M. mirabilis* (10 m origin): Diversity differed significantly across treatments (ANOVA: $F_{(2, 21)}$ = 14.7, p < 0.001). T0 (n = 12) had significantly lower diversity than both control T25 (n = 6; p = 0.05) and transplant T25 (n = 6; p < 0.001), suggesting a time effect. (b) *M. mirabilis* (20 m origin): significant difference observed (ANOVA: $F_{(2, 21)}$ = 14.74, p < 0.001), with T0 (n = 12) differing from control T25 (n = 6; p = 0.0375) and transplant T25 (n = 6; p < 0.001). (c) *M. decactis* (10 m origin): No significant differences in Shannon diversity across treatments (Kruskal–Wallis: χ^2 = 3.027, df = 2, p = 0.220, n = 24). (d) *M. decactis* (20 m origin): Shannon diversity differed significantly (Kruskal–Wallis: χ^2

= 11.615, df = 2, p = 0.003, n = 23). Wilcoxon post hoc tests showed significant difference between control T0 (n = 11) and control T25 (n = 6; p < 0.001); other pairwise comparisons were not significant (p > 0.05).

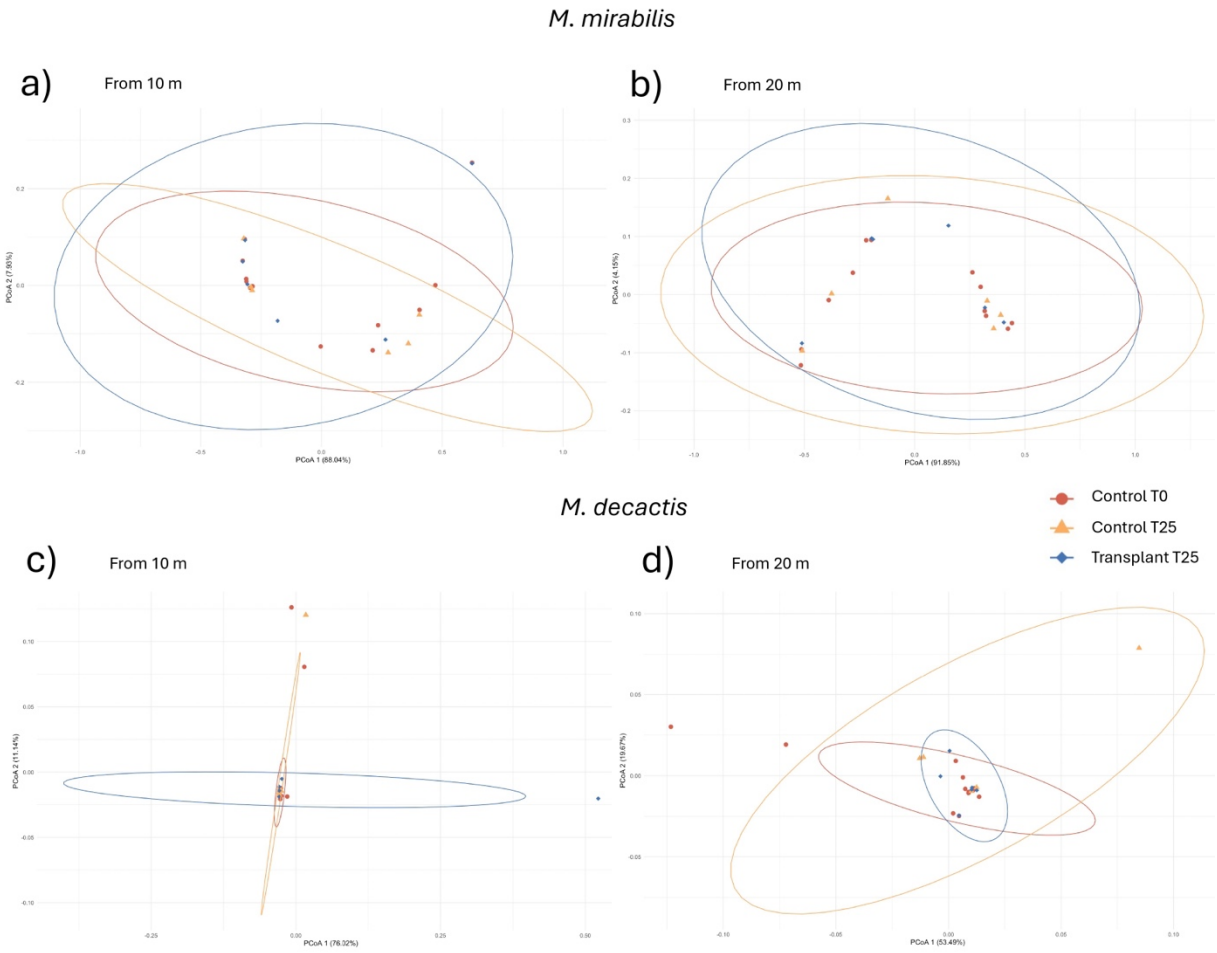

Figure 4.5 Principal Coordinates Analysis (PCoA) of Symbiodiniaceae community structure (Bray–Curtis distances). All analyses were performed at the DIV level. (a) *M. mirabilis* (10 m origin): PERMANOVA showed significant differences across groups (pseudo-F = 4.662, df = 2, p = 0.013, n = 24). Control T0 vs. control T25 differed significantly (p = 0.039); other comparisons were not significant. Transplanted colonies were more dispersed, with no clear clustering. (b) *M. mirabilis* (20 m origin): PERMANOVA: pseudo-F = 22.97, df = 2, p = 0.001, n = 24. All pairwise comparisons were significant (p = 0.003–0.042), though PCoA did not show distinct grouping. (c) *M. decactis* (10 m origin): PERMANOVA: pseudo-F = 2.553, df = 2, p = 0.001, n = 24. Control T0 vs. transplant T25 differed (p = 0.003); other comparisons not significant. (d) *M. decactis* (20 m origin): PERMANOVA: pseudo-F = 2.574, df = 2, p = 0.016, n = 23. Significant difference between control T0 and transplant T25 (p = 0.009); other comparisons not significant.

4.1.2.2 *M. mirabilis* (20 m origin)

Symbiodiniaceae communities in *M. mirabilis* originating from 20 m shifted over time, with increased diversity and significant changes in community composition, but no clear effect of transplantation (Figure 4.4b, 4.5b). Shannon diversity differed significantly across treatments (ANOVA: $F_{(2, 21)} = 14.74$, $p < 0.001$). Control colonies at T0 (n = 12) had significantly lower diversity than both control T25 (n = 6, p = 0.0375) and transplanted T25 colonies (n = 6, p < 0.001), while the T25 groups did not differ from each other. Observed

richness did not differ significantly across groups (Kruskal–Wallis: χ^2 = 4.14, df = 2, p = 0.126, n = 24; Supplementary figure A2b).

PCoA did not show distinct clustering (Figure 4.5b). However, significant differences in community structure were detected (PERMANOVA: pseudo-F = 22.97, df = 2, p = 0.001, n = 24), with all pairwise comparisons significant: control T0 vs. control T25 (p = 0.003), control T0 vs. transplant T25 (p = 0.003), and control T25 vs. transplanted T25 (p = 0.042).

4.1.2.3 *M. decactis* (10 m origin)

In *M. decactis* from 10 m, Symbiodiniaceae alpha diversity was similar across control T0 (n = 12), control T25 (n = 6), and transplant T25 (n = 6) groups. Neither Shannon diversity (Kruskal–Wallis: χ^2 = 3.03, df = 2, p = 0.220, n = 24; Figure 4.4c) nor observed richness (Kruskal–Wallis: χ^2 = 0.70, df = 2, p = 0.704, n = 24; Supplementary figure A2c) differed among treatments.

PCoA showed partial separation across treatments. PERMANOVA revealed a treatment effect (pseudo-F = 2.553, df = 2, p = 0.001, n = 24), with a significant difference between control T0 and transplant T25 (p = 0.003), though no difference was found between control T0 and control T25 (p = 1.000), and transplant T25 and control T25 (p = 0.060) (Figure 4.4c).

4.1.2.4 *M. decactis* (20 m origin)

Symbiodiniaceae Shannon diversity differed significantly among treatments (Kruskal–Wallis: χ^2 = 11.62, df = 2, p = 0.003, n = 23; Figure 4.4d). Control T0 colonies (n = 11) exhibited significantly higher diversity than control T25 colonies (n = 6; p < 0.001), while comparisons involving the transplant group were not significant (control T0 vs. transplant T25: p = 0.073; control T25 vs. transplant T25: p = 1.000). Observed richness did not differ across treatments (Kruskal–Wallis: χ^2 = 0.027, df = 2, p = 0.987, n = 23; Supplementary figure A2d).

PCoA indicated partial clustering of transplanted colonies. PERMANOVA revealed a significant overall effect of treatment (pseudo-F = 2.574, df = 2, p = 0.016, n = 23), with pairwise comparisons showing a significant difference between control T0 and transplant T25 (p = 0.009); other comparisons were not significant (Figure 4.5d).

4.1.2 Bleaching effect on Symbiodiniaceae communities

Bleached colonies of *M. pharensis* were more frequently dominated by type B15 Symbiodiniaceae, while non-bleached colonies were consistently dominated by B7 types (Figure 4.6). All non-bleached colonies (n = 32) harbored B7-type ITS2-profiles, including B7-B7e, B7-B7d-B7e, and B7-B7f. In contrast, bleached colonies (n = 10) showed higher prevalence of B15-type profiles (B15d-B15a-B15b-B19bi-B15c-B15e-B15f). One bleached sample exhibited a mixed profile. When grouped by dominant Symbiodiniaceae type, the pattern showed a clear contrast between B7 in non-bleached colonies and B15 in bleached ones.

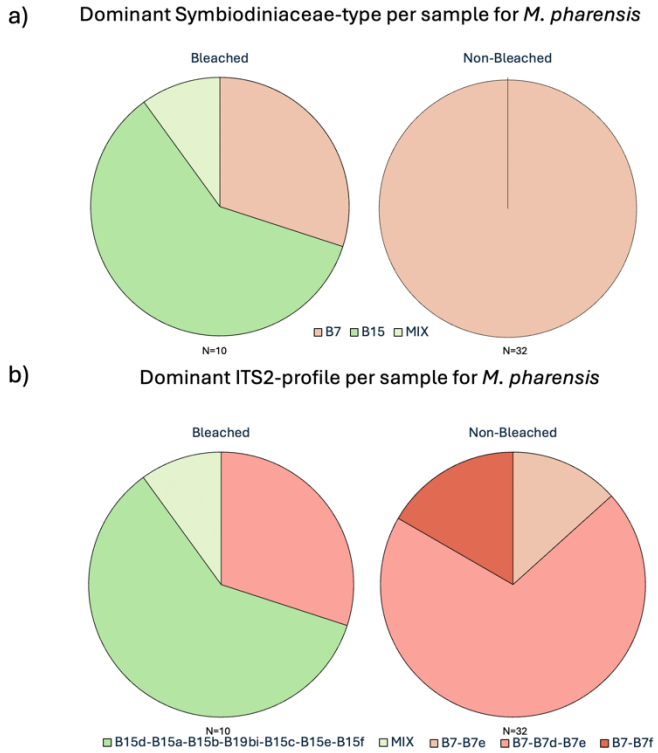

Figure 4.6 Dominant Symbiodiniaceae types and ITS2-profiles in bleached and non-bleached *M. pharensis* colonies. (a) Proportion of dominant Symbiodiniaceae ITS2-type groups per sample. All non-bleached colonies (n = 32) were dominated by type B7, while bleached colonies (n = 10) were primarily dominated by type B15. (b) Dominant ITS2-profiles per sample. Bleached colonies were mostly dominated by the composite B15d-B15a-B15b-B19bi-B15c-B15e-B15f profile, whereas non-bleached colonies were dominated by B7-B7d-B7e.

Alpha diversity metrics did not differ significantly between bleached (n = 10) and non-bleached (n = 32) *M. pharensis* colonies (Figure 4.7b–c). Shannon diversity (Wilcoxon rank sum: W = 198, n_1 = 10, n_2 = 32, p = 0.6306) and observed richness (Wilcoxon rank sum: W = 144, n_1 = 10, n_2 = 32, p = 0.3227) showed no significant differences between groups. PCoA showed some clustering of bleached and non-bleached colonies (Figure 4.7a), however this was not confirmed by PERMANOVA (pseudo-F = 1.175, df = 2, p = 0.333, n = 42).

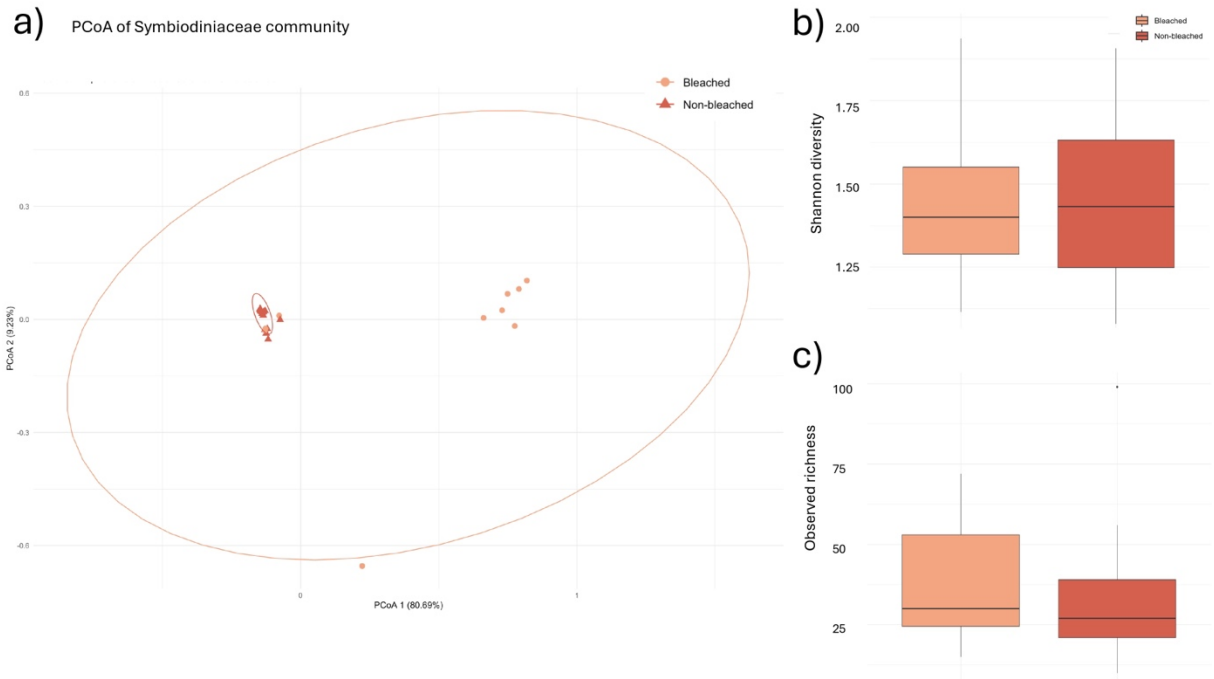

Figure 4.7 Symbiodiniaceae diversity and community composition in bleached and non-bleached *M. pharensis* colonies. All analyses shown were performed at the DIV level. (a) Principal Coordinates Analysis (PCoA) based on Bray–Curtis dissimilarities. Bleached samples showed greater dispersion, but no significant clustering by bleaching status was observed (PERMANOVA: pseudo-F = 1.175, df = 2, p = 0.333, n = 42). (b) Shannon diversity (Wilcoxon rank sum tests: W = 198, n_1 = 10, n_2 = 32, p = 0.6306) and (c) observed richness (Wilcoxon rank sum tests: W = 144, n_1 = 10, n_2 = 32, p = 0.3227) did not differ significantly between groups.

4.2 Bacteria community structure

An initial average of 203,160 raw reads per sample underwent quality filtering, contaminant removal, and taxonomic assignment based on the SILVA 138.2 database. Across all coral samples, a total of 2,581 bacterial OTUs were detected after filtering and rarefaction. On average, samples contained 207.4 ± 112.4 OTUs. Taxonomic classification assigned sequences to 61 phyla, 149 classes, 379 orders, 651 families, and 1,604 genera. The bacterial community was strongly dominated by Alphaproteobacteria, which accounted for 37.5% the overall relative abundance. Other abundant classes included Clostridia (9.8%), Acidimicrobiia (9.1%), Gammaproteobacteria (8.3%), and Planctomycetes (5.9%). Less dominant but still widespread classes included Actinobacteria (3.6%), Anaerolineae (3.0%), Chlorobia (2.6%), Bacteroidia (2.4%), and Thermoanaerobaculia (2.1%).

4.2.1 Bacterial communities are host species-specific

Bacterial community composition differed significantly among the three *Madracis* species, with multiple OTUs displaying strong host specificity (Figure 4.8). Across all

hosts, the most represented bacterial classes were Alphaproteobacteria, Acidimicrobiia, Actinobacteria, Clostridia, and Gammaproteobacteria.

DESeq2 Likelihood Ratio Tests (LRT) identified 300 OTUs with significant differential abundance across species (LRT padj < 0.05). The 10 most abundant OTUs per species were visualized in a bubble plot and further evaluated using pairwise Wald tests (Supplementary table A1). The complete set of pairwise comparisons are visualized in volcano plots (Supplementary figures A3-A5), which highlight OTUs with strong differential abundance (log_2 fold change > 2, equivalent to ≥4-fold differences). *M. pharensis* showed the strongest differentiation, with 249 OTUs significantly more abundant than in *M. mirabilis* and 147 more abundant than in *M. decactis*. In contrast, only 13 OTUs were more abundant in *M. mirabilis* and 9 in *M. decactis*, respectively. The comparison between *M. decactis* and *M. mirabilis* revealed 103 OTUs enriched in *M. decactis* and 27 in *M. mirabilis*. These plots show both the magnitude and direction of change, illustrating that *M. pharensis* consistently hosted more, significantly enriched OTUs than *M. mirabilis* or *M. decactis*.

Among the OTUs highlighted in the bubble plot (Figure 4.8a), several were also supported by DESeq2-based differential abundance testing. OTU 599 (Paracoccaceae) was highly abundant in both *M. decactis* (23.9 ± 19.6%) and *M. mirabilis* (29.2 ± 15.2%) and was significantly enriched in *M. mirabilis* compared to *M. pharensis* (log_2FC = 7.2, padj < 0.001). OTU 1328 (Actinomarinales) showed elevated abundance in *M. pharensis* (9.8 ± 6.0%) and was significantly enriched relative to both *M. decactis* (log_2FC = 7.3, padj < 0.001) and *M. mirabilis* (log_2FC = 8.6, padj < 0.001). OTU 2105 (Pseudomonadaceae) was significantly enriched in *M. decactis* compared to *M. mirabilis* (log_2FC = 7.1, padj < 0.001) and *M. pharensis* (log_2FC = 6.5, padj < 0.001) OTU 31 (Pirellulaceae) was more abundant in *M. mirabilis*, and significantly enriched compared to both *M. decactis* (log_2FC = 4.1, padj = 0.003) and *M. pharensis* (log_2FC = 4.7, padj < 0.001) OTU 12039 (Caminicellaceae) was significantly enriched in *M. pharensis* relative to *M. decactis* (log_2FC = 7.5, padj = 0.003) and *M. mirabilis* (log_2FC = 7.6, padj = 0.001).

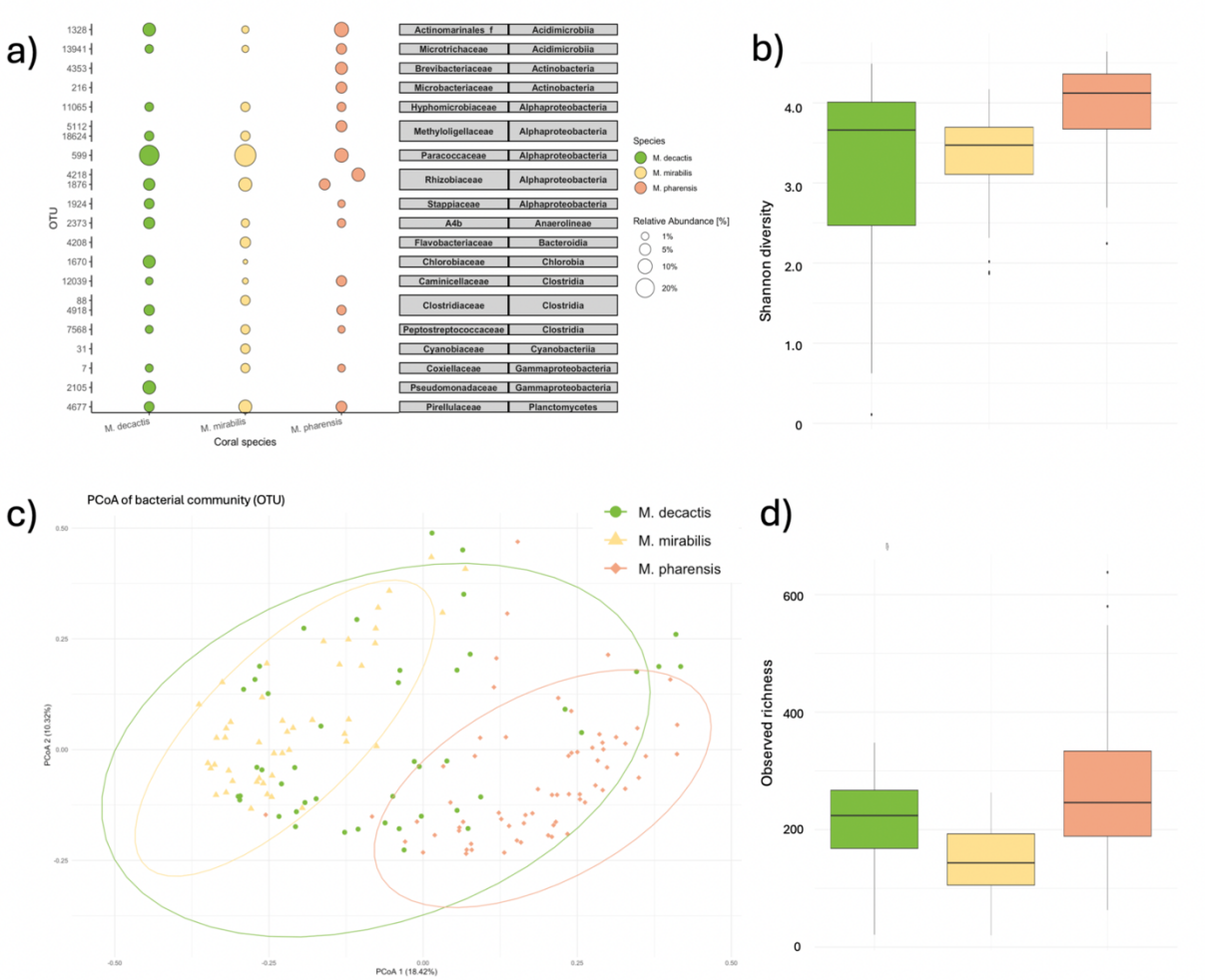

Figure 4.8 Bacterial community structure at the OTU level across *Madracis* species. (a) Bubble plot showing the mean relative abundance (%) of the top 10 most abundant OTUs across *M. decactis* (n = 45), *M. mirabilis* (n = 46), and *M. pharensis* (n = 36). Circle size corresponds to the average relative abundance per species. Taxonomic annotations are shown at the family and class level. Several OTUs showed strong host specificity, including OTU 599 (Paracoccaceae: 23.9 ± 19.6% in *M. decactis*, 29.2 ± 15.2% in *M. mirabilis*), OTU 1328 (Actinomarinales: 9.8 ± 6.0% in *M. pharensis*), OTU 12039 (Caminicellaceae: 3.5 ± 5.4% in *M. pharensis*), and OTU 2105 (Pseudomonadaceae: 7.3 ± 17.6% in *M. decactis*). Differential abundance for these OTUs was confirmed using DESeq2 pairwise tests (see supplementary table A1). (b) Shannon diversity differed significantly among species (Kruskal–Wallis: $\chi^2 = 40.19$, df = 2, $p < 0.001$, n = 127), with all Wilcoxon post hoc comparisons significant ($p < 0.001$). (c) Principal Coordinates Analysis (PCoA) based on Bray–Curtis dissimilarity revealed clear clustering by species (PERMANOVA: pseudo-F = 13.74, df = 2, $p < 0.001$, n = 127), especially between *M. mirabilis* and *M. pharensis*. (d) Observed richness also differed significantly among species (Kruskal–Wallis: $\chi^2 = 41.13$, $p < 0.001$, n = 127), with *M. mirabilis* displaying significantly lower richness than both *M. decactis* ($p < 0.001$) and *M. pharensis* ($p < 0.001$).

Bacterial community composition and alpha diversity differed significantly among *M. decactis* (n = 45), *M. mirabilis* (n = 46), and *M. pharensis* (n = 36) (Figure 4.8). Alpha diversity was highest in *M. pharensis*, intermediate in *M. decactis*, and lowest in *M. mirabilis*. Shannon diversity differed significantly across species (Kruskal–Wallis: $\chi^2 = 40.19$, df = 2, $p < 0.001$, n = 127), and pairwise tests confirmed significant differences between all species pairs (all $p < 0.001$). Observed richness also varied (Kruskal–Wallis: $\chi^2 = 41.13$, $p < 0.001$, n = 127), with *M. mirabilis* showing significantly lower richness than both *M. decactis* ($p < 0.001$) and *M. pharensis* ($p < 0.001$).

A PCoA showed clear clustering in the bacterial community composition of the three *Madracis* species, with clear clustering particularly between *M. mirabilis* and *M. pharensis* (Figure 4.8c). PERMANOVA based on Bray–Curtis distances confirmed these clusters and revealed significant differences in bacterial community composition among coral species (pseudo-F = 13.74, df = 2, $p < 0.001$, n = 127). Pairwise comparisons indicated dissimilarities between all the species: *M. mirabilis* vs. *M. pharensis* ($p < 0.001$), *M. decactis* vs. *M. mirabilis* ($p < 0.001$) and *M. pharensis* vs. *M. decactis* ($p < 0.001$).

4.2.2 Bacterial communities in bleached and non-bleached *M. pharensis*

Bacterial communities in *M. pharensis* exhibited broadly similar structure between bleached (n = 9) and non-bleached (n = 27) colonies, with overlapping dominant taxa and only subtle shifts in OTU-level composition (Figure 4.9). Alphaproteobacteria was consistently present under both conditions, including OTU 599 (Paracoccaceae; bleached: 12.5 ± 7.8%, non-bleached: 11.6 ± 10.0%), OTU 1876 (Rhizobiaceae; 3.9 ± 2.3% vs. 4.2 ± 2.7%), and OTU 4280 (Caminicellaceae; 7.2 ± 10.5% vs. 3.2 ± 3.5%). Minor differences were observed, such as higher relative abundances of OTUs from Microtrichaceae, Pirellulaceae, and Thermoanaerobaculaceae in bleached colonies, and increased Chlorobiaceae (e.g., OTU 1738: 0.4 ± 0.8% vs. 4.1 ± 11.5%) in non-bleached colonies. However, differential abundance testing using DESeq2 did not identify any significantly different OTUs (padj < 0.05) between bleached and non-bleached samples, suggesting that these patterns reflect variability in dominant taxa rather than systematic shifts in bacterial community composition.

Shannon diversity did not differ significantly between groups (Wilcoxon rank sum test: W = 121, $n_1 = 9$, $n_2 = 27$, $p = 0.103$), nor did observed richness (W = 117, $n_1 = 9$, $n_2 = 27$, $p = 0.210$). PCoA (Figure 4.9c) did not show clear clustering between bleached and non-bleached samples, and this was confirmed by PERMANOVA (pseudo-F = 1.21, df = 2, $p = 0.314$, n = 36).

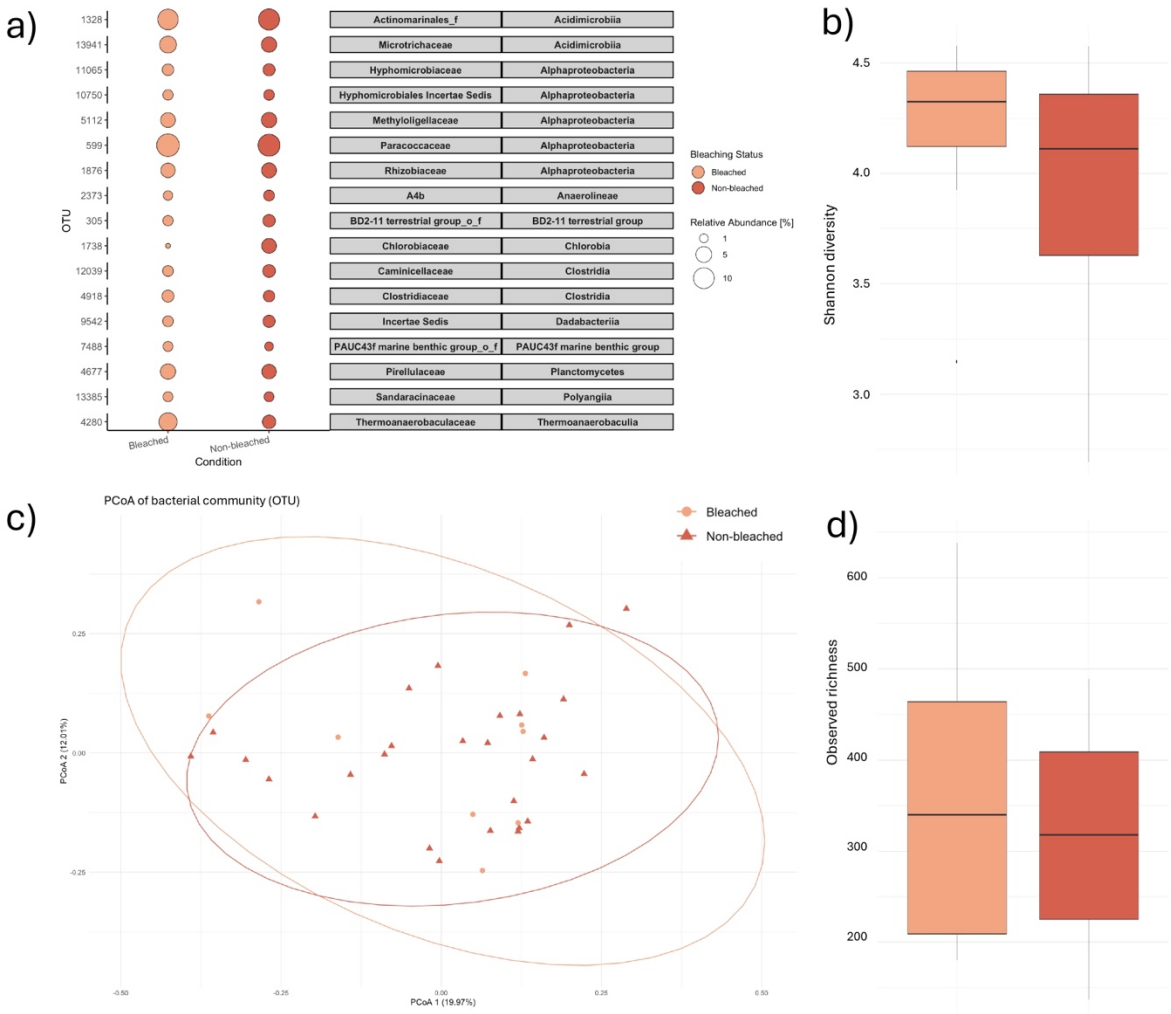

Figure 4.9 Bacterial communities in bleached and non-bleached *M. pharensis* colonies. (a) Relative abundance of the top 17 OTUs, grouped by bacterial family and class. Circle size represents mean abundance (%) across bleached (n = 9, light red) and non-bleached (n = 27, dark red) samples. Dominant OTUs include OTU 599 (Paracoccaceae), OTU 1876 (Rhizobiaceae), and OTU 4280 (Caminicellaceae), all of which were present in both conditions with minor differences in relative abundance. (b) Shannon diversity (Wilcoxon rank sum: W = 121, n_1 = 9, n_2 = 27, p = 0.103) and (d) observed richness (W = 117, n_1 = 9, n_2 = 27, p = 0.210) did not differ significantly between groups. (c) Principal Coordinates Analysis (PCoA) based on Bray–Curtis dissimilarities. Ellipses show 95% confidence intervals. PERMANOVA showed no significant difference in bacterial community composition by bleaching status (pseudo-F = 1.21, df = 2, p = 0.314, n = 36).

4.2.3 Drivers of bacterial communities in *M. mirabilis* and *M. decactis*

Timepoint was the only factor that significantly affected bacterial community composition across all datasets, while transplant treatment also had a significant effect in most cases (PERMANOVA $p < 0.01$; Supplementary figure A6). In contrast, other variables, including colony identity, depth group, Symbiodiniaceae main profile, and ITS2-profile, were not consistent predictors of community structure.

4.2.3.1 *Madracis mirabilis*

Although only one OTU (OTU2979, Cyanobacteriia, Cyanobiaceae) was significantly different across *M. mirabilis* transplant treatments based on the DESeq2 LRT (χ^2 = 27.10, padj = 0.0396), several OTUs showed notable shifts in relative abundance across treatments and depths (Figure 4.10). The significantly affected OTU was not among the most abundant taxa and was therefore not investigated further, as it did not indicate a broader community shift.

Alphaproteobacteria OTUs, particularly from the families Paracoccaceae (OTU599: 29.2% ± 15.2%), Rhizobiaceae (OTU1876: 7.8% ± 6.6%), and Stappiaceae (OTU2420: 3.6% ± 4.3%), remained consistently abundant across all conditions. OTUs affiliated with Clostridiaceae (OTU2373: 1.4% ± 7.3%), Peptostreptococcaceae (OTU7568: 1.3% ± 2.1%), and Lachnospiraceae (OTU5721: 1.1% ± 2.5%) also displayed moderate but stable abundances.

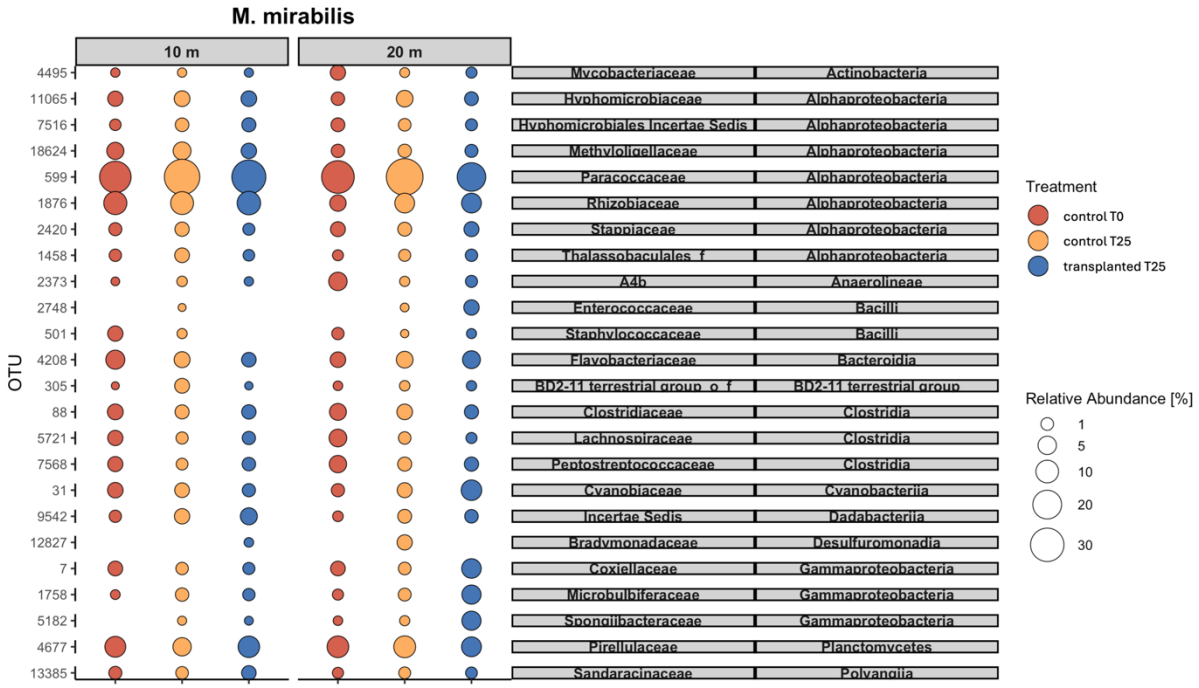

Figure 4.10 Mean relative abundance of the top 10 most abundant bacterial OTUs within each treatment group of *M. mirabilis* across transplant treatments originating from 10 m and 20 m. OTUs are grouped by bacterial family (right) and class (left). Circle size reflects mean relative abundance (%) within each group, colored by treatment: control T0 (red, n = 11), control T25 (orange, n = 6), and transplanted T25 (blue, n = 6). OTU 599 (Paracoccaceae: 29.2% ± 15.2%) was the most dominant.

Interestingly, several Gammaproteobacteria—including OTUs from Coxiellaceae (OTU7), Microbulbiferaceae (OTU1758), and Spongibacteraceae (OTU5182)—showed increased relative abundance in *M. mirabilis* colonies transplanted from 20 to 10 meters.

The mean relative abundance of OTU 7 was 6.2% ± 11.5% in the transplanted group, compared to 2.1% ± 2.6% in the T0 controls and 1.0% ± 1.5% in the T25 controls. Similarly, OTU 1758 increased to 5.4% ± 13.1% in transplants, from 0.2% ± 0.6% (T0) and 0.6% ± 1.1% (T25), and OTU 5182 rose to 5.8% ± 8.8% in transplants compared to 0.1% ± 0.4% (T0) and 0.2% ± 0.6% (T25). While these changes were not statistically significant, they represent notable shifts in average abundance following transplantation.

Shannon diversity did not differ significantly between treatments at either depth (all $p > 0.05$; Supplementary figure A7). However, observed richness increased significantly over time in both depth groups (ANOVA 10 m: $F_{(2,20)} = 9.90$, $p = 0.001$; 20 m; $F_{(2,20)} = 4.80$, $p = 0.020$) (Figure 4.11 a-b).

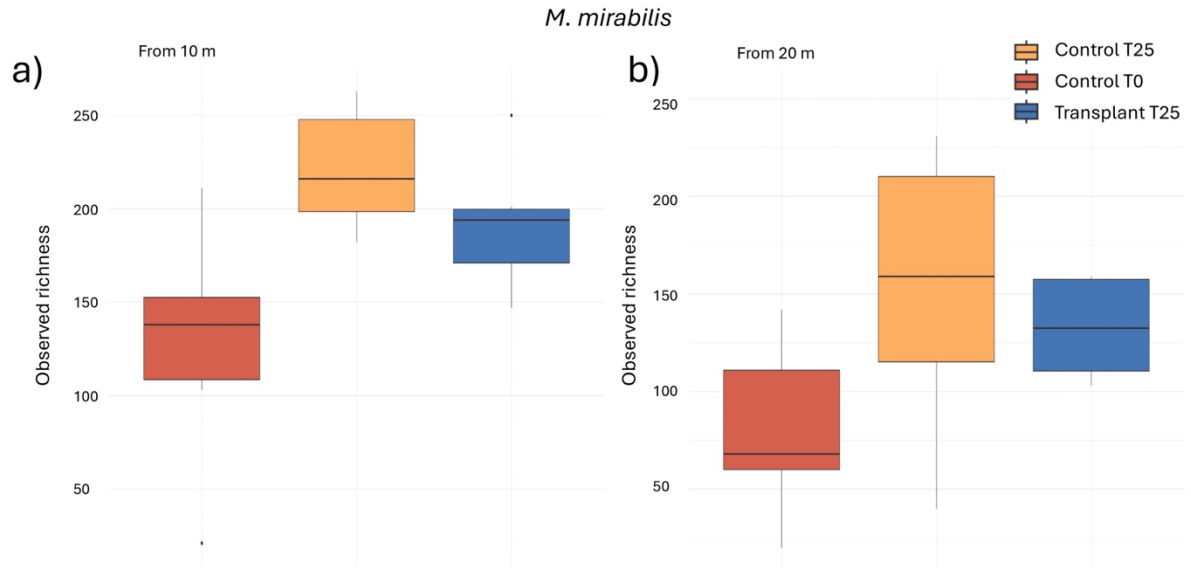

Figure 4.11 Observed richness (number of OTUs) in bacterial communities associated with *M. mirabilis* across transplantation treatments, grouped by depth of origin. (a) Colonies originating from 10 m: control T0 (red, n = 11), control T25 (orange, n = 6), transplant T25 (blue, n = 6). Significant differences in richness were detected (ANOVA: $F_{(2, 20)} = 9.90$, $p = 0.001$). Post hoc Tukey HSD tests showed significantly higher richness in control T25 colonies compared to T0 ($p = 0.0012$), and in transplant T25 colonies compared to T0 ($p = 0.0267$), with no significant difference between the T25 groups ($p = 0.458$). (b) Colonies originating from 20 m: control T0 (red, n = 11), control T25 (orange, n = 6), transplant T25 (blue, n = 6). ANOVA also detected significant differences in richness ($F_{(2, 20)} = 4.80$, $p = 0.020$). Control T25 colonies had significantly higher richness than T0 ($p = 0.041$), while transplant T25 colonies showed marginally higher richness than T0 ($p = 0.057$). No significant difference was observed between the two T25 groups ($p = 0.989$).

PCoA plots suggested mild clustering of bacterial communities by treatment (Figure 4.12a–b). These visual patterns were supported by PERMANOVA at 20 m, which detected a significant effect of treatment (pseudo-F = 1.42, df = 2, $p = 0.017$, n = 23). Pairwise comparisons revealed significant differences between control T0 and transplanted T25 ($p = 0.030$), and between control T25 and transplanted T25 ($p = 0.047$), while no significant difference was observed between control T0 and control T25 ($p =$

0.080). For colonies from 10 m, PERMANOVA did not detect a significant treatment effect (pseudo-F = 1.35, df = 2, p = 0.077, n = 23), despite some visual separation in the PCoA.

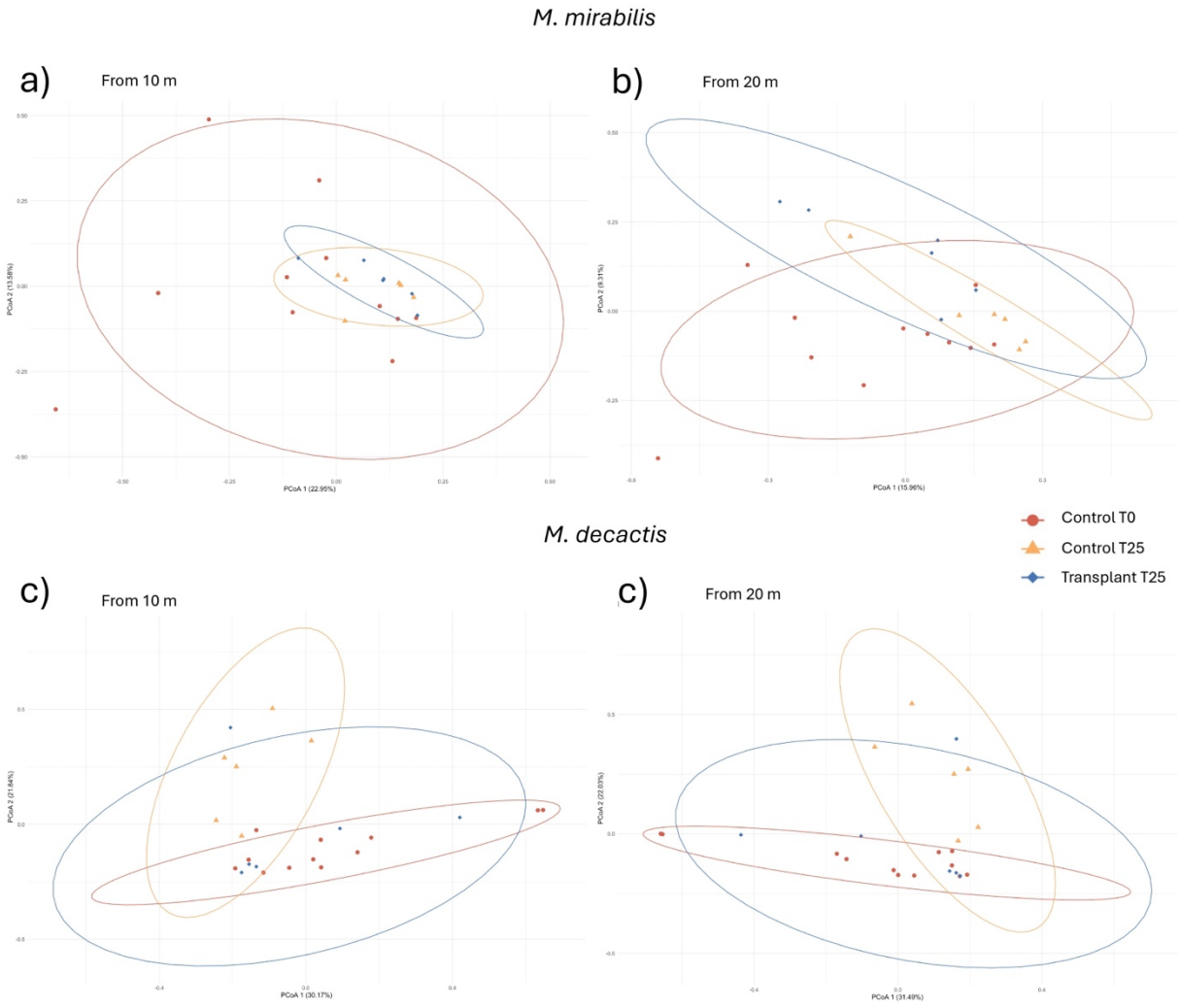

Figure 4.12 Principal Coordinates Analysis (PCoA) of bacterial community composition in *M. mirabilis* and *M. decactis*, based on Bray–Curtis dissimilarities at the OTU level. Samples are grouped by treatment: control T0 (red), control T25 (orange), and transplanted T25 (blue). Ellipses represent 95% confidence intervals. a) *M. mirabilis* from 10 m (n = 11, 6, 6): significant treatment differences were detected (PERMANOVA: pseudo-F = 1.88, df = 2, p = 0.0163, n = 23), with a strong pairwise difference between control T0 and control T25 (p < 0.001); other comparisons were not significant. b) *M. mirabilis* from 20 m (n = 11, 6, 6): bacterial communities differed significantly across treatments (pseudo-F = 1.42, df = 2, p = 0.0174, n = 23), with significant pairwise differences between control T25 and transplant T25 (p = 0.0471), and between control T0 and transplant T25 (p = 0.03); control T0 vs. control T25 was not significant (p = 0.0796). c) *M. decactis* from 10 m (n = 12, 6, 6): PERMANOVA revealed significant differences (pseudo-F = 2.10, df = 2, p = 0.0134, n = 24), driven by a difference between control T0 and control T25 (p < 0.001); other pairwise comparisons were not significant. d) *M. decactis* from 20 m (n = 10, 5, 6): significant treatment differences were also observed (pseudo-F = 1.88, df = 2, p = 0.0163, n = 21), with control T0 differing from control T25 (p = 0.0152); other pairwise comparisons were not significant.

4.2.3.2 *Madracis decactis*

Although a single OTU (OTU124, Gammaproteobacteria, Pseudomonadaceae) was identified as significantly different across *M. decactis* transplant treatments based on the DESeq2 LRT (χ^2 = 42.60, padj < 0.001), no other OTUs showed significant treatment

effects. The significantly affected OTU was not among the dominant taxa and was therefore not explored further, as it did not reflect a broader community-level shift.

Nonetheless, several dominant bacterial taxa were consistently detected across samples (Figure 4.13). Alphaproteobacteria from Paracoccaceae (OTU599: 23.9% ± 19.6%), Rhizobiaceae (OTU1876: 5.1% ± 4.3%), and Stappiaceae (OTU1924: 3.1% ± 4.2%) were present across all treatments and depths. OTU 18624 (Methyloligellaceae: 2.4% ± 2.4%) was also commonly observed regardless of depth. These results suggest that the dominant bacterial taxa associated with *M. decactis* remained relatively stable during the experimental period, with no strong effects of depth or transplant status detected.

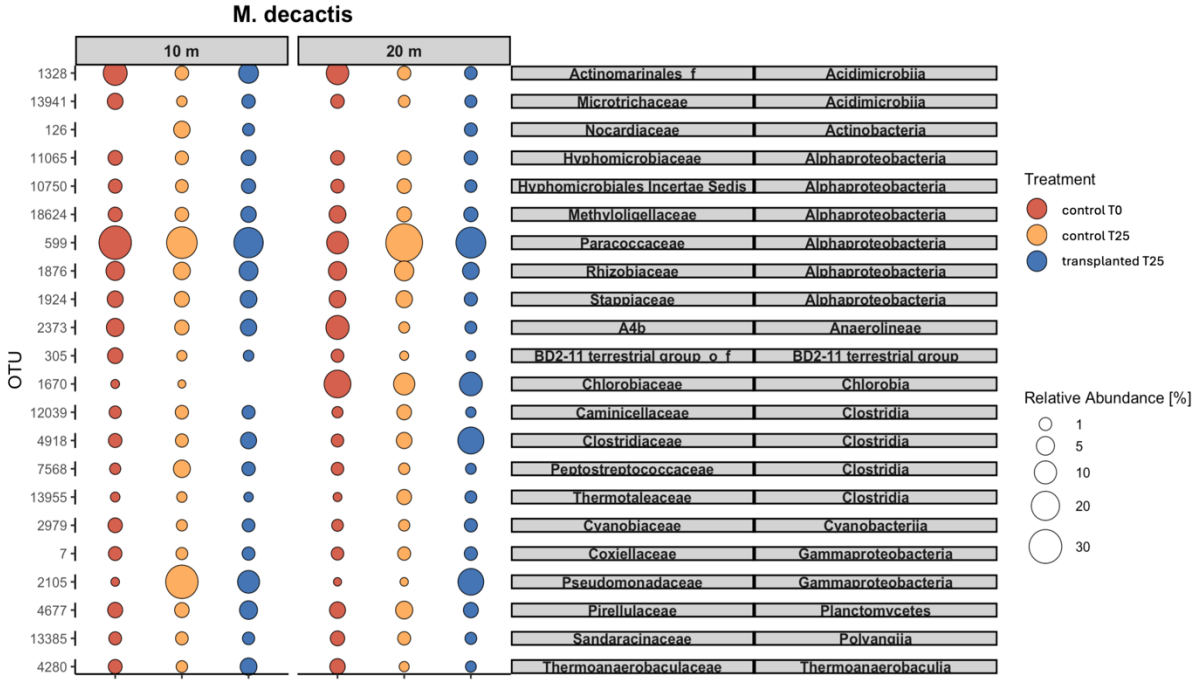

Figure 4.13 Mean relative abundance of the top 10 most abundant bacterial OTUs within each treatment group of *M. decactis* across transplant treatments from 10 m and 20 m. OTUs are grouped by bacterial family (right) and class (left). Circle size reflects mean relative abundance (%) within each group, colored by treatment: control T0 (red, n = 12 for 10 m; n = 10 for 20 m), control T25 (orange, n = 6), and transplanted T25 (blue, n = 6). OTU599 (Paracoccaceae: 23.9% ± 19.6%) and OTU1876 (Rhizobiaceae: 5.1% ± 4.3%) were among the most dominant.

Shannon diversity and observed richness did not differ significantly across treatments at either depth (all $p > 0.05$; Supplementary figures A7, A8). Alpha diversity remained relatively stable regardless of transplant treatment or time. PCoA plots revealed moderate clustering by treatment group at both depths (Figure 4.11c-d). PERMANOVA revealed significant differences among treatments at 10 m (pseudo-F = 2.10, df = 2, $p = 0.013$, n = 24), with pairwise differences between control T0 and control T25 ($p < 0.001$) and not any of the other groups. At 20 m, treatment effects were also

significant (pseudo-F = 1.88, df = 2, p = 0.016, n = 21), with differences between control T0 and T25 colonies (p = 0.015). No other pairwise comparisons were significant.

4.3 Linking microbial communities

4.3.1 Bacterial community across Symbiodiniaceae main profiles

Bacterial community composition in *M. pharensis* varied significantly across Symbiodiniaceae main profiles (B7, B13, B15), with consistent trends in both alpha and beta diversity (Figure 4.14). PCoA analysis revealed clear clustering by profile, especially among B13- and B15-type colonies, with B7 samples displaying broader dispersion. This pattern was confirmed by PERMANOVA, which detected significant differences among groups (PERMANOVA: pseudo-F = 6.38, df = 2, $p < 0.001$, n = 127). Pairwise comparisons further revealed that B13 differed significantly from both B15 ($p < 0.001$) and B7 ($p < 0.001$), while B7 and B15 were not significantly different from each other (p = 0.129).

Alpha diversity patterns mirrored the beta diversity results. Shannon diversity differed significantly among main profiles (Kruskal-Wallis: $\chi^2 = 14.30$, df = 2, $p < 0.001$, n = 127), with pairwise tests indicating significantly higher diversity in B15 than in B13 ($p < 0.001$), and moderate differences between B13 and B7 (p = 0.048) and between B15 and B7 (p = 0.012). Observed richness also varied significantly (Kruskal-Wallis $\chi^2 = 28.00$, df = 2, $p < 0.001$), with higher richness in B15 colonies compared to B13 (p = 0.0027) and B7 ($p < 0.001$). No significant difference in richness was detected between B15 and B7 (p = 0.103).

Bacterial community composition also varied significantly across Symbiodiniaceae main profiles, with 179 OTUs identified as differentially abundant (LRT: padj < 0.05). The 15 most abundant OTUs were visualized in a bubble plot (Figure 4.14a) and further evaluated using DESeq2 pairwise Wald tests (Supplementary table A2). The full set of pairwise comparisons is illustrated in volcano plots (Supplementary figures A9-A11), highlighting OTUs with large fold changes between profiles. Multiple OTUs were enriched ≥ 4-fold in specific profiles, particularly in corals hosting the B13 and B15 types. The strongest differences were observed between profiles B15 and B13, with 112 OTUs enriched in B15 and only 6 in B13. In contrast, profile B7 had 199 OTUs significantly more

abundant than B13, while only 7 OTUs were enriched in B13. Comparisons involving B15 and B7 revealed fewer differentially abundant OTUs, with 9 enriched in B15 and 3 in B7.

Among the most abundant OTUs, several exhibited significant enrichments in specific Symbiodiniaceae profiles. OTU 599 (Paracoccaceae) was most abundant in B13 colonies (29.4 ± 15.3%) and was significantly enriched in B13 compared to both B15 (log_2FC = 3.0, padj < 0.001) and B7 (log_2FC = 2.2, padj = 0.002). Similarly, OTU 4677 (Pirellulaceae) was enriched in B13 relative to B7 (log_2FC = 3.6, padj = 0.005). OTU 1328 (Actinomarinales) and OTU 11065 (Hyphomicrobiaceae) were significantly enriched in B15 compared to B13 (log_2FC = 3.4, padj = 0.001 and log_2FC = 2.7, padj = 0.02, respectively), while OTU 1670 (Stappiaceae) was enriched in B7 relative to B15 (log_2FC = 3.8, padj = 0.007).

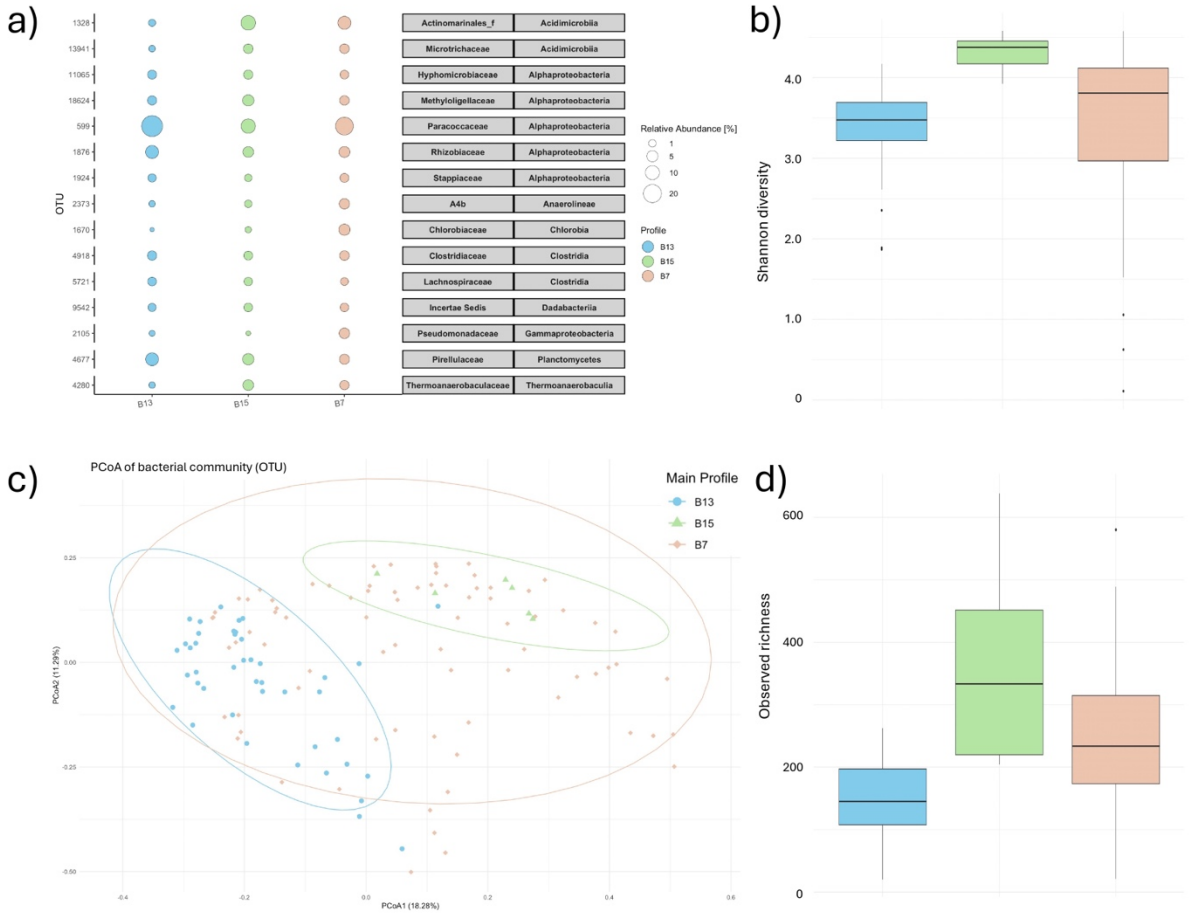

Figure 4.14 Bacterial community structure in *M. pharensis* across Symbiodiniaceae main profiles B13 (blue, n = 45), B15 (green, n = 6), and B7 (pink, n = 77). All analyses shown were performed at the OTU level. (a) Bubble plot showing the relative abundance of the top 15 most abundant OTUs across Symbiodiniaceae main profiles (B13, B15, B7). OTUs are grouped by bacterial class (left) and family (right). Circle size reflects the mean relative abundance (%) per main profile. OTU 599 (Paracoccaceae) was the most abundant across all profiles but peaked in B13 (29.4% ± 15.3%). Other prominent OTUs included OTU 4677 (Pirellulaceae), OTU 1328 (Actinomarinales), and OTU 11065 (Hyphomicrobiaceae), which varied in abundance across profiles. Several of these OTUs were also supported by DESeq2-based pairwise comparisons as significantly enriched in specific profiles (see supplementary table A2). (b) Shannon diversity differed significantly among profiles (Kruskal–Wallis: χ^2 = 14.30, df = 2, p < 0.001, n = 127), with

Wilcoxon post hoc comparisons indicating that diversity was significantly higher in profile B15 compared to the others. (c) Principal Coordinates Analysis (PCoA) based on Bray–Curtis dissimilarity shows clustering by main profile, with ellipses representing 95% confidence intervals. Differences in community composition were confirmed by PERMANOVA (pseudo-F = 6.38, df = 2, $p < 0.001$, n = 127). (d) Observed richness also differed significantly across groups (Kruskal-Wallis: $\chi^2 = 28.00$, df = 2, $p < 0.001$, n = 127), with B15 dominated colonies exhibiting the highest richness.

In addition to differential abundance patterns identified by DESeq2, Indicator Species Analysis (IndVal) revealed OTUs specifically associated with Symbiodiniaceae main profiles, providing complementary insight into host–microbe associations (Supplementary table A3). A total of 21 OTUs exhibited strong indicator values (IndVal ≥ 0.7, $p < 0.05$), including several that were also enriched in DESeq2 analyses. OTU 599 (Paracoccaceae), for instance, was a strong indicator of B13 (IndVal = 0.83, p = 0.001), consistent with its high relative abundance and significant DESeq2 enrichment in B13 colonies. Similarly, OTU 11065 (Hyphomicrobiaceae) showed strong association with B15 (IndVal = 0.72, p = 0.001) and was also significantly enriched in B15 based on DESeq2 results. OTU 1328 (Actinomarinales), another B15 indicator (IndVal = 0.75, p = 0.001), aligned with the DESeq2 enrichment pattern. For B7, OTU 1670 (Stappiaceae) was a strong indicator (IndVal = 0.76, p = 0.001), while OTU 4677 (Pirellulaceae), previously noted as enriched in B13, was also identified as an indicator for this profile (IndVal = 0.74, p = 0.002). These overlapping results reinforce the distinct bacterial signatures associated with each symbiont profile, with B15 exhibiting the largest number of profile-specific indicator taxa.

To explore the relationship between bacterial community composition and Symbiodiniaceae ITS2-profile in more detail, a pairwise PERMANOVA was conducted across all eight ITS2-profile groupings (Supplementary figure A12). The global PERMANOVA showed a significant effect of profile on bacterial community structure (pseudo-F = 2.86, df = 2, $p < 0.001$, n = 127). Pairwise comparisons revealed that samples dominated by the B15d-B15a-B15b-B19bi-B15c-B15e-B15f ITS2-profile differed significantly from all other groups ($p \leq 0.05$). Several additional significant differences were detected, particularly between B13- and B7-associated groupings (e.g., B13/B7-B13a-B13b-B7d-B13c vs. B7-B7d-B7e, $p \leq 0.05$). In contrast, comparisons within B7-type groupings (e.g., B7-B7d-B7e vs. B7-B7f) and within B13-type groupings (e.g., B13/B7-B13a-B13b-B7d-B13c vs. B13a-B13b-B7) were not significant (all $p > 0.05$), suggesting compositional similarity within those clusters.

4.3.2 Host species, and not Symbiodiniaceae shape bacterial community

Host species shaped the bacterial community structure more strongly than Symbiodiniaceae ITS2-profile in *Madracis* corals. A Canonical Correspondence Analysis (CCA) constrained by both factors revealed a significant model (Chi^2 = 0.7293, F = 1.31, p = 0.007), indicating that host species and ITS2-profile together explained a meaningful proportion of community variation (Figure 4.15). Marginal tests showed that host species had a significant effect (Chi^2 = 0.3052, F = 2.76, p = 0.001), whereas ITS2-profile did not (Chi^2 = 0.4394, F = 0.99, p = 0.241). Among the canonical axes, only CCA1 significantly explained variation (Chi^2 = 0.2045, F = 3.30, p = 0.026), while subsequent axes were non-significant (all p > 0.2). The ordination (Figure 4.15) shows clear separation of bacterial communities by the three host species. These results suggest that coral host identity is a stronger driver of bacterial community composition than ITS2-profile.

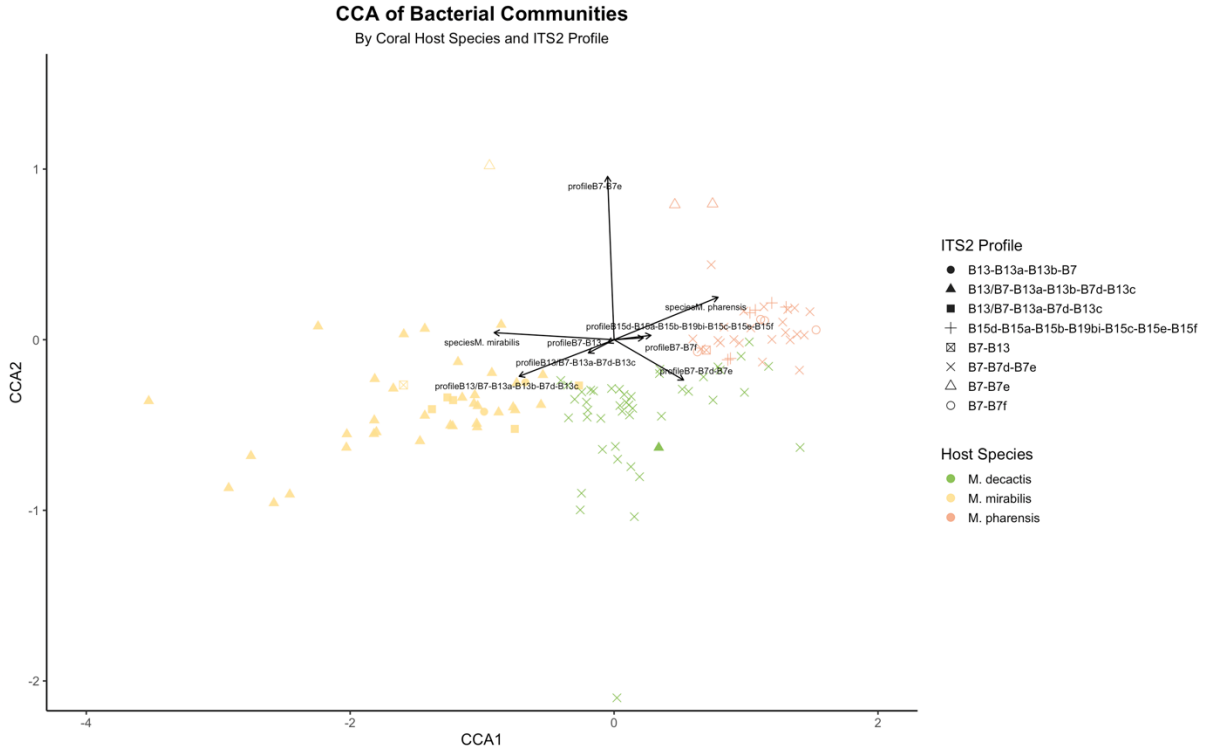

Figure 4.15 Canonical Correspondence Analysis (CCA) of bacterial community composition constrained by coral host species and Symbiodiniaceae ITS2-profile. Analysis at the OTU level. Points are colored by host species (green = *M. decactis* (n = 45), yellow = *M. mirabilis* (n = 46), pink = *M. pharensis* (n = 36)) and shaped by ITS2-profile. Arrows indicate the direction and strength of explanatory variables. CCA1 explained a significant portion of the variation (Chi^2 = 0.2045, F = 3.30, p = 0.026). While species identity had a significant overall effect on bacterial community structure (Chi^2 = 0.2904, F = 2.34, p = 0.001); ITS2-profile did not (Chi^2 = 0.4389, F = 1.01, p = 0.200).

In addition, the influence of Symbiodiniaceae ITS2-profiles and experimental treatment (transplantation or bleaching) on bacterial community composition within each host species was investigated by CCA. Although none of the models were

statistically significant overall, CCA ordinations suggested some visual clustering patterns that were not confirmed by the statistical tests (Supplementary figures A13, A14 and A15).

In *M. mirabilis* (n = 46), bacterial communities showed mild visual clustering across transplant treatments, particularly between control T0 and T25 groups, but the overall model was not significant (Chi^2 = 1.13, F = 0.87, p = 0.543), and no individual axes explained significant variation (CCA1: Chi^2 = 0.23, F = 1.91, p = 0.111) (Supplementary figure A13). Similarly, in *M. pharensis* (n = 36), communities from bleached and non-bleached colonies showed apparent grouping, but this was not supported statistically (Chi^2 = 0.53, F = 1.08, p = 0.255; CCA1: p = 0.168 (Supplementary figure A14).

In contrast, the CCA model for *M. decactis* (n = 45) was not significant overall (Chi^2 = 0.51, F = 1.03, p = 0.091), but permutation tests of individual terms revealed a significant effect of transplant status (Chi^2 = 0.46, F = 1.11, p = 0.005), whereas ITS2-profile had no significant effect (p = 0.804; Supplementary Figure A15). No individual axes explained a significant portion of the variance (e.g., Axis 1: Chi^2 = 0.15, F = 1.78, p = 0.086). However, visual inspection suggested some treatment-related structuring, particularly among transplanted and control T25 colonies from 20 m depth.

4.3.3 Correlations of Symbiodiniaceae and bacterial community

To assess the overall relationship between Symbiodiniaceae and bacterial communities, a Mantel test was first conducted using Bray–Curtis dissimilarities. This revealed a weak but statistically significant correlation across all samples (r = 0.093, p = 0.012, Spearman, 999 permutations; Supplementary figure A16). However, when tested separately by host species, these correlations disappeared: *M. pharensis* (r = 0.026, p = 0.382), *M. mirabilis* (r = –0.134, p = 0.885), and *M. decactis* (r = –0.210, p = 0.982), indicating that the global correlation is likely driven by subtle interspecific patterns rather than consistent within-species coordination between symbiont compartments.

To further explore potential interactions, pairwise Spearman correlations were calculated between ITS2-profiles and bacterial OTUs within each host species. Significant associations were defined by Spearman's ρ > 0.5 and a Benjamini–Hochberg adjusted p-value < 0.05. *M. pharensis* exhibited the highest number of significant OTU/ITS2-profile associations. These were predominantly affiliated with

Alphaproteobacteria, especially Paracoccaceae, and were most strongly linked to profiles A2aw-A2ag-A13 and A1er-A1dh (Supplementary figure A17).

In *M. mirabilis*, fewer but generally stronger correlations were detected, mostly involving the profile A4-A4dk-A4ay and OTUs from diverse bacterial families including Staphylococcaceae, Devosiaceae, Sandaracinaceae, and Spirochaetaceae (Supplementary figure A18a). In *M. decactis*, a similarly low number of significant correlations involved OTUs from Flavobacteriaceae, Halomonadaceae, Arcobacteraceae, and Rhizobiaceae, most strongly associated with profiles A2aw-A2ag-A13 and A3-A3ac. OTU299 showed the highest correlation ($\rho = 0.64$) with profile A3-A3ac (Supplementary figure A18b). Despite the absence of strong overall coordination in the Mantel tests, several ITS2-profiles showed localized associations with specific bacterial taxa.

5 Discussion

This thesis investigated how environmental stressors, specifically changes in light intensity and temperature, shape the microbial communities of reef-building corals, and whether host identity, Symbiodiniaceae composition, or environmental stressors primarily determine bacterial community structure. Utilizing a depth reciprocal transplantation experiment and a natural bleaching event, the thesis assessed: (1) the response of Symbiodiniaceae and bacterial communities to light variation, (2) the impact of thermal bleaching, and (3) the interaction between Symbiodiniaceae and bacterial communities, as well as drivers of bacterial community variation. It was hypothesized that stress exposure would promote shifts toward more tolerant Symbiodiniaceae types, increased abundance of stress-associated bacteria, and that these microbial shifts would reflect underlying associations with host species identity and symbiont type.

The findings demonstrate that both bacterial and Symbiodiniaceae communities are strongly shaped by host species identity. In addition, each microbial group exhibited distinct responses to transplantation and bleaching. Symbiodiniaceae communities primarily shifted in response to bleaching, particularly in terms of dominant types, while transplantation effects were more evident in diversity metrics. Bacterial communities also responded to transplantation, with shifts in composition that varied by host species. Importantly, the experiment started during a period of elevated cumulative heat stress, which may have already altered microbial communities prior to transplantation and thus contributed to the patterns observed (Maher et al., 2020). These changes in microbial communities may help explain how the coral holobiont responds to environmental stress. Such shifts have been suggested as early signs of stress (Bourne et al., 2008; Glasl et al., 2017) and as part of the coral's ability to adapt to changing conditions (van Oppen et al., 2015; Voolstra & Ziegler, 2020).

Overall, these findings underscore the complexity and context-dependence of coral holobiont responses. The flexibility of microbial associations may be central to coral resilience, particularly as climate-driven stress events become more frequent. By simultaneously examining the roles of bleaching, transplantation, and host identity, this study offers insight into the hierarchical drivers of microbial community dynamics under environmental stressors.

5.1 Host specific microbial communities

5.1.1 Host specific Symbiodiniaceae communities

Symbiodiniaceae communities were clearly structured by coral host species, reflecting strong host-specific associations. Each *Madracis* species supported distinct symbiont assemblages, with differences in overall diversity and community structure suggesting species-specific patterns of symbiont flexibility and stability. These results align with previous findings that Symbiodiniaceae communities often exhibit host-specificity, driven by both evolutionary divergence and ecological compatibility (LaJeunesse et al., 2018; Thornhill et al., 2005).

Dominant Symbiodiniaceae ITS2 main profiles also varied systematically by host, though all belonged to the genus *Breviolum*, highlighting host-specific symbiont associations within a single symbiont lineage. *M. mirabilis* was almost exclusively dominated by the B13 type, while *M. pharensis* primarily hosted B7, with a substantial presence of B15. *M. decactis* exhibited a pattern, where B7 remained almost exclusive overall (Figures 4.3, 4.4, and 4.7). These distribution patterns reflect both host identity and depth-related ecological function. For example, Frade et al. (2008b) reported that B7 occurred across all *Madracis* species and depths, functioning as a generalist, while B13 was restricted to the shallow-specialist *M. mirabilis*, and B15 dominated deeper colonies of *M. pharensis*. The widespread presence of B7 in *M. decactis* and *M. pharensis* may indicate a more generalist symbiotic strategy, while B13 dominance in *M. mirabilis* suggests irradiance-driven specialization. Importantly, broader research has shown that certain Symbiodiniaceae types, such as *Durusdinium* (type D1), trade thermal tolerance for reduced nutrient transfer efficiency (Cooper et al., 2011; Stat & Gates, 2011), emphasizing the ecological consequences of symbiont composition. Overall, *Durusdinium* was present at very low abundances across all samples, suggesting that *Madracis* corals may be unable to acquire or maintain this thermotolerant genus even under elevated environmental stress.

These host-specific associations highlight the central role of coral identity in shaping Symbiodiniaceae community structure and, ultimately, holobiont responses to environmental change. The higher symbiont diversity observed in *M. decactis* may indicate greater ecological plasticity, potentially enabling this species to cope more

effectively with fluctuating conditions. In contrast, the lower diversity in *M. mirabilis* may reflect a more specialized but potentially constrained strategy. Such differences are likely rooted in evolutionary relationships and physiological compatibility between host and symbiont (LaJeunesse et al., 2018). Notably, previous studies have shown that cryptic or rare symbionts can contribute to coral resilience by facilitating acclimatization or reorganization under stress (Ziegler et al., 2018). As climate-driven thermal anomalies increase (Hughes et al., 2018), the ability to host flexible or stress-tolerant symbionts may become a key determinant of coral persistence.

5.1.2 Host specific bacterial communities

Bacterial communities also exhibited strong host-specific structuring across the three *Madracis* species. PCoA revealed distinct clustering of bacterial communities by host, supported by significant differences in both alpha and beta diversity (Figure 4.9b, d).

Although several dominant bacterial classes—such as Alphaproteobacteria, Clostridia, and Acidimicrobiia—were shared across *Madracis* species, clear host-specific microbial signatures emerged. These patterns suggest that host identity plays a major role in structuring bacterial communities, with distinct microbial assemblages associated with each species. *M. pharensis* hosted a particularly differentiated microbiome, marked by consistent enrichment of specific taxa not observed in the other two species. Likewise, *M. mirabilis* and *M. decactis* each supported unique bacterial lineages.

These host-specific patterns are consistent with previous studies highlighting the influence of host traits on microbiome composition (Hernandez-Agreda et al., 2016; Pollock et al., 2018). They support the broader understanding that coral-associated microbial communities are shaped not only by environmental factors but also by stable, evolutionarily rooted host–microbe interactions (Voolstra & Ziegler, 2020; Ziegler et al., 2019). These taxon-level differences underscore the role of host identity as a key driver of microbial community structure.

Alpha and beta diversity metrics reinforced these findings. *M. pharensis* exhibited the highest bacterial Shannon diversity and richness, indicating a broader and potentially more flexible microbial repertoire. *M. mirabilis* consistently displayed the lowest diversity, suggesting a more specialized or tightly regulated microbiome, whereas *M.*

decactis showed intermediate diversity. These results, confirmed by PERMANOVA and PCoA, reflect widely reported patterns of phylosymbiosis in corals where microbial communities mirror host evolutionary relationships (Pollock et al., 2018).

Overall, the distinct bacterial communities observed among *Madracis* species underscore the central role of host identity in structuring coral microbiomes. These differences likely contribute to species-specific holobiont responses to environmental stress, including bleaching and transplantation. Recognizing these host-specific microbial baselines is therefore critical for interpreting stress-induced shifts and evaluating coral resilience under climate change.

5.1.3 Co-occurrence patterns between Symbiodiniaceae and Bacteria

Symbiodiniaceae identity was associated with distinct bacterial community patterns, particularly in colonies dominated by B15 and B13 ITS2-profiles. DESeq2 and Indicator Species Analysis both identified OTUs significantly enriched in these profiles, including strong associations of OTUs from Paracoccaceae and Pirellulaceae with B13, and Actinomarinales and Hyphomicrobiaceae with B15. Notably, B15-dominated colonies also harbored the highest number of profile-specific indicator taxa, suggesting a more defined and possibly specialized bacterial assemblage.

However, this apparent specificity may reflect host-driven effects rather than direct symbiont–microbe interactions. B15 was exclusively found in *M. pharensis*, which itself had a distinct bacterial community. Interestingly, when comparing B15 and B7, only a small number of OTUs were significantly different between profiles (Figure A9), despite their contrasting Symbiodiniaceae composition. This limited differentiation further supports the interpretation that bacterial community structure is primarily shaped by host identity, with symbiont profile exerting only minor influence. In contrast, B7 occurred across all host species, and B13 was primarily associated with *M. mirabilis*. These patterns mirror the clustering observed in PCoA plots of bacterial composition by host species and by ITS2-profile (Figures 4.9c and 4.15c, respectively), which show strikingly similar groupings. This suggests that the apparent symbiont-associated microbial differences may instead result from host-specific structuring. Indeed, CCA (Figure 4.16) confirmed that host species, not ITS2-profile, was the primary driver of bacterial community composition when both factors were included in the model.

While Symbiodiniaceae may shape local microbial niches via metabolites such as DMSP or by influencing oxygen gradients, their impact appears secondary to broader host-mediated effects (Rädecker et al., 2015; Vanwonterghem & Webster, 2020). This interpretation aligns with previous research emphasizing host immune traits, skeletal architecture, and metabolic regulation as dominant forces shaping coral microbiomes (Hernandez-Agreda et al., 2016; Vanwonterghem & Webster, 2020; Ziegler et al., 2017). Ultimately, the strong microbial signature associated with B15 likely reflects the distinctiveness of *M. pharensis* as a bacterial host, rather than a uniquely microbiome-shaping role of the B15 symbiont.

OTU-level co-occurrence analysis further supported a host-dominated assembly process. In *M. mirabilis*, the A4.A4dk.A4ay ITS2-profile was associated with bacterial taxa like Gracilibacteria and Dehalococcoidia; however, these associations did not persist across hosts. Similarly, while OTUs from Alphaproteobacteria (especially Paracoccaceae) co-occurred with multiple Symbiodiniaceae profiles in *M. pharensis*, the same symbiont types in *M. decactis* were associated with different bacterial groups. These mismatches highlight the influence of host identity as a strong ecological filter shaping bacterial assemblages, regardless of symbiont identity (Morrow et al., 2022).

A weak association between Symbiodiniaceae and bacterial community composition was detected across all samples, but this relationship did not hold when examined within individual host species. This suggests that the apparent correlation is primarily driven by differences between host species, rather than by consistent co-structuring within hosts. Similar patterns of host-driven microbial compartmentalization have been reported in other coral systems (Voolstra & Ziegler, 2020; Ziegler et al., 2019), highlighting the dominant role of host identity in shaping microbial assemblages over potential symbiont–bacteria interactions.

Importantly, weak correlations at the community level do not preclude meaningful functional interactions at finer biological scales. Matthews et al. (2020) emphasize that specific bacterial taxa may support Symbiodiniaceae functions such as nutrient uptake, oxidative stress mitigation, or metabolite exchange, even in the absence of broad community-level co-variation. Thus, although the findings suggest limited within-host co-structuring, they do not rule out functional dependencies between Symbiodiniaceae and associated bacteria. Emerging models propose that key interactions, such as nitrogen

cycling, reactive oxygen species detoxification, or DMSP breakdown, may underlie critical metabolic co-dependencies within the coral holobiont (Frade et al., 2015; Rädecker et al., 2015; Vanwonterghem & Webster, 2020).

5.2 Microbial response to bleaching

5.2.1 Symbiodiniaceae in bleached and non-bleached corals

Symbiodiniaceae composition differed markedly between bleached and non-bleached *M. pharensis* colonies. All non-bleached colonies were dominated by the B7 ITS2 main profile, while B15 was exclusively found in bleached individuals (Figure 4.7). This raises the question of whether the shift in composition resulted from symbiont shuffling following bleaching, or whether colonies dominated by B15 were more susceptible to thermal stress.

The possibility of post-bleaching symbiont shuffling is supported by several studies that have documented changes in symbiont dominance as corals reorganize their communities in response to thermal stress (Cunning et al., 2018; Ros et al., 2021; Silverstein et al., 2015). In this scenario, the prevalence of B15 in bleached colonies could reflect a stress-induced restructuring rather than pre-existing susceptibility. However, an alternative and perhaps more likely explanation is that symbiont identity influenced bleaching sensitivity from the outset.

Frade et al. (2008b) described B7 as a generalist symbiont broadly distributed across hosts and depths, while B15 was more restricted to deeper habitats associated, assumingly with lower temperatures. Accordingly, B15-dominated colonies may be less capable of withstanding abrupt thermal anomalies. Furthermore, Frade et al. (2008a) reported that both B7 and B15 are naturally present in healthy *M. pharensis*, indicating that these profiles are part of the species' typical symbiotic repertoire rather than acquired opportunistically.

These findings highlight the importance of accounting for host-specific symbiont assemblages and the relative prevalence of stress-tolerant versus sensitive Symbiodiniaceae types when assessing coral bleaching vulnerability. As ocean warming continues to intensify (Rhein et al., 2013), understanding how symbiont identity

influences stress resilience will be critical for predicting coral responses and informing conservation strategies.

5.2.2 Bacteria in bleached and non-bleached corals

Bacterial communities in *M. pharensis* remained compositionally stable under bleaching stress. No significant differences were detected between bleached and non-bleached colonies, indicating a high degree of microbial stability. OTUs from the bacterial families (Paracoccaceae, Methyloligellaceae, Rhizobiaceae, and Hyphomicrobiaceae) were consistently present across both groups. This stability mirrors findings in other coral species, such as *Porites lobata* and *Pocillopora acuta*, where microbial assemblages remained unchanged during bleaching events (Botté et al., 2022; Hadaidi et al., 2017).

Notably, stress-associated bacterial orders including Vibrionales, Rhodobacterales, and Flavobacteriales, were not dominant in bleached colonies. These taxa are often linked to microbial dysbiosis and coral stress responses (Bourne et al., 2008; McDevitt-Irwin et al., 2017; Mouchka et al., 2010), and their absence suggests that bleaching in *M. pharensis* did not trigger acute microbial destabilization. Instead, this species may maintain a host-regulated microbiome capable of buffering moderate environmental stress.

Two persistently detected families, Rhizobiaceae and Paracoccaceae, belong to the order Rhizobiales, which has been associated with stress-related shifts in other coral microbiomes (McDevitt-Irwin et al., 2017). While their presence here does not indicate dysbiosis per se, it may reflect a subtle background signal of physiological stress consistent with elevated environmental pressures during the bleaching period.

Recent studies have demonstrated that shifts in microbial communities can occur prior to visible signs of coral bleaching, underscoring their value as early indicators of stress (McDevitt-Irwin et al., 2017; Ziegler et al., 2017). Supporting this, microbial restructuring often precedes macroscopic symptoms such as tissue paling or necrosis (Thompson et al., 2015; Lee et al., 2016). Consequently, the apparent stability of microbial communities in *M. pharensis* does not necessarily indicate the absence of stress, but rather suggests that both bleached and non-bleached colonies may have experienced similarly stressful conditions even if only some showed visible bleaching.

Importantly, compositional stability does not preclude functional changes. Previous studies have documented that microbial communities may remain taxonomically stable while undergoing shifts in gene expression, such as upregulation of virulence or stress-response genes within genera like *Vibrio* (Littman et al., 2011; Thurber et al., 2009). This highlights the need to consider functional as well as taxonomic metrics when evaluating coral health and microbial dynamics under stress.

The microbial stability observed in *M. pharensis* aligns with species-specific patterns reported by Ziegler et al. (2019), who found that coral species exhibit divergent microbiome responses to transplantation stress. For example, *Acropora hemprichii* showed substantial restructuring, while *Pocillopora verrucosa* maintained a stable microbiome. In this context, the inert microbial response in *M. pharensis* may reflect a tightly regulated or inherently stable microbial community shaped by host traits rather than environmental stressors.

5.2.3 Co-occurrence during bleaching

Neither bleaching status, Symbiodiniaceae ITS2-profile, nor depth significantly explained bacterial community composition in *M. pharensis*. These findings suggest that bacterial community structure in this species is not strongly influenced by symbiont identity or bleaching condition. Instead, it is likely shaped by host-intrinsic factors or stable microhabitat features that buffer against external stressors. This interpretation aligns with previous studies highlighting the dominant role of host physiology and internal regulation in structuring coral-associated microbiomes (Hernandez-Agreda et al., 2017; Voolstra & Ziegler, 2020).

5.3 Host driven responses to environmental change

Comparing *M. mirabilis* and *M. decactis* under identical experimental conditions revealed species-specific microbial dynamics. The contrasting microbial responses observed in the two species, suggest a strong role for host identity in shaping microbiome dynamics under environmental variability. Although both species experienced changes in environmental conditions, including fluctuating irradiance and a reduction in thermal stress over time, their microbial communities responded in both similar and different ways. Together, these results support the idea that coral host species exert a strong

influence over microbiome structure and response potential. While environmental conditions clearly shape microbial assemblages, the extent and nature of these responses appear to be filtered through host-specific traits.

5.3.1 Symbiodiniaceae response in *M. mirabilis*

The Symbiodiniaceae community in *M. mirabilis* exhibited limited compositional change following transplantation. No distinct clustering was observed between control and transplanted colonies, and the dominant symbiont type (B13) remained consistently prevalent, with slightly higher occurrence at timepoint 25 (T25) compared to timepoint 0 (T0). In addition, Shannon diversity increased at T25, suggesting a modest temporal shift in community complexity despite the stability in dominant symbiont composition. This pattern indicates that while the primary symbiont was retained, the overall diversity of the community increased slightly over time.

The absence of major restructuring underscores the role of host-mediated filtering in shaping symbiont assemblages, consistent with studies emphasizing coral host identity as a key determinant of Symbiodiniaceae composition (Cunning et al., 2018; LaJeunesse et al., 2018; Thornhill et al., 2005). While some coral species exhibit symbiont shuffling in response to environmental stress (e.g., *Montastraea cavernosa*; Silverstein et al., 2015), the apparent stability in *M. mirabilis* suggests an inherently stable symbiotic partnership that persists across environmental shifts.

The observed increase in Shannon diversity at T25 may reflect easing thermal stress rather than a direct effect of transplantation. Between November 16th and December 12th, 2023, NOAA Coral Reef Watch data showed a decline in Degree Heating Weeks (DHW) from 20 to 16 and a reduction in bleaching alert level from "Alert Level" to "Watch" (NOAA, n.d.; Figure 5.1). Given that the maximum monthly mean (MMM) sea surface temperature (SST) around Aruba, Bonaire, and Curaçao is approximately 28 °C, and that bleaching thresholds are exceeded with even a 1 °C increase, a small drop in

temperature (~1 °C) can substantially alleviate physiological stress in corals (Figure 5.1).

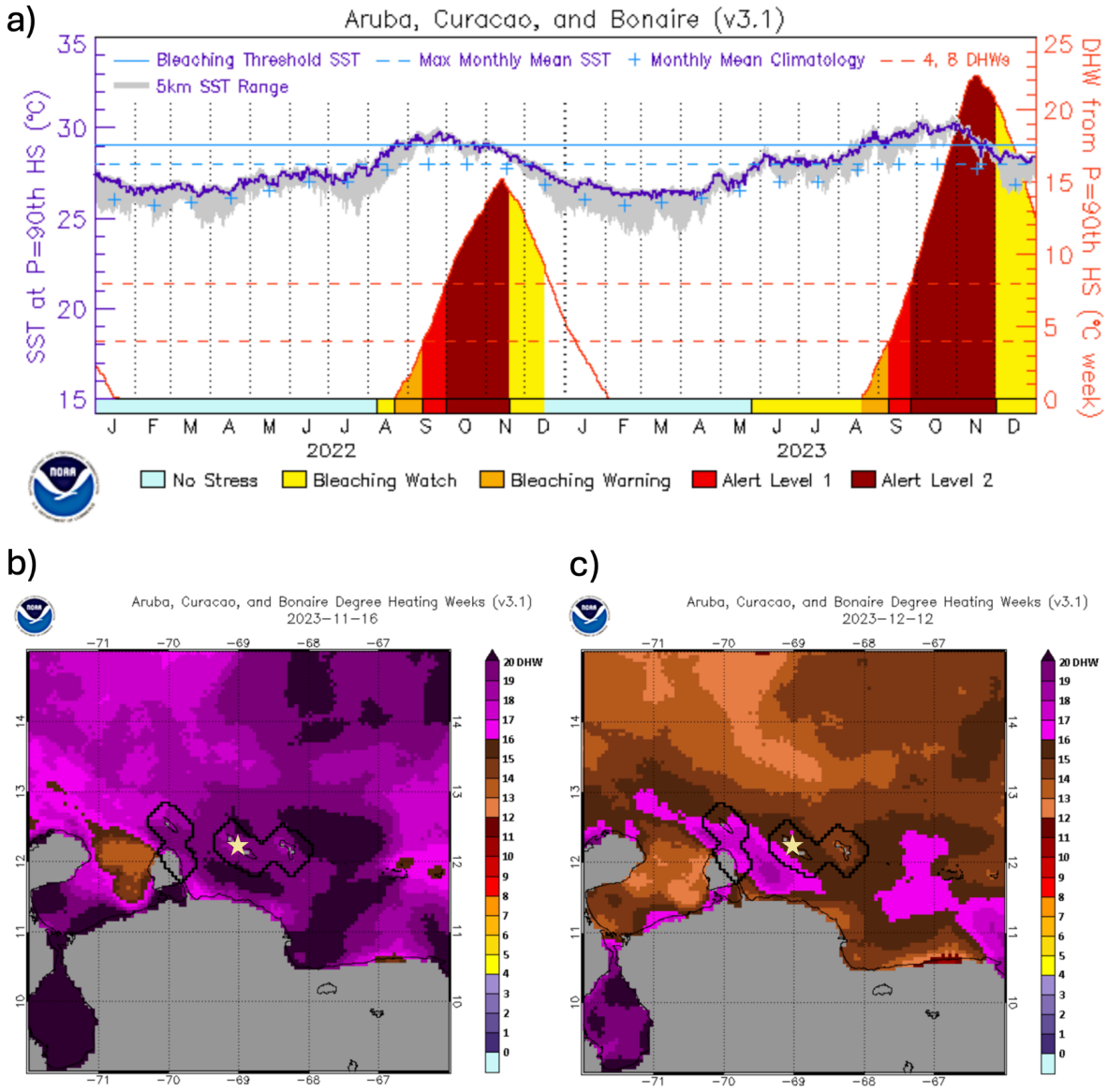

Figure 5.1 a) Sea surface temperature (SST) and Degree Heating Weeks (DHW) for the southern Caribbean (Aruba, Curaçao, and Bonaire), based on NOAA Coral Reef Watch (v3.1) data from January 2022 to December 2023 (NOAA, n.d). Time-series of daily SST at the 90th percentile hotspot (purple line) with the 5 km SST range shaded in gray. The maximum monthly mean (MMM), the bleaching threshold (MMM +1°C), and climatological SST are indicated with horizontal lines. Background colors represent thermal stress alert levels, and the red line (right y-axis) shows cumulative DHW, peaking at Alert Level 2 in late 2023 before declining. (b–c) Spatial DHW maps for November 16th (b) and December 12th (c), 2023, show a marked decline in thermal stress across the region, with DHW decreasing from ~20 to ~16 in core reef zones. These patterns indicate a regional easing of thermal stress in late 2023, which may have supported subtle symbiont community adjustments, as reflected in elevated alpha diversity measures observed during this period. The yellow star shows the location of Curaçao.

This subtle relaxation of thermal pressure may have facilitated early-stage reorganization of the Symbiodiniaceae community. While elevated diversity has sometimes been associated with stress-induced instability (Howe-Kerr et al., 2020), it can also reflect transient increases in background or rare types as conditions stabilize

(Ziegler et al., 2018). Therefore, the diversity increase observed at T25 may indicate a temporary expansion of community complexity during recovery, rather than long-term compositional turnover driven by transplantation alone.

5.3.2 Symbiodiniaceae response in *M. decactis*

In *M. decactis*, subtle but consistent shifts in Symbiodiniaceae community composition were observed over time, regardless of transplantation treatment. While B7 remained the dominant symbiont in most colonies, one colony displayed a shift toward B13 dominance at the later timepoint (T25). Additionally, Shannon diversity showed a declining trend over time, with a noticeable decrease from timepoint T0 to T25.

Although B13 is not directly linked to thermal tolerance, it has been more frequently observed in shallow-water coral communities exposed to higher irradiance levels (Frade et al., 2008b). In this context, the small but parallel increase in B13 across both species may reflect a mild, post-stress adjustment in symbiont composition—potentially favoring types better suited to elevated light or temperature conditions. Notably, B13 is not typically dominant in *M. decactis*, making its increased presence in this species particularly interesting (Frade et al., 2008b). While the observed shifts were subtle and did not resemble the large-scale symbiont turnover documented in studies involving *Durusdinium* following bleaching events (Silverstein et al., 2015; Cunning et al., 2018), the consistent direction of change may indicate the early stages of community restructuring in response to recent environmental stress.

In general, richness remained stable, but differences in Shannon diversity were detected. While not statistically significant, Shannon diversity tended to decrease over time in *M. decactis*, in contrast to an increasing trend observed in *M. mirabilis*. This divergence points to species-specific responses to shared environmental shifts, reinforcing findings that microbial and symbiont plasticity can vary significantly between coral taxa (Ziegler et al., 2019; Ros et al., 2021).

Overall, these results suggest that even moderate environmental change can prompt subtle reorganization of Symbiodiniaceae communities, independent of direct transplantation effects. However, the absence of clear community clustering across treatments reinforces the conclusion that host identity remains the primary determinant of symbiont composition in *M. decactis* (LaJeunesse et al., 2018; Thornhill et al., 2005).

5.3.3 Bacterial response in *M. mirabilis*

Transplantation from 20 m to 10 m induced subtle shifts in the bacterial community composition of *M. mirabilis*, suggesting that upward relocation—alongside a roughly twofold increase in light intensity—elicited a mild stress response within the holobiont. Similar environmentally driven microbial shifts have been observed in other coral transplantation studies, supporting the idea that coral microbiomes can rapidly adjust to changing conditions (Voolstra & Ziegler, 2020; Ziegler et al., 2017; Ziegler et al., 2019).

PERMANOVA detected significant treatment effects in colonies originating from 20 m, with transplanted samples differing from both control groups, which did not differ significantly from each other. In contrast, no significant treatment effect was observed in colonies from 10 m. These results indicate that upward transplantation, drove microbial restructuring for corals originating from 20 m. This restructuring was accompanied by increased relative abundance of several Gammaproteobacteria OTUs, including members of Coxiellaceae, Microbulbiferaceae, and Spongibacteraceae. Although not statistically significant by DESeq2, their consistent enrichment in transplanted colonies supports a biologically relevant pattern. Gammaproteobacteria include both beneficial and opportunistic taxa and are known to respond to stress or environmental disturbance (McDevitt-Irwin et al., 2017; Pogoreutz et al., 2018). Their increase may reflect microbial adjustments to elevated light or temperature fluctuations, consistent with the coral probiotic hypothesis, which posits that microbiome flexibility aids holobiont acclimatization (Reshef et al., 2006; Ziegler et al., 2020).

All enriched Gammaproteobacteria OTUs were also present in control samples, indicating microbial "shuffling" rather than recruitment of novel taxa (Ziegler et al., 2017). This supports the view that *M. mirabilis* hosts a flexible microbial repertoire that can shift relative abundances without altering core membership. In contrast, key Alphaproteobacteria (e.g., Paracoccaceae, Rhizobiaceae, Stappiaceae) and Clostridia (e.g., Clostridiaceae, Lachnospiraceae) remained stable across treatments, reflecting a conserved bacterial core as reported in other coral species (Hernandez-Agreda et al., 2017).

Bacterial richness also increased over time, regardless of transplantation treatment or depth, suggesting that easing thermal stress—rather than transplantation—

was the primary driver of this trend. Between November and December 2023, NOAA data showed a decline in DHW and a reduction in bleaching alert level, indicating a broader environmental recovery (NOAA, n.d.). This pattern mirrors findings in *Acropora* and *Porites*, where richness increased following thermal stress as part of early-stage microbiome reorganization (Maher et al., 2020). Together, these results suggest that *M. mirabilis* maintains a resilient and responsive microbial community, capable of adjusting to changing environmental conditions through internal restructuring rather than community replacement.

5.3.4 Bacterial response in *M. decactis*

Bacterial communities in *M. decactis* remained relatively stable over the course of the experiment, with no significant changes in alpha diversity across treatments or timepoints. This indicates that microbial richness was not strongly affected by either transplantation or temporal factors. Beta diversity analyses did reveal some shifts in community composition—particularly between control T0 and control T25 samples at both 10 m and 20 m. However, because treatment and time were confounded in the PERMANOVA design, the exact causes of these changes could not be determined. Overall, the bacterial community response was consistent across depths and did not clearly reflect a transplantation effect.

Only one OTU showed statistically significant differential abundance across treatment groups, although a few displayed depth- or timepoint-restricted patterns. While these patterns may reflect sensitivity to environmental factors like light or temperature, the lack of consistent statistical support limits strong interpretation. Core taxa from Alphaproteobacteria and Clostridia remained stable, highlighting a conserved microbial backbone in *M. decactis* (Hernandez-Agreda et al., 2017).

Unlike *M. mirabilis*, which showed signs of microbial flexibility in response to light and temperature shifts, *M. decactis* maintained a relatively conservative microbiome structure. This is consistent with patterns observed in *Pocillopora*, where microbial richness remained low and community composition stable across stress gradients (Maher et al., 2020). Together, these findings suggest that *M. decactis* may rely on a tightly regulated, host-filtered microbiome that resists compositional disruption even under changing environmental conditions.

5.3.5 Co-occurrence patterns in *M. mirabilis and M. decactis*

CCA revealed weak or non-significant effects of transplantation status and Symbiodiniaceae ITS2-profile on bacterial community structure in both *M. mirabilis* and *M. decactis*. In *M. mirabilis*, the ordination showed no clear separation of groups, suggesting that neither transplantation nor symbiont identity played a strong role in shaping microbial communities. This supports earlier observations that bacterial communities in *M. mirabilis* remained compositionally stable across treatments, with only modest changes in the relative abundance of certain taxa—such as Gammaproteobacteria, following upward transplantation. These shifts did not amount to broad community restructuring and were not clearly distinguishable in ordination space, reinforcing the interpretation of a resilient and host-regulated microbiome.

In *M. decactis*, the CCA ordination suggested slightly more apparent separation between treatment groups, particularly between transplanted and non-transplanted colonies at 20 m. However, these patterns were weak and not strongly supported overall. As in *M. mirabilis*, symbiont profile had no clear influence on bacterial community structure, indicating a decoupling of bacterial and Symbiodiniaceae community dynamics.

Together, these findings suggest that bacterial communities in both species were primarily structured by host identity and internal regulatory mechanisms, rather than short-term environmental change or symbiont composition. This aligns with previous work highlighting the dominant role of host factors—such as immune filtering or stable physicochemical niches—in shaping coral-associated microbiomes (Hernandez-Agreda et al., 2017; Grottoli et al., 2018). While subtle microbial shifts may occur in response to stress or recovery, their overall impact on community composition appears limited within the timeframe of this experiment.

5.4 Limitations and future directions

While this study provides a comparative view of coral holobiont responses across host species and environmental stressors, some methodological constraints may have limited the resolution of some findings. One key limitation is the use of OTU (Operational Taxonomic Unit)-based analysis for bacterial communities, which may obscure fine-

scale variation that could be resolved using ASV (Amplicon Sequence Variant)-based approaches. ASVs represent exact biological sequences and can distinguish variants differing by as little as one nucleotide, offering higher taxonomic resolution than traditional OTU clustering (Callahan et al., 2017). This becomes particularly relevant when attempting to detect subtle co-occurrence patterns between specific bacterial taxa and Symbiodiniaceae types.

A second limitation stems from the DNA extraction protocol, which was based on whole coral tissue slurries without physically separating Symbiodiniaceae cells from host tissue. This likely reduced the ability to determine whether bacterial taxa were specifically associated with the host or the algal symbionts, as microbial signals from both compartments were combined. To address this, future studies could perform parallel DNA extractions targeting separated host and symbiont fractions, ideally alongside a bulk holobiont extraction from the same colony. Physical separation can be achieved using differential centrifugation or airbrush-based tissue disruption followed by fractionation, as demonstrated in recent coral metabolomics protocols (Matthews et al., 2023). In addition, while 16S rRNA gene sequencing is a powerful tool for characterizing microbial taxonomic diversity, it provides limited insight into the functional capabilities of microbial communities. Closely related taxa often differ in gene content, and similar functions can be encoded by phylogenetically distant lineages, meaning that taxonomic composition may not reliably reflect metabolic potential (Louca et al., 2016). Future work incorporating metagenomics or metatranscriptomics would therefore be valuable for resolving functional differences that are not detectable using 16S-based approaches.

In addition to improving microbial resolution, bleaching-related dynamics would benefit from time-series sampling across different stages of stress—before, during, and after bleaching—to determine whether observed symbiont shifts reflect stable tolerance or transient stress-induced responses. Furthermore, increased temporal replication for *M. mirabilis* and *M. decactis* would help clarify whether the subtle bacterial changes observed in this study represent consistent thermal responses or short-term variability. More broadly, continued investigation into coral holobiont structure and function remains essential for understanding reef resilience. Elucidating how microbial communities interact with host identity and symbiont composition under changing environmental conditions will be key to predicting coral responses in a warming ocean.

6 Conclusion

This thesis investigated how microbial communities in three *Madracis* coral species respond to environmental stressors, with a focus on the hierarchical roles of host identity, Symbiodiniaceae composition, and environmental conditions. Using high-throughput sequencing of Symbiodiniaceae ITS2 and full-length bacterial 16S rRNA genes, it characterized shifts in microbial structure, diversity during a reciprocal depth transplantation experiment and a natural bleaching event.

By jointly analyzing bacterial and Symbiodiniaceae communities, this thesis offers an integrated perspective on coral holobiont responses to distinct stress scenarios. Host identity emerged as the strongest predictor of microbial structure across species. Although Symbiodiniaceae main profiles were associated with bacterial community patterns, their effects were closely tied to host identity and did not independently shape microbiome composition. Notably, *M. mirabilis* and *M. decactis* exhibited contrasting microbial responses under similar environmental conditions, while *M. pharensis* showed clear differences in dominant Symbiodiniaceae types between bleached and non-bleached colonies. These findings highlight the role of host traits in governing holobiont stability and reveal species-specific flexibility in response to environmental stress.

These results support a hierarchical model of coral holobiont organization, wherein host species provide the foundational template for microbial community assembly, and environmental factors, act as modulators that fine-tune symbiont composition and abundance. While the potential for microbial flexibility exists, particularly in certain bacterial taxa, this flexibility appears bounded by host regulatory mechanisms and may vary considerably among coral species.

As climate change increases the frequency and severity of stress events on coral reefs, understanding the interplay between host traits, microbial dynamics, and environmental conditions will be critical for predicting coral resilience. This thesis contributes to that understanding and future research integrating functional gene profiling, longer-term monitoring, and broader taxonomic sampling will be essential to fully unravel the complex, multi-partner interactions that define coral holobiont responses under global change.

Appendix A

Supplementary figures

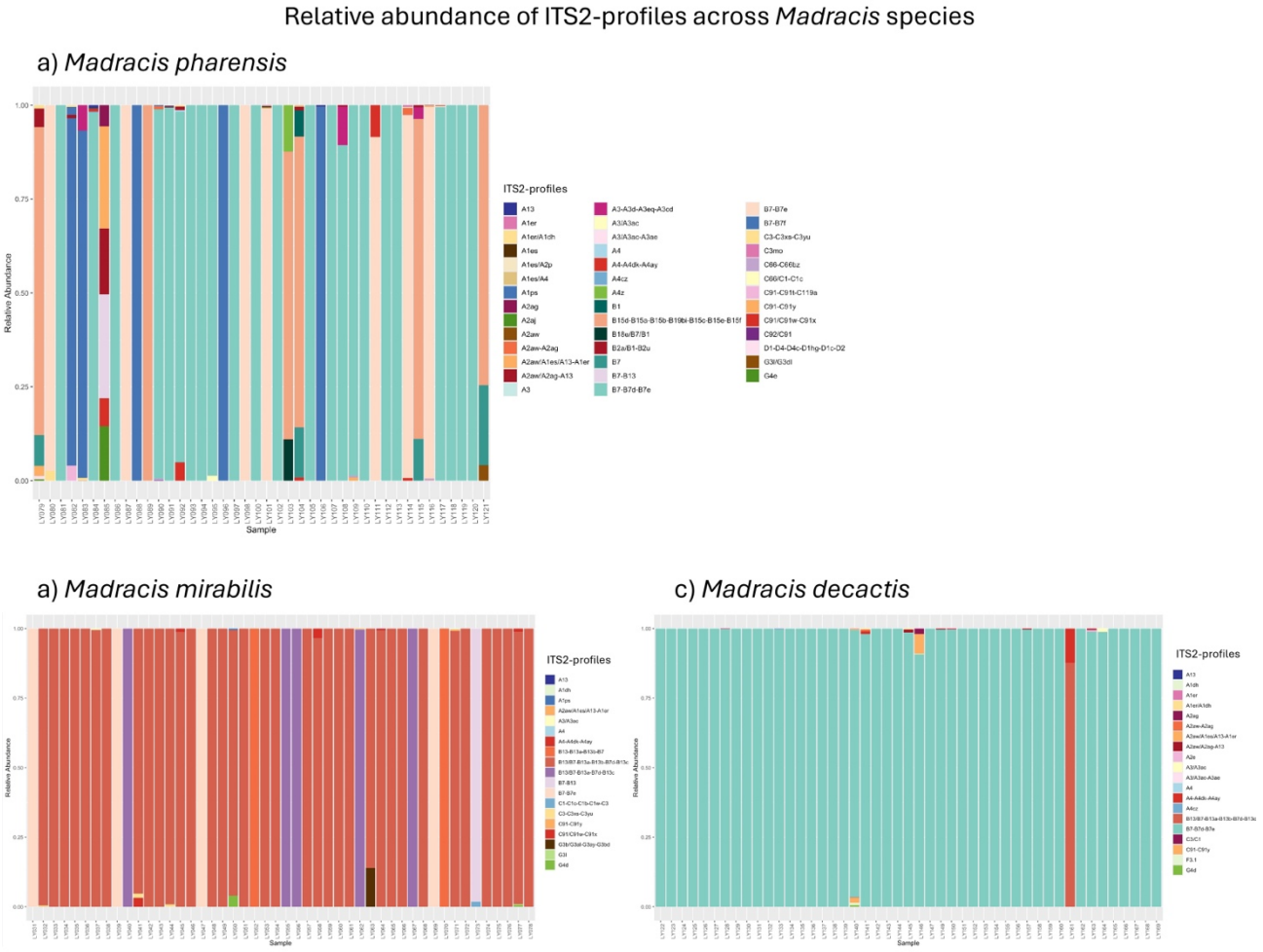

Figure A1 Relative abundance of the top 10 most abundant ITS2-profiles per sample across three *Madracis* species. Each bar represents the proportional contribution of ITS2-profiles within a single coral colony. (a) *M. pharensis* showed high ITS2-profile diversity, with multiple co-dominant profiles present across samples. (b) *M. mirabilis* colonies were predominantly dominated by a single B13-type profile. (c) *M. decactis* samples were also largely dominated by a single ITS2-profile.

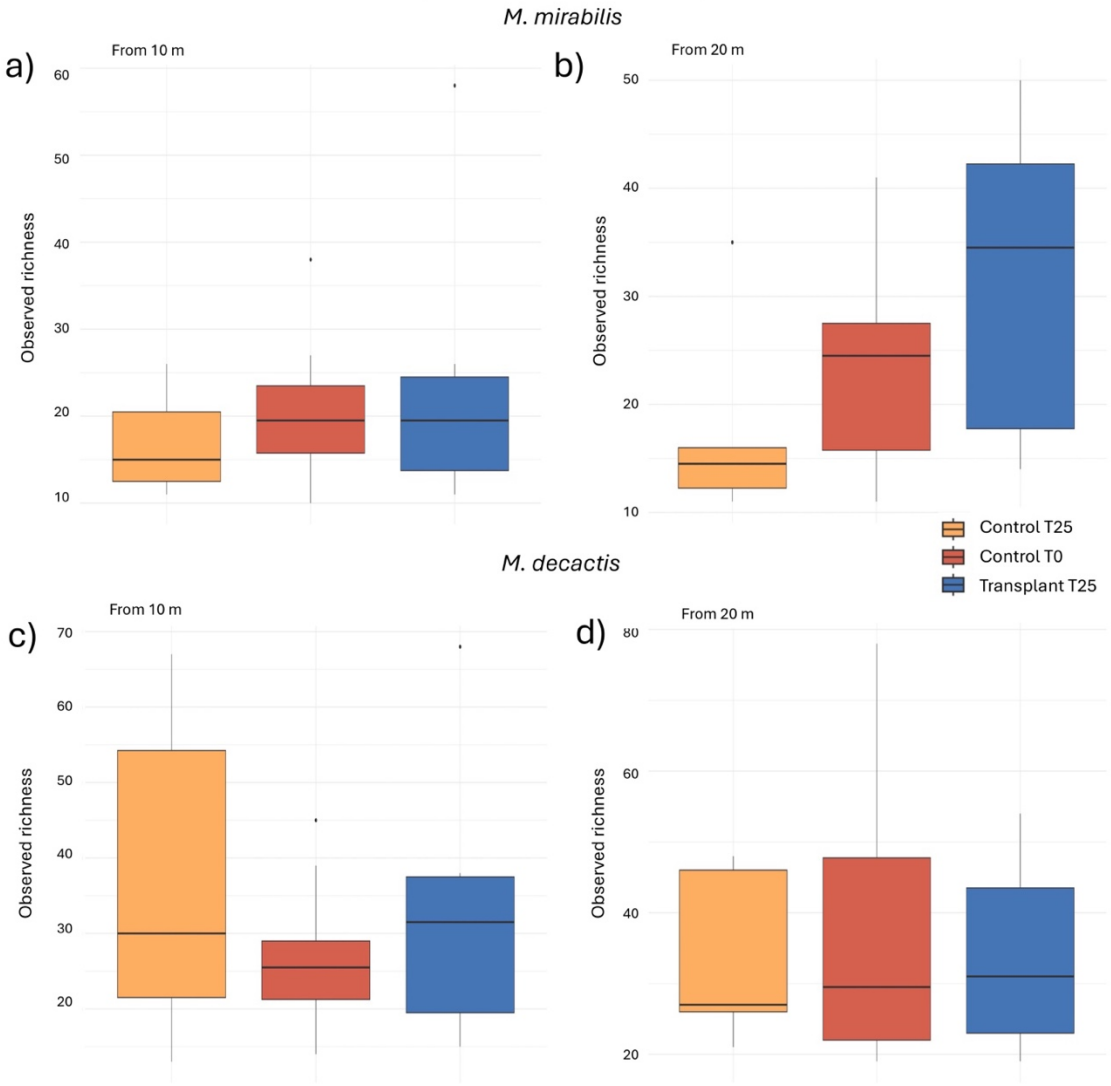

Figure A2 Observed richness of Symbiodiniaceae communities across transplant treatments. All analyses were performed at the DIV level. (a) *M. mirabilis* (10 m): No significant differences in richness (Kruskal–Wallis: $\chi^2 = 0.816$, df = 2, p = 0.665, n = 24). (b) *M. mirabilis* (20 m): Richness did not differ significantly (Kruskal–Wallis: $\chi^2 = 4.142$, df = 2, p = 0.126, n = 24). (c) M. decactis (10 m): No significant differences (Kruskal–Wallis: $\chi^2 = 0.702$, df = 2, p = 0.704, n = 24). (d) *M. decactis* (20 m): No significant differences (Kruskal–Wallis: $\chi^2 = 0.027$, df = 2, p = 0.987, n = 23).

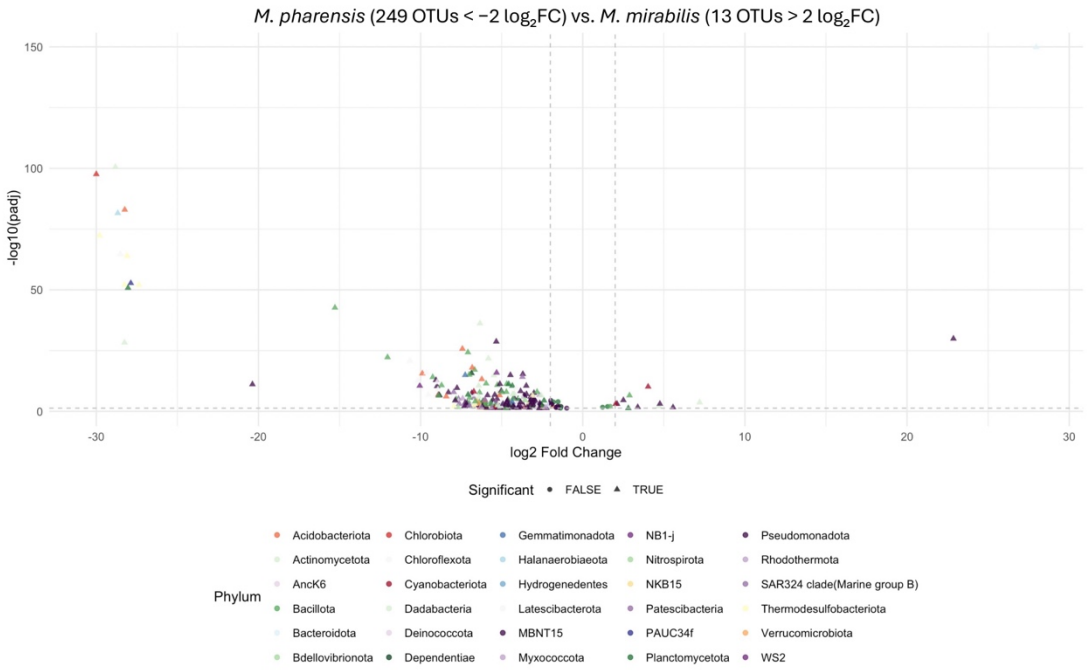

Figure A3 Differentially abundant bacterial OTUs between *M. pharensis* and *M. mirabilis* based on DESeq2 Wald test results. The volcano plot shows $\log_2$ fold changes in OTU abundance (x-axis) versus $-\log_{10}$ adjusted p-values (y-axis). Each point represents an OTU, with triangles indicating significant differences (padj < 0.05) and colors corresponding to bacterial phyla. Vertical dashed lines mark ±2 $\log_2$ fold change (4×increase), and the horizontal line marks the adjusted p = 0.05 threshold. The comparison revealed 249 OTUs significantly more abundant in *M. pharensis* ($\log_2$FC < −2) and 13 OTUs more abundant in *M. mirabilis* ($\log_2$FC > 2).

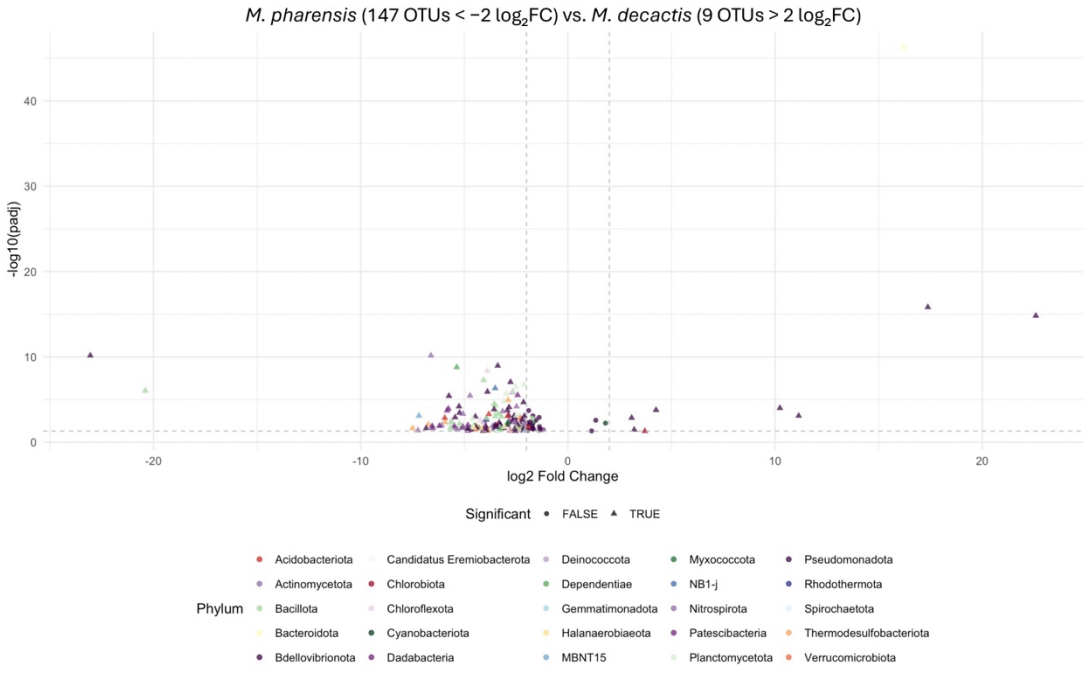

Figure A4 Differentially abundant bacterial OTUs between *M. pharensis* and *M. decactis* based on DESeq2 Wald test results. The volcano plot shows $\log_2$ fold changes in OTU abundance (x-axis) versus $-\log_{10}$ adjusted p-values (y-axis). Each point represents an OTU, with triangles indicating significant differences (padj < 0.05) and colors corresponding to bacterial phyla. Vertical dashed lines mark ±2 $\log_2$ fold change (4×increase), and the horizontal line marks the adjusted p = 0.05 threshold. The comparison revealed 147 OTUs significantly more abundant in *M. pharensis* ($\log_2$FC < −2) and 9 OTUs more abundant in *M. decactis* ($\log_2$FC > 2).

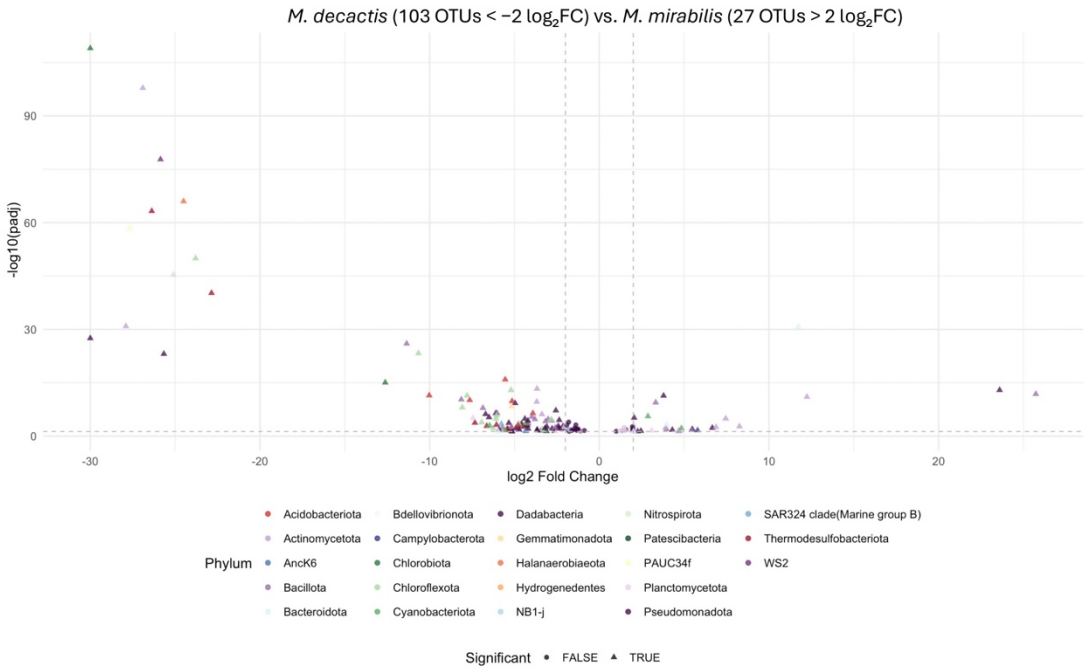

Figure A5 Differentially abundant bacterial OTUs between *M. decactis and M. mirabilis* based on DESeq2 Wald test results. The volcano plot shows $\log_2$ fold changes in OTU abundance (x-axis) versus $-\log_{10}$ adjusted p-values (y-axis). Each point represents an OTU, with triangles indicating significant differences (padj < 0.05) and colors corresponding to bacterial phyla. Vertical dashed lines mark ±2 $\log_2$ fold change (4×increase), and the horizontal line marks the adjusted p = 0.05 threshold. The comparison revealed 103 OTUs significantly more abundant in *M. decactis* ($\log_2$FC < −2) and 27 OTUs more abundant in *M. mirabilis* ($\log_2$FC > 2).

Figure A6 Heatmap of PERMANOVA p-values testing the influence of six factors: colony identity, depth group, main Symbiodiniaceae profile, ITS2-profile, timepoint, and transplant treatment, on bacterial community composition in *M.* mirabilis (n = 46) and *M. decactis* (n = 45) at two depths. Significant effects (p < 0.05) are primarily associated with timepoint and transplantation treatment, particularly for *M. mirabilis* at 20 m and *M. decactis* at both depths. Other variables showed no consistent influence, although depth group and main profile were significant in *M. mirabilis* at 20 m.

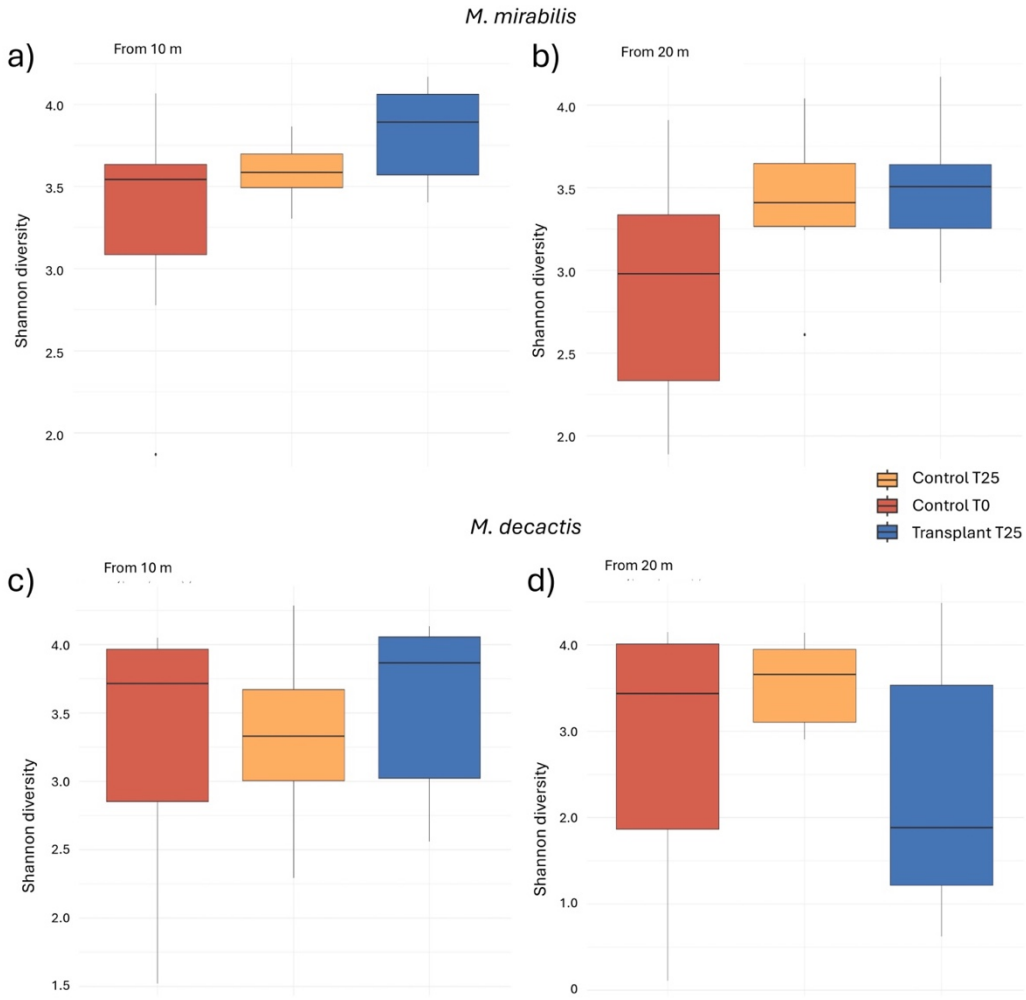

Figure A7 Shannon diversity of bacterial communities in *M. mirabilis* and *M. decactis* across transplantation treatments. All analyses shown were performed at the OTU level. (a–b) *M. mirabilis* from 10 m and 20 m origin, respectively (n = 11, 6, 6 per group). (c–d) *M. decactis* from 10 m and 20 m origin, respectively (n = 12, 6, 6 for 10 m; n = 10, 5, 6 for 20 m). No significant differences in Shannon diversity were detected across treatments for either species at either depth (all ANOVA $p > 0.05$). Boxplots are colored by treatment: control T0 (red), control T25 (orange), and transplanted T25 (blue).

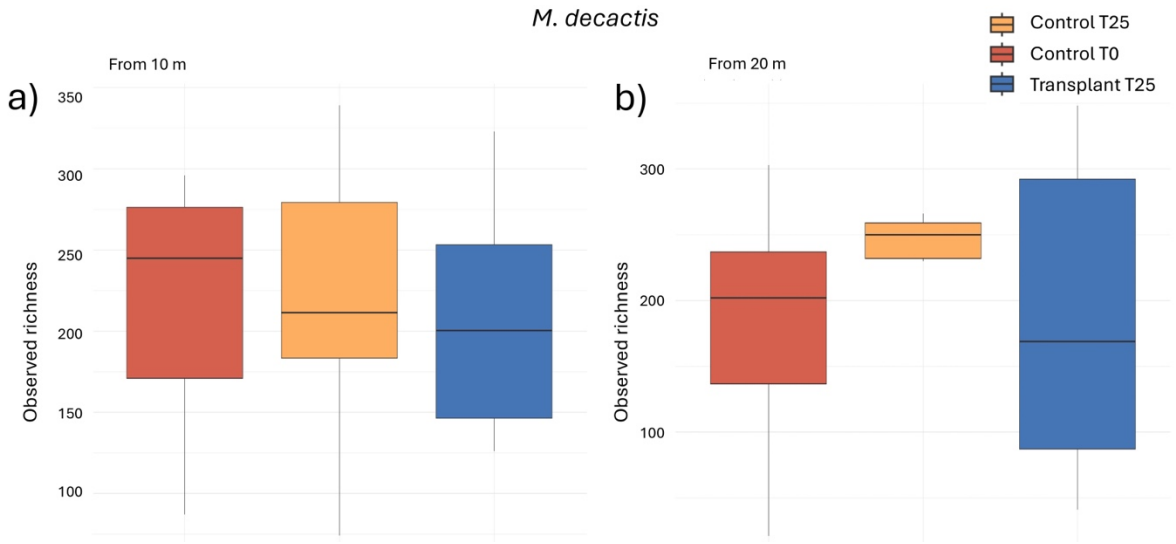

Figure A8 Observed richness (number of OTUs) in bacterial communities of *M. decactis* across transplantation treatments. (a–b) *M. decactis* from 10 m and 20 m origin, respectively (n = 12, 6, 6 for 10 m; n = 10, 5, 6 for 20 m). No significant differences in richness were observed for *M. decactis* at either depth (all $p > 0.05$). Treatments are colored as follows: control T0 (red), control T25 (orange), and transplanted T25 (blue).

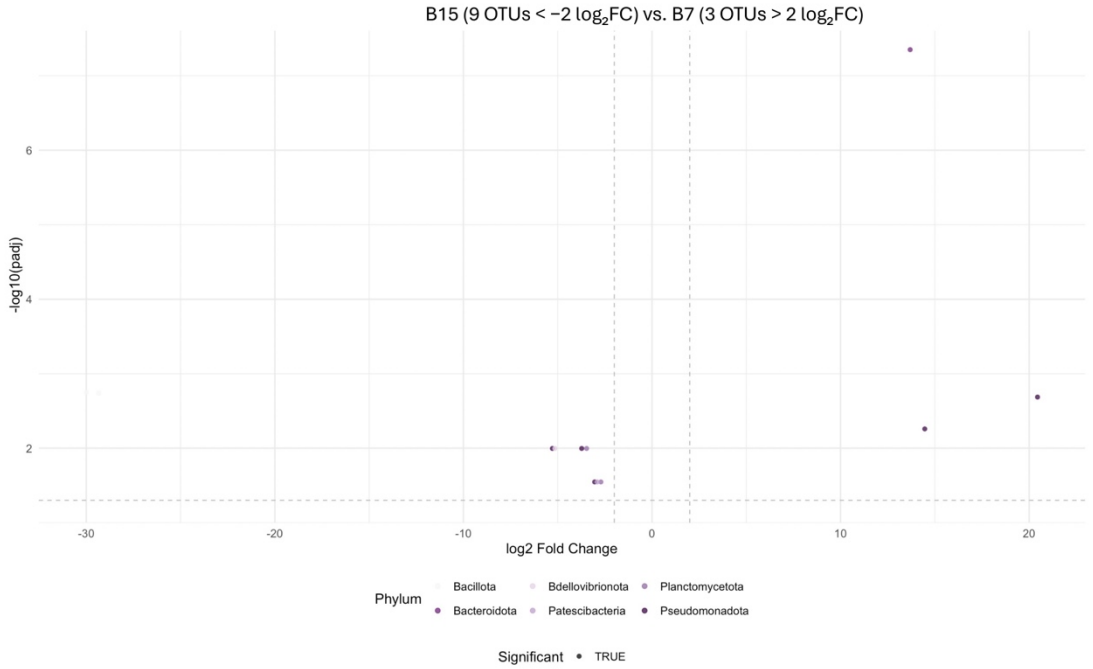

Figure A9 Differentially abundant bacterial OTUs between ITS2 main profile B15 and B7 based on DESeq2 Wald test results. The volcano plot shows $\log_2$ fold changes in OTU abundance (x-axis) versus $-\log_{10}$ adjusted p-values (y-axis). Each point represents an OTU, with triangles indicating significant differences (padj < 0.05) and colors corresponding to bacterial phyla. Vertical dashed lines mark ±2 $\log_2$ fold change (4×increase), and the horizontal line marks the adjusted p = 0.05 threshold. The comparison revealed 9 OTUs significantly more abundant in B15 ($\log_2FC < -2$) and 3 OTUs more abundant in B7 ($\log_2FC > 2$).

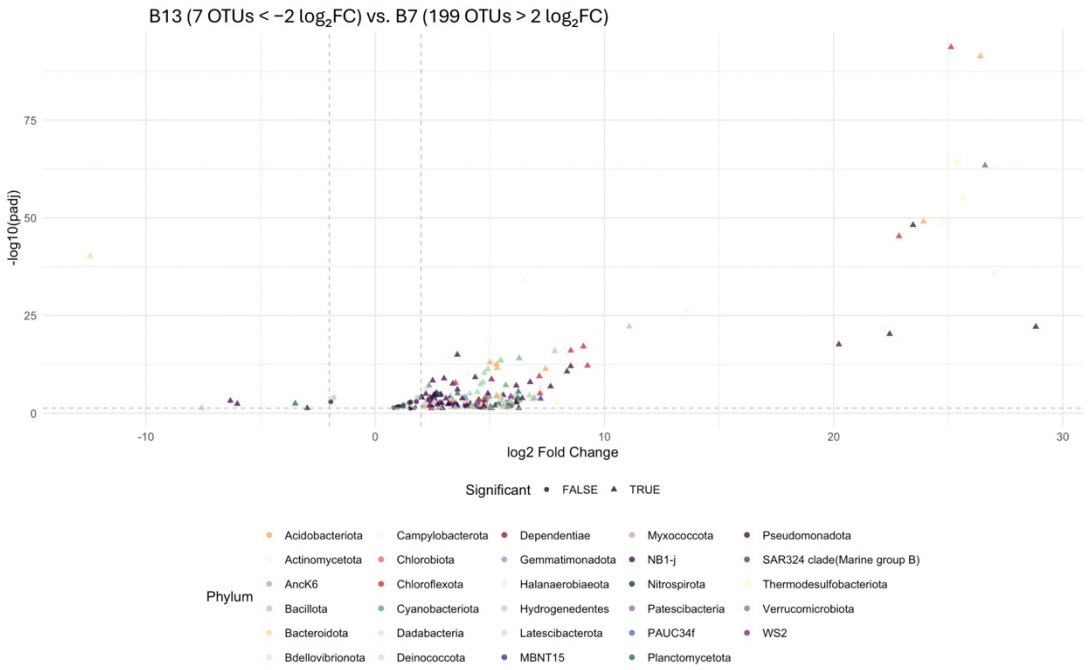

Figure A10 Differentially abundant bacterial OTUs between ITS2 main profile B13 and B7 based on DESeq2 Wald test results. The volcano plot shows $\log_2$ fold changes in OTU abundance (x-axis) versus $-\log_{10}$ adjusted p-values (y-axis). Each point represents an OTU, with triangles indicating significant differences (padj < 0.05) and colors corresponding to bacterial phyla. Vertical dashed lines mark ±2 $\log_2$ fold change (4×increase), and the horizontal line marks the adjusted p = 0.05 threshold. The comparison revealed 7 OTUs significantly more abundant in B13 ($\log_2$FC < −2) and 199 OTUs more abundant in B7 ($\log_2$FC > 2).

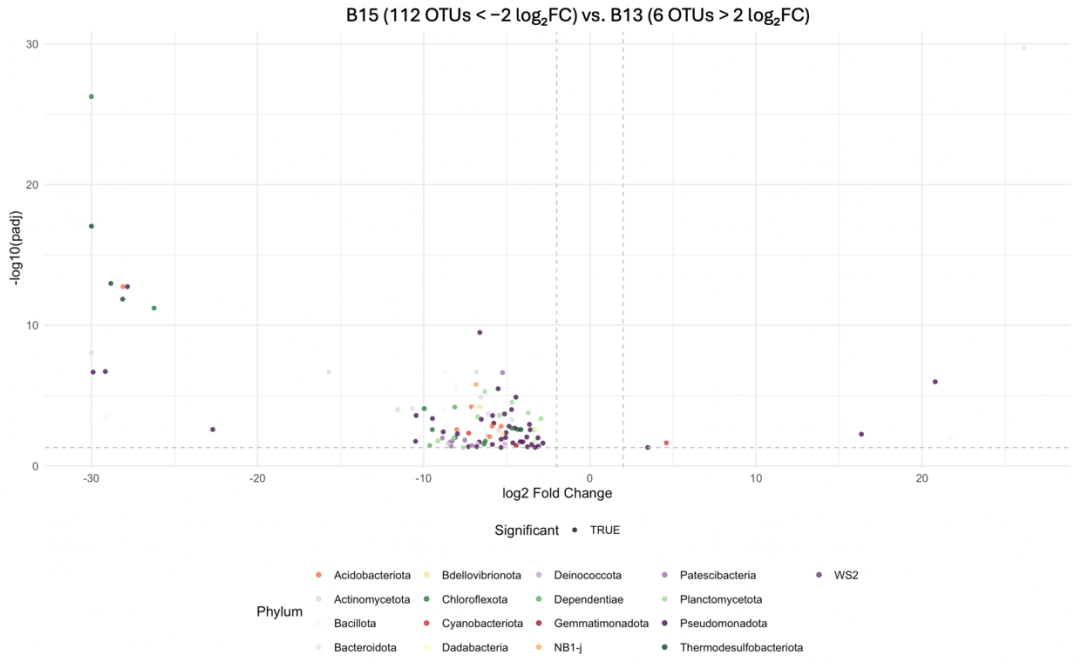

Figure A11 Differentially abundant bacterial OTUs between ITS2 main profile B15 and B13 based on DESeq2 Wald test results. The volcano plot shows $\log_2$ fold changes in OTU abundance (x-axis) versus $-\log_{10}$ adjusted p-values (y-axis). Each point represents an OTU, with triangles indicating significant differences (padj < 0.05) and colors corresponding to bacterial phyla. Vertical dashed lines mark ±2 $\log_2$ fold change (4×increase), and the horizontal line marks the adjusted p = 0.05 threshold. The comparison revealed 112 OTUs significantly more abundant in B15 ($\log_2$FC < −2) and 6 OTUs more abundant in B13 ($\log_2$FC > 2).

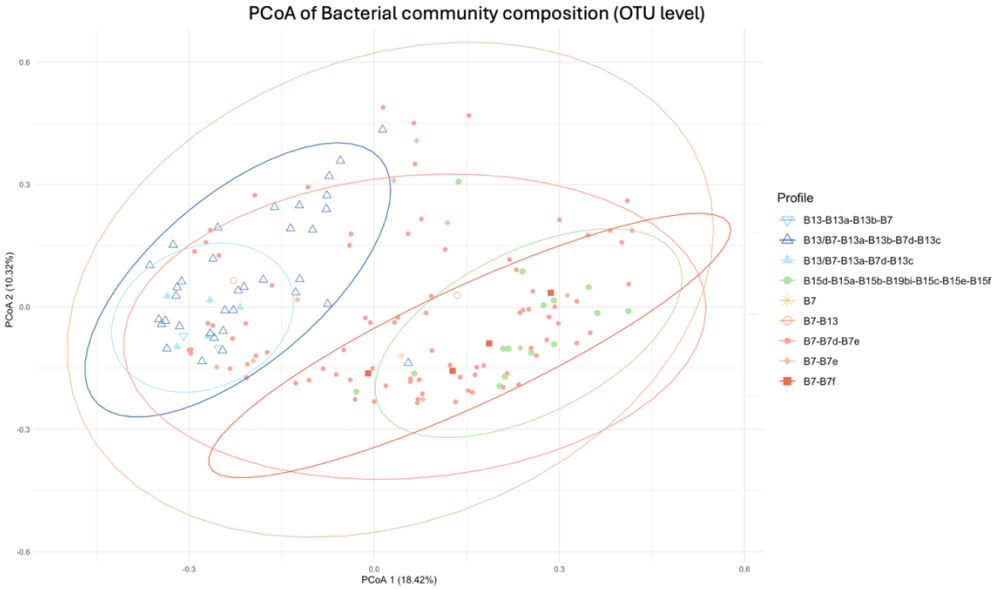

Figure A12 Principal Coordinates Analysis (PCoA) of bacterial community composition based on Bray–Curtis dissimilarities at the OTU level, grouped by Symbiodiniaceae ITS2-profile combinations (n = 9). Ellipses represent 95% confidence intervals. A global PERMANOVA revealed a significant effect of ITS2-profile on bacterial community composition (pseudo-F = 2.86, df = 2, $p < 0.001$, n = 127). Pairwise PERMANOVA comparisons indicated significant differences ($p \leq 0.05$) between the following groups: B15d-B15a-B15b-B19bi-B15c-B15e-B15f vs. all other profiles, B13/B7-B13a-B13b-B7d-B13c vs. B7-B13, B7-B7d-B7e, and B7-B7f, and B13a-B13b-B7 vs. B7-B13. All other pairwise comparisons were not significant ($p > 0.05$).

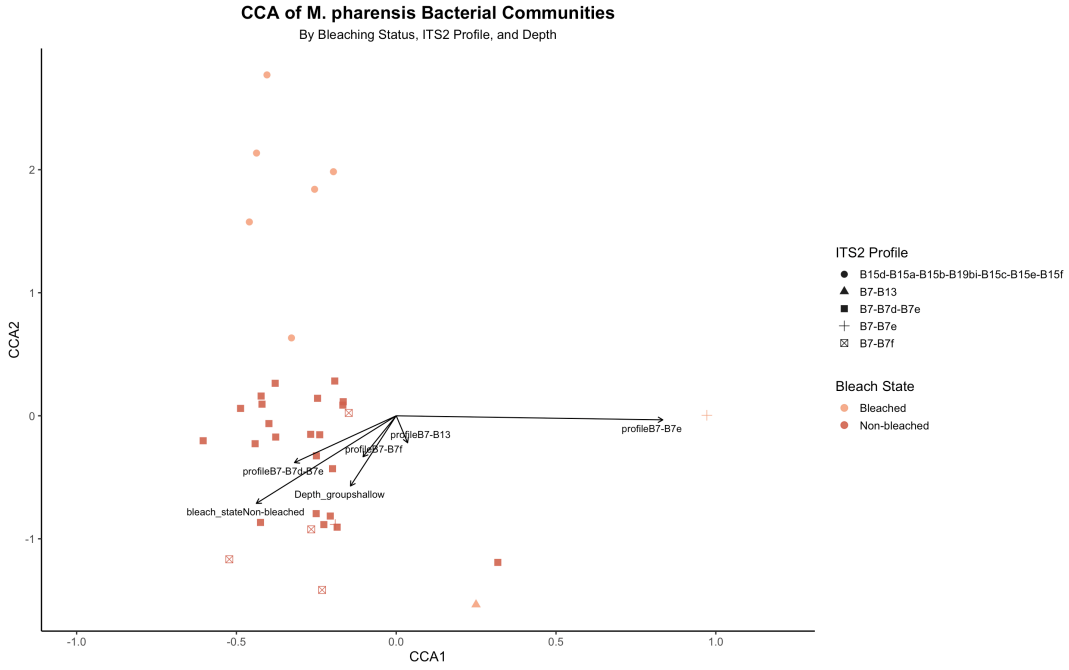

Figure A13 Canonical Correspondence Analysis (CCA) of bacterial community composition in *M. pharensis*, constrained by bleaching status, dominant ITS2-profile, and depth. Points are colored by bleaching status: non-bleached (dark red, n = 27) and bleached (light red, n = 9), and shaped by dominant ITS2-profile. The overall model was not significant ($Chi^2 = 0.531$, F = 1.08, p = 0.255), and none of the explanatory variables or canonical axes significantly explained variation in bacterial composition (all $p > 0.05$). Analysis at the OTU level.

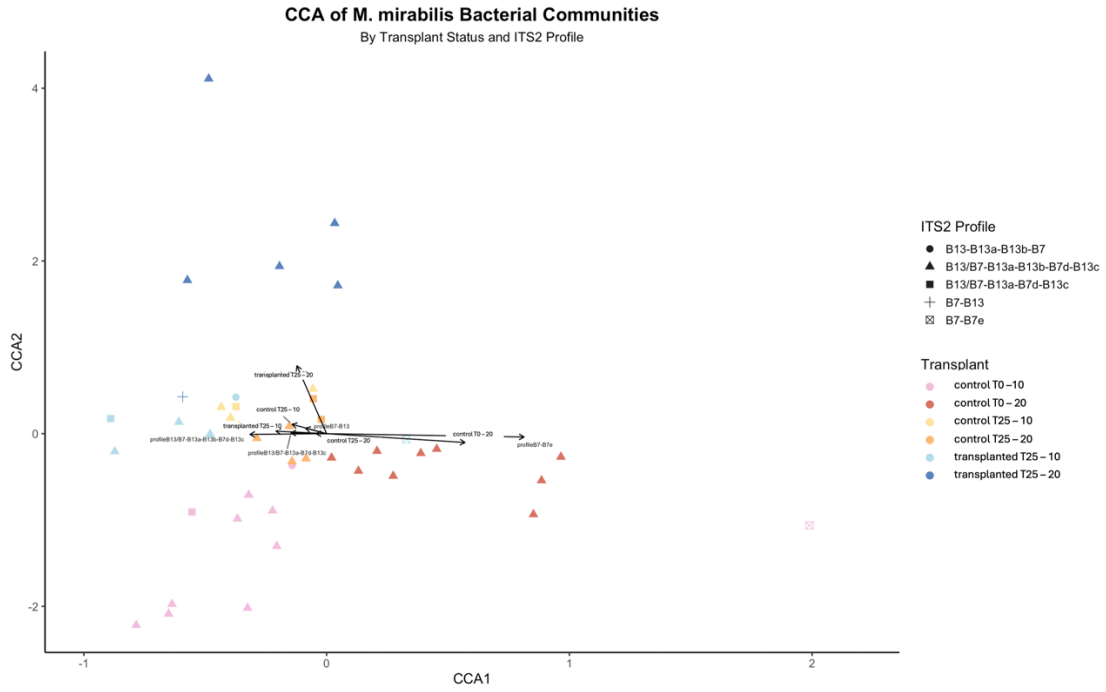

Figure A14 Canonical Correspondence Analysis (CCA) of bacterial community composition in *M. mirabilis*, constrained by transplant treatment and dominant ITS2-profile. Points are colored by treatment and depth: control T0 from 10 m (pink, n = 11), control T0 from 20 m (red, n = 11), control T25 from 10 m (yellow, n = 6), control T25 from 20 m (orange, n = 6), transplant T25 from 10 m (light blue, n = 6), and transplant T25 from 20 m (dark blue, n = 6). Points are shaped by dominant ITS2-profile. The overall model was not significant (Chi^2 = 1.135, F = 0.87, p = 0.543), and no constrained axes significantly explained variation (all p > 0.1). Analysis at the OTU level.

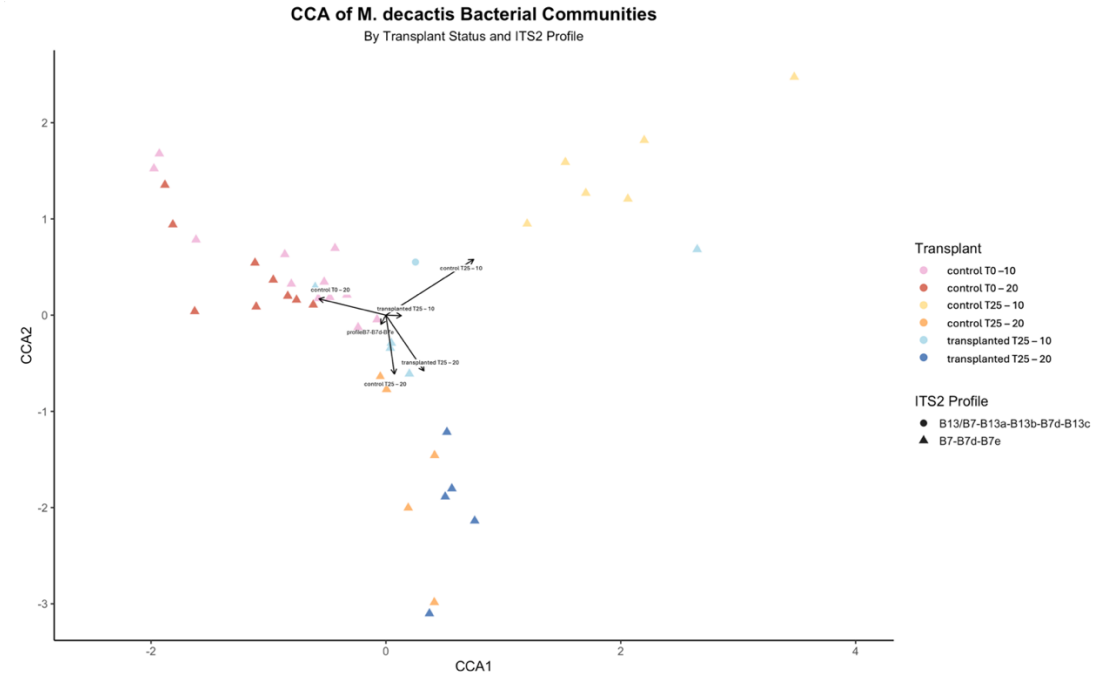

Figure A15 Canonical Correspondence Analysis (CCA) of bacterial community composition in *M. decactis*, constrained by transplant treatment and dominant ITS2-profile. Points are colored by treatment and depth: control T0 from 10 m (pink, n = 12), control T0 from 20 m (red, n = 10), control T25 from 10 m (yellow, n = 6), control T25 from 20 m (orange, n = 6), transplant T25 from 10 m (light blue, n = 6), and transplant T25 from 20 m (dark blue, n = 6). Points are shaped by dominant ITS2-profile. The overall model was not significant (Chi^2 = 0.513, F = 1.03, p = 0.091). Among the constrained variables, transplant status was significant (Chi^2 = 0.460, F = 1.11, p = 0.005), while neither ITS2-profile did not explain variation. All canonical axes were non-significant (p > 0.05). Analysis at the OTU level.

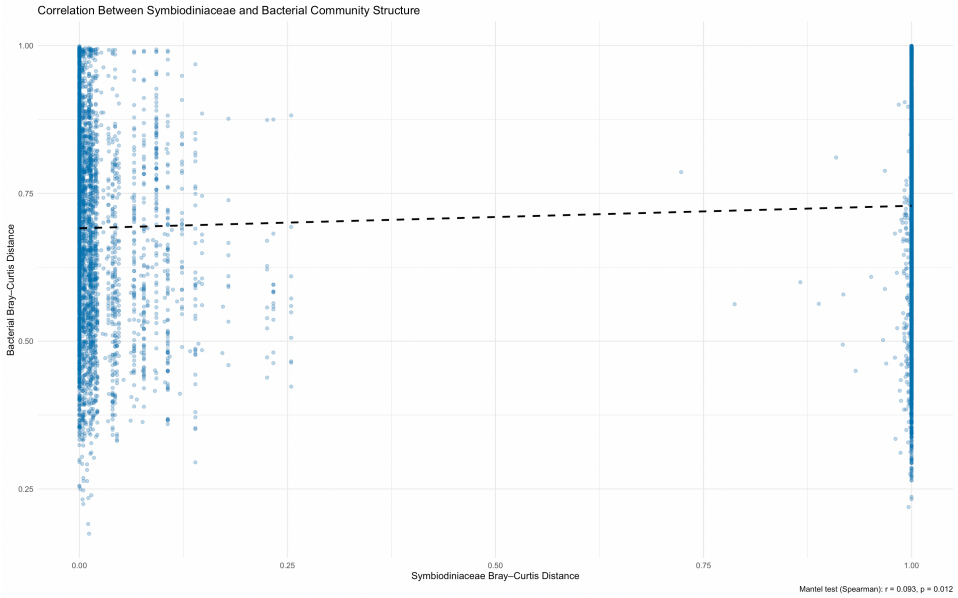

Figure A16 Mantel test showing the relationship between Symbiodiniaceae and bacterial community structure across all samples. The scatterplot shows pairwise Bray–Curtis dissimilarities between Symbiodiniaceae and bacterial communities. Each point represents a sample pair. A weak but statistically significant correlation was found (Spearman's r = 0.093, p = 0.012), while host-specific tests were not significant (all p > 0.05), indicating that observed covariation is limited and mostly interspecific. The dashed line represents the fitted regression between Bray–Curtis distances for Symbiodiniaceae and bacterial communities.

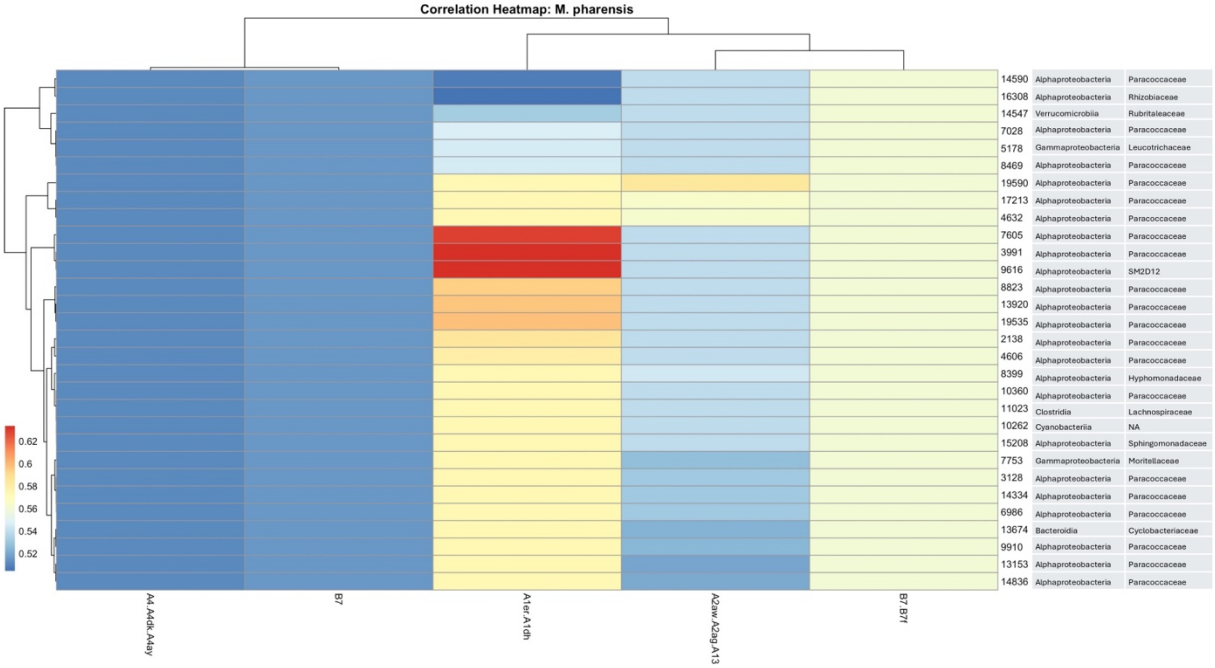

Figure A17 Correlation heatmap of bacterial OTUs and Symbiodiniaceae ITS2-profiles in *M. pharensis*. Significant positive correlations (ρ > 0.5, adjusted p ≤ 0.05) are shown between bacterial OTUs and ITS2-profiles. OTUs are annotated with Class and Family, and clustered based on correlation profiles. Most associations were detected with A2aw-A2ag-A13 and A1er-A1dh, especially involving members of Paracoccaceae. The color scale represents Spearman ρ values coefficients, with warmer shades indicating stronger correlations.

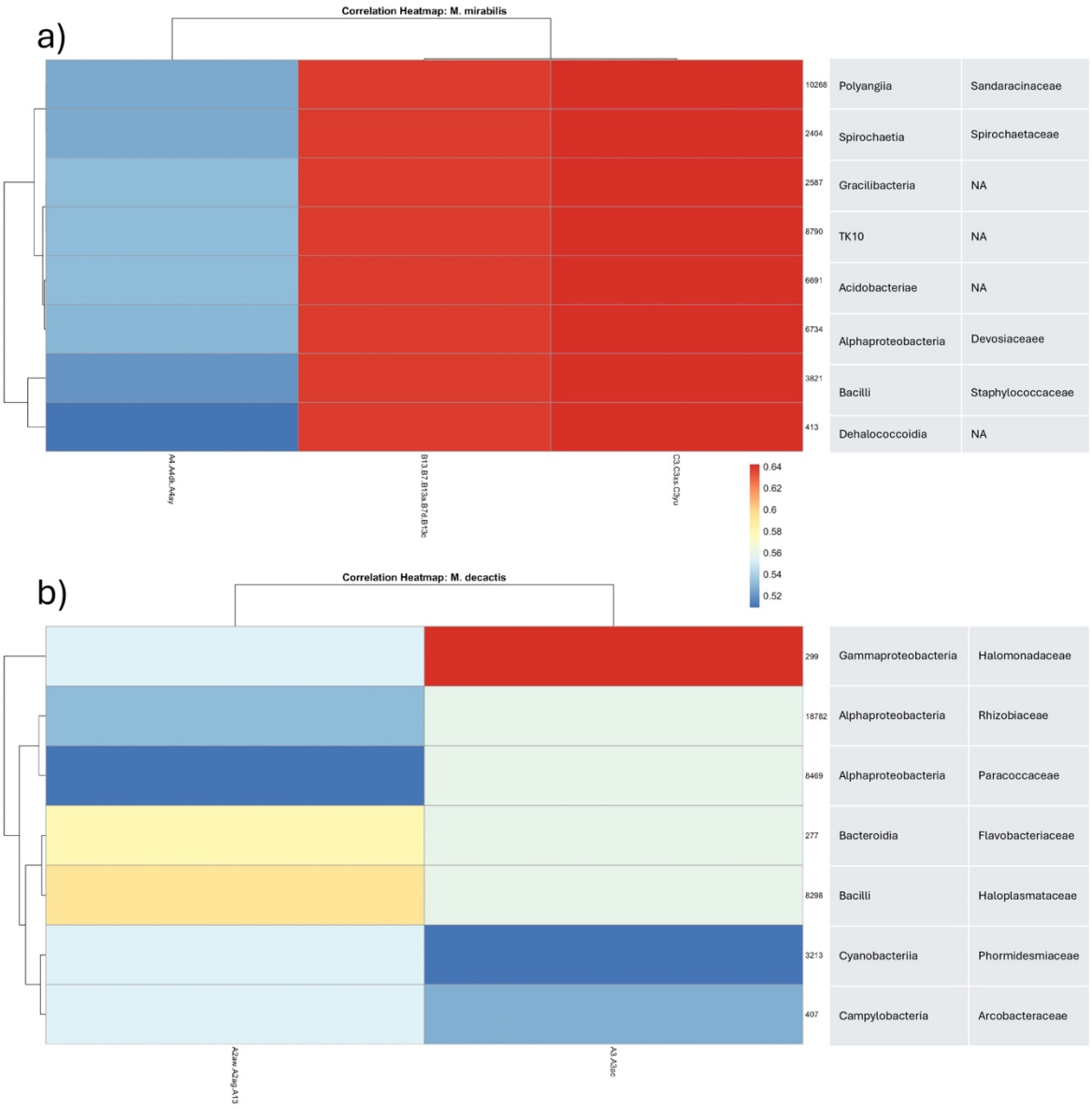

Figure A18 Correlation heatmaps of bacterial OTUs and Symbiodiniaceae ITS2-profiles for *M. mirabilis* (a) and *M. decactis* (b). Each heatmap shows significant positive correlations (Spearman's ρ > 0.5, adjusted p ≤ 0.05) between bacterial OTUs and ITS2-profiles. Warmer colors indicate stronger correlations. Taxonomic annotations (Class and Family) are shown for each OTU. In *M. mirabilis* (a), most correlations involved the profile A4-A4dk-A4ay and diverse bacterial families. In *M. decactis* (b), moderate correlations were observed with both A2aw-A2ag-A13 and A3-A3ac, including OTUs from Rhizobiaceae, Arcobacteraceae, and others. The color scale represents Spearman ρ values coefficients, with warmer shades indicating stronger correlations.

Supplementary tables

Table A1 Pairwise DESeq2 results for differentially abundant OTUs among *Madracis* species. This table summarizes OTUs shown in the species-level bubble plot (Figure 4.8) that were also found to be significantly differentially abundant in pairwise comparisons between coral hosts (*M. decactis*, *M. mirabilis*, and *M. pharensis*). Differential abundance analysis was performed using Wald tests in DESeq2, with $\log_2$ fold changes ($\log_2$FC) calculated between groups and Benjamini-Hochberg adjusted p-values (padj) < 0.05 considered significant. The "Enriched in" column indicates the species in which the OTU was significantly more abundant relative to the comparison group. Only OTUs that matched both the visual bubble plot (based on mean relative abundance) and passed DESeq2 significance thresholds in pairwise contrasts are included.

OTU	Comparison	Enriched_in	log2Fold Change	padj	Class	Family
11065	mirabilis_vs_decactis	mirabilis	1.000	0.04260	Alphaproteobacteria	Hyphomicrobiaceae
12039	mirabilis_vs_decactis	decactis	-3.014	< 0.001	Clostridia	Caminicellaceae
1328	mirabilis_vs_decactis	decactis	-3.669	< 0.001	Acidimicrobiia	Actinomarinales_f
13941	mirabilis_vs_decactis	decactis	-3.687	< 0.001	Acidimicrobiia	Microtrichaceae
1670	mirabilis_vs_decactis	decactis	-12.62	< 0.001	Chlorobia	Chlorobiaceae
1924	mirabilis_vs_decactis	decactis	-4.960	< 0.001	Alphaproteobacteria	Stappiaceae
2105	mirabilis_vs_decactis	decactis	-30.00	< 0.001	Gammaproteobacteria	Pseudomonadaceae
2373	mirabilis_vs_decactis	decactis	-5.201	< 0.001	Anaerolineae	A4b
4208	mirabilis_vs_decactis	mirabilis	11.74	< 0.001	Bacteroidia	Flavobacteriaceae
4918	mirabilis_vs_decactis	decactis	-1.104	0.04020	Clostridia	Clostridiaceae
5112	mirabilis_vs_decactis	decactis	-2.561	< 0.001	Alphaproteobacteria	Methyloligellaceae
7	mirabilis_vs_decactis	mirabilis	3.789	< 0.001	Gammaproteobacteria	Coxiellaceae
88	mirabilis_vs_decactis	mirabilis	3.324	< 0.001	Clostridia	Clostridiaceae
12039	mirabilis_vs_pharensis	pharensis	-7.083	< 0.001	Clostridia	Caminicellaceae
1328	mirabilis_vs_pharensis	pharensis	-6.338	< 0.001	Acidimicrobiia	Actinomarinales_f
13941	mirabilis_vs_pharensis	pharensis	-5.820	< 0.001	Acidimicrobiia	Microtrichaceae
1670	mirabilis_vs_pharensis	pharensis	-8.902	< 0.001	Chlorobia	Chlorobiaceae
18624	mirabilis_vs_pharensis	pharensis	-1.971	< 0.001	Alphaproteobacteria	Methyloligellaceae
2105	mirabilis_vs_pharensis	pharensis	-20.38	< 0.001	Gammaproteobacteria	Pseudomonadaceae
2373	mirabilis_vs_pharensis	pharensis	-3.804	< 0.001	Anaerolineae	A4b
31	mirabilis_vs_pharensis	mirabilis	2.031	< 0.001	Cyanobacteriia	Cyanobiaceae
4208	mirabilis_vs_pharensis	mirabilis	27.96	< 0.001	Bacteroidia	Flavobacteriaceae
4677	mirabilis_vs_pharensis	pharensis	-1.803	< 0.001	Planctomycetes	Pirellulaceae
4918	mirabilis_vs_pharensis	pharensis	-2.819	< 0.001	Clostridia	Clostridiaceae
5112	mirabilis_vs_pharensis	pharensis	-5.333	< 0.001	Alphaproteobacteria	Methyloligellaceae
7	mirabilis_vs_pharensis	mirabilis	2.505	< 0.001	Gammaproteobacteria	Coxiellaceae
7568	mirabilis_vs_pharensis	mirabilis	1.691	0.008627	Clostridia	Peptostreptococcaceae
88	mirabilis_vs_pharensis	mirabilis	2.883	< 0.001	Clostridia	Clostridiaceae
4218	mirabilis_vs_pharensis	pharensis	-4.589	0.002693	Alphaproteobacteria	Rhizobiaceae
4353	mirabilis_vs_pharensis	pharensis	-5.237	0.003196	Actinobacteria	Brevibacteriaceae

11065	decactis_vs_pharensis	pharensis	-1.687	< 0.001	Alphaproteobacteria	Hyphomicrobiaceae
12039	decactis_vs_pharensis	pharensis	-4.069	< 0.001	Clostridia	Caminicellaceae
1328	decactis_vs_pharensis	pharensis	-2.670	< 0.001	Acidimicrobiia	Actinomarinales_f
13941	decactis_vs_pharensis	pharensis	-2.131	0.001710	Acidimicrobiia	Microtrichaceae
1670	decactis_vs_pharensis	decactis	3.715	0.04875	Chlorobia	Chlorobiaceae
18624	decactis_vs_pharensis	pharensis	-2.141	< 0.001	Alphaproteobacteria	Methyloligellaceae
1924	decactis_vs_pharensis	decactis	3.077	0.001368	Alphaproteobacteria	Stappiaceae
2105	decactis_vs_pharensis	decactis	11.14	< 0.001	Gammaproteobacteria	Pseudomonadaceae
31	decactis_vs_pharensis	decactis	1.813	0.005730	Cyanobacteriia	Cyanobiaceae
4208	decactis_vs_pharensis	decactis	16.22	< 0.001	Bacteroidia	Flavobacteriaceae
4677	decactis_vs_pharensis	pharensis	-2.509	< 0.001	Planctomycetes	Pirellulaceae
4918	decactis_vs_pharensis	pharensis	-1.715	0.001581	Clostridia	Clostridiaceae
5112	decactis_vs_pharensis	pharensis	-2.772	< 0.001	Alphaproteobacteria	Methyloligellaceae

Table A2 Pairwise differential abundance comparisons of selected OTUs across Symbiodiniaceae main profiles (B7, B13, B15) using DESeq2 Wald tests. The table includes OTUs that were among the top 15 most abundant (as visualized in Figure 4.14a). Comparisons were performed between all combinations of B7, B13, and B15 profiles. The enriched group is based on the direction of $\log_2$ fold change ($\log_2$FC), and adjusted p-values (padj) indicate significance after multiple testing correction. Only comparisons with padj < 0.05 are shown.

OTU	**Comparison**	**Enriched_in**	**log2Fold Change**	**padj**	**Class**	**Family**
4677	B7_vs_B15	B15	-2.709	0.02835	Planctomycetes	Pirellulaceae
1328	B7_vs_B13	B7	6.511	< 0.001	Acidimicrobiia	Actinomarinales_f
13941	B7_vs_B13	B7	4.947	< 0.001	Acidimicrobiia	Microtrichaceae
1924	B7_vs_B13	B7	4.361	< 0.001	Alphaproteobacteria	Stappiaceae
2105	B7_vs_B13	B7	28.82	< 0.001	Gammaproteobacteria	Pseudomonadaceae
4280	B7_vs_B13	B7	5.005	< 0.001	Thermoanaerobaculia	Thermoanaerobaculaceae
4677	B7_vs_B13	B7	1.003	0.02706	Planctomycetes	Pirellulaceae
4918	B7_vs_B13	B7	1.833	< 0.001	Clostridia	Clostridiaceae
9542	B7_vs_B13	B7	2.208	< 0.001	Dadabacteriia	Incertae Sedis
1328	B13_vs_B15	B15	-6.82	< 0.001	Acidimicrobiia	Actinomarinales_f
13941	B13_vs_B15	B15	-4.714	< 0.001	Acidimicrobiia	Microtrichaceae
1924	B13_vs_B15	B15	-4.195	0.01907	Alphaproteobacteria	Stappiaceae
2105	B13_vs_B15	B15	-22.70	0.002570	Gammaproteobacteria	Pseudomonadaceae
4280	B13_vs_B15	B15	-5.343	0.001530	Thermoanaerobaculia	Thermoanaerobaculaceae
4677	B13_vs_B15	B15	-3.712	< 0.001	Planctomycetes	Pirellulaceae
4918	B13_vs_B15	B15	-4.447	< 0.001	Clostridia	Clostridiaceae
9542	B13_vs_B15	B15	-3.223	0.002570	Dadabacteriia	Incertae Sedis

Table A3 Indicator bacterial OTUs associated with Symbiodiniaceae main profiles (B7, B13, B15) based on Indicator Value (IndVal) analysis. OTUs with IndVal ≥ 0.7 and $p < 0.05$ were retained as strong indicators. Indicator values represent the strength of association between each OTU and the main profile group, with 1.0 indicating perfect specificity and fidelity.

OTU	Main_profile	IndVal	p-value	Class	Family
4208	B13	0.9145	0.001	Bacteroidia	Flavobacteriaceae
31	B13	0.8287	0.004	Cyanobacteriia	Cyanobiaceae
88	B13	0.8139	0.031	Clostridia	Clostridiaceae
2420	B13	0.7964	0.019	Alphaproteobacteria	Stappiaceae
1796	B13	0.7760	0.012	Alphaproteobacteria	Paracoccaceae
12925	B13	0.7458	0.022	Alphaproteobacteria	Paracoccaceae
1876	B13	0.7387	0.026	Alphaproteobacteria	Rhizobiaceae
1322	B13	0.7382	0.029	Planctomycetes	Pirellulaceae
599	B13	0.7150	0.032	Alphaproteobacteria	Paracoccaceae
10788	B15	0.9419	0.001	Thermoleophilia	67-14
7502	B15	0.9052	0.002	Latescibacterota_c	Latescibacterota_c_o_f
4602	B15	0.8872	0.001	Anaerolineae	Anaerolineaceae
138	B15	0.8716	0.001	Actinobacteria	Nocardiaceae
17131	B15	0.8665	0.005	Alphaproteobacteria	Paracoccaceae
19214	B15	0.8519	0.002	Gammaproteobacteria	I3A_f
16183	B15	0.8381	0.001	Planctomycetes	Planctomycetes_o_f
712	B15	0.8379	0.001	Actinobacteria	Mycobacteriaceae
7422	B15	0.8275	0.002	Vicinamibacteria	Subgroup 9_f
17463	B15	0.8264	0.001	Gracilibacteria	Candidatus Peribacteria_f
6967	B15	0.8256	0.003	Vicinamibacteria	Subgroup 17_f
5153	B15	0.8238	0.001	Phycisphaerae	SG8-4
13142	B15	0.8237	0.005	Babeliae	Vermiphilaceae
5096	B15	0.8115	0.003	NB1-j_c	NB1-j_c_o_f
2426	B15	0.8107	0.001	Thermoleophilia	Gaiellales_f
5112	B15	0.8094	0.001	Alphaproteobacteria	Methyloligellaceae
6995	B15	0.8054	0.002	Alphaproteobacteria	Alphaproteobacteria_o_f
357	B15	0.8052	0.001	Gammaproteobacteria	UBA10353 marine group_f
1338	B15	0.8018	0.004	Clostridia	Oscillospiraceae
2087	B15	0.7988	0.002	Actinobacteria	Brevibacteriaceae
453	B15	0.7986	0.001	Alphaproteobacteria	Rhizobiaceae
1892	B15	0.7947	0.001	Alphaproteobacteria	Rhizobiaceae
4255	B15	0.7934	0.002	Gammaproteobacteria	KI89A clade
120	B15	0.7905	0.006	Alphaproteobacteria	Hyphomicrobiaceae
3222	B15	0.7885	0.003	Gammaproteobacteria	Arenicellaceae

10787	B15	0.7770	0.004	Acidimicrobiia	Microtrichales_f
9076	B15	0.7735	0.018	Clostridia	Lachnospiraceae
4663	B15	0.7695	0.003	Planctomycetes	Rubinisphaeraceae
15437	B15	0.7690	0.008	Alphaproteobacteria	Hyphomicrobiaceae
15911	B15	0.7681	0.008	Clostridia	Caminicellaceae
135	B15	0.7647	0.003	Alphaproteobacteria	Rhizobiaceae
4280	B15	0.7626	0.046	Thermoanaerobaculia	Thermoanaerobaculaceae
7212	B15	0.7588	0.001	Gracilibacteria	Gracilibacteria_o_f
7403	B15	0.7571	0.005	JG30-KF-CM66	JG30-KF-CM66_o_f
7331	B15	0.7562	0.003	Dehalococcoidia	S085_f
1312	B15	0.7550	0.001	Clostridia	Anaerovoracaceae
7344	B15	0.7540	0.014	Polyangiia	Haliangiaceae
10128	B15	0.7536	0.005	WS2_c	WS2_c_o_f
14037	B15	0.7513	0.002	KD4-96	KD4-96_o_f
1264	B15	0.7509	0.017	Clostridia	Lachnospiraceae
8561	B15	0.7491	0.006	Vampirivibrionia	Gastranaerophilaceae
1328	B15	0.7485	0.036	Acidimicrobiia	Actinomarinales_f
8170	B15	0.7469	0.007	Anaerolineae	Caldilineaceae
5156	B15	0.7449	0.002	Kiritimatiellia	WCHB1-41_f
7174	B15	0.7424	0.023	Oligoflexia	Oligoflexaceae
5198	B15	0.7418	0.027	Saccharimonadia	Saccharimonadales_f
6167	B15	0.7341	0.011	Planctomycetes	Gemmataceae
13025	B15	0.7307	0.024	Clostridia	Caminicellaceae
14925	B15	0.7285	0.02	Gammaproteobacteria	EC3_f
18108	B15	0.7272	0.004	Desulfomonilia	Desulfomonilaceae
16531	B15	0.7262	0.005	Chloroflexia	AKYG1722
708	B15	0.7174	0.006	Alphaproteobacteria	Sphingomonadaceae
8776	B15	0.7109	0.013	Microgenomatia	Candidatus Levybacteria_f
3868	B15	0.7018	0.006	Anaerolineae	Aggregatilineales_f
43	B15	0.7016	0.006	Bacilli	Bacillaceae
2373	B7	0.8055	0.03	Anaerolineae	A4b
1924	B7	0.7538	0.042	Alphaproteobacteria	Stappiaceae

Appendix B

Transplantation experiment

For the transplantation experiment “stationary” racks (80x60 cm) and “mobile” racks (40x56 cm) were constructed, using PVC pipes, wire mesh, and metal rods, all secured with zip ties. The PVC pipes formed the frame, with holes drilled into them to allow water flow for sinking. The stationary racks were fitted with 60 cm metal rods, inserted through pre-drilled holes at the corners and middle, to serve as pillars for anchoring them to the ground. The mobile racks were placed on the stationary racks, with loose wire mesh attached to the bottom and tighter mesh on top. The racks were set up at depths of 10 and 20 meters, with one mobile rack at each depth being transplanted and the other left as a control group at its original depth.

Corals were found and collected around the same depth as the experiment was conducted (10- and 20-meters depth). Twelve colonies of each species, *M. mirablis* and *M. decactis,* were collected. Each colony was split, with one part used for transplantation and the other serving as a control. After being acclimatized for five days, the transplantation was conducted by swapping one of the mobile racks between the two depths and keeping one mobile rack as control. The colonies were reattached at their new depth to the stationary racks using zip ties.

Samples were collected from each colony at two timepoints: day 0 (timepoint 0, T0) and day 25 (timepoint 25, T25). This yielded a total of n = 48 samples for both *M. mirabilis* and *M. decactis*.

Appendix C
Sample preparation and symbiont measurements

Airbrushing

Falcon tubes, Eppendorf tubes (designated for 2 photosymbionts, 2 chlorophyll, 6 genetics, 4 spec, and 2 BSA samples), and ziplock bags were labeled according to the sample numbers. The coral specimens were then rinsed thoroughly with 1X PBS. A 10 mL aliquot of 1X PBS was added to each ziplock bag, into which the coral was placed and held in position for the air brushing procedure. A clean pipette tip was affixed to the airgun for each sample. The tissue adhering to the coral skeleton was airbrushed, taking care to avoid damage to the skeleton while ensuring thorough coverage from one side to the other. The resulting tissue slurry, consisting of both tissue and PBS, was transferred into a pre-labeled falcon tube. An additional 5 mL of 1X PBS was added to the ziplock bag, sealed, and mixed thoroughly to maximize the transfer of tissue into the falcon tube. The falcon tube was then filled with 1X PBS to a final volume of 15 mL, with any excess volume recorded.

The samples within the falcon tubes were vortexed for 1 minute at 20 rpm (x100). The homogenate was aliquoted into 10 pre-labeled tubes. Prior to aliquoting, the sample was vortexed, and a pipette was used to resuspend and homogenize the sample each time. The following aliquots were prepared:

a) 2 aliquots for photosymbionts density (500 µL each)
b) 2 aliquots for chlorophyll content (1000 µL each)
c) 6 aliquots for genetic analysis (1000 µL each)
d) Empty Eppendorf tubes were prepared for the transfer of the supernatant from the genetics aliquots to the spec fluorometer and BSA tubes.

The aliquots intended for photosymbiont cell density analysis were fixed with formalin. To this end, 500 µL of the homogenate was mixed with 500 µL of 10% formalin. These aliquots were stored at room temperature.

Then centrifugation steps were as follows for the different aliquots:

a) The chlorophyll (2 aliquots) and genetics (6 aliquots) samples were centrifuged at 16,000 g (rcf) for 5 minutes.
b) The genetics samples (6 aliquots) were subjected to a higher speed centrifugation at 20,000 g (rcf) for 30 minutes. The supernatant was subsequently transferred to the spec fluorometer and BSA tubes.

Note: This project utilized only the aliquots for genetic analysis, photosymbiont density and chlorophyll content, while the remaining aliquots were allocated to other parallel projects.

Photosymbiont cell counting

A 10 µL aliquot of the fixed sample was placed into one of the divisions of a hemocytometer, with the cover slip already in place. The cell count was performed using a counter, with a minimum of 8 “counting units” analyzed to obtain representative data, ensuring that the coefficient of variation (CV) among counting units remained below 15%. The CV, defined as the ratio of the standard deviation to the mean (CV = SD/mean), was calculated. If the number of cells in any counting unit was fewer than 15, the sample was concentrated by centrifuging at 5,000 g (rcf) for 5 minutes, followed by removal of 750 µL of liquid, thereby concentrating the coral tissue by a factor of 4. The sample was then recounted.

To prevent cross-contamination between samples, the hemocytometer and cover slip were cleaned with ethanol between uses, and the counting process was repeated for each new sample. The cell count was then extrapolated to the total volume of the sample, providing an estimate of the total tissue content.

Photosymbiont density measurements

Each airbrushed coral skeleton was first cleaned by rinsing with water and then placed in a labeled ziplock bag or Falcon tube containing a bleach solution. The skeleton was left in the solution for 2–3 days or until it turned completely white. Afterward, it was thoroughly rinsed with tap water to remove any residual bleach, and excess water was drained. The skeleton was then dried in a laboratory oven at 40°C until fully dehydrated.

Once dry, the coral skeleton was carefully wrapped in aluminum foil, ensuring complete coverage of all surfaces without overlapping the foil by more than one layer. The weight of the aluminum foil used was measured and extrapolated to estimate the surface area of the skeleton, with the weight (in milligrams) corresponding to the surface area (in cm^2). This was achieved by first creating a calibration curve based on known surface areas of aluminum foil, which were weighed. Finally, the photosymbiont cell count was used to calculate the photosymbiont cell density in the coral tissue, expressed as the number of cells per area (# cells/cm^2).

Chlorophyll content

The tissue pellets were defrosted on ice and resuspended by adding 50 µL of dimethyl sulfoxide (DMSO), followed by vortexing. Then, 950 µL of acetone was added, and the samples were vortexed again. The tubes were wrapped in aluminum foil to protect from light and incubated in the dark at 4°C for 24 hours to extract the chlorophyll.

After incubation, the samples were centrifuged at 16,000×g for 10 minutes to separate the supernatant from the tissue pellet. The supernatant (200 µL per well) was transferred into a 96-well plate, with triplicate measurements taken for accuracy. Absorbance was measured at 630, 663, and 750 nm using a BioTek™ microplate reader, with the 750 nm absorbance serving as a reference.

Chlorophyll concentrations were calculated using the equations from Jeffrey and Humphrey (1975) for 100% acetone:

Chlorophyll a: *Chl a* [µg mL^{-1}] = 11.43 x A_{663} – 0.64 x A_{630}

Chlorophyll c2: *Chl c2* [µg mL^{-1}] = 27.09 x A_{630} – 3.63 x A_{663}

The total amount of chlorophyll was determined by multiplying the concentration by the extraction volume. Finally, values were normalized to the tissue blastate and aliquot volume and standardized to the tissue's surface area.

Appendix D
DNA extractions

The DNA extractions were performed using a ZymoBIOMICS™ DNA Miniprep Kit based on the manufacturers protocol with some modifications (Zymo Research, 2023).

The 6 x 1.5 mL microcentrifuge tubes for each sample were subjected to UV radiation for 30 minutes. Reagents required for the day were aliquoted, ensuring no precipitation was present. Clean microcentrifuge tubes were then labeled accordingly.

To each coral tissue pellet, 150 µL of ultrapure water was added, followed by vortexing. The mixture was then transferred into a microcentrifuge tube, and the samples were centrifuged at 15,000 x g for 10 minutes. The supernatant was discarded after centrifugation. Next, 750 µL of lysis solution was added to each tube, vortexed, and the contents were transferred to ZR BashingBead™ Lysis Tubes.

The ZR BashingBead™ Lysis Tubes were placed in a bead beater with a 2 mL tube holder assembly, and bead beating was performed at 25 Hz for 5 cycles of 1 minute each. The holder assembly was rotated between runs.

At this stage, an optional stopping point was available where samples could be stored in the refrigerator for several hours if necessary. For this procedure, the samples were stored for approximately one hour before continuing.

Upon resumption, the ZR BashingBead™ Lysis Tubes were centrifuged at 10,000 x g for 1 minute. Up to 400 µL of the supernatant was transferred to a Zymo-Spin™ III-F Filter in a new Collection Tube and centrifuged at 8,000 x g for 1 minute. The Zymo-Spin™ III-F Filter was discarded.

To the filtrate in the Collection Tube, 1,200 µL of ZymoBIOMICS™ DNA Binding Buffer was added and mixed gently with a pipette. Then, 800 µL of the mixture was transferred to a Zymo-Spin™ IICR Column in a new Collection Tube and centrifuged at 10,000 x g for 1 minute. The flow-through was discarded, and the process was repeated with the remaining mixture.

The Zymo-Spin™ IICR Column was transferred to a new Collection Tube and washed sequentially with 400 µL of ZymoBIOMICS™ DNA Wash Buffer 1, 700 µL of DNA Wash Buffer 2, and 200 µL of DNA Wash Buffer 2. After each wash, centrifugation was performed at 10,000 x g for 1 minute, discarding the flow-through after each step.

The Zymo-Spin™ IICR Column was then transferred to a clean 1.5 mL microcentrifuge tube. To elute the DNA, 50 µL of ZymoBIOMICS™ DNase/RNase-Free Water was added directly to the column matrix, followed by a 1-minute incubation. The mixture was then centrifuged at 10,000 x g for 1 minute.

A Zymo-Spin™ III-HRC Filter was prepared by placing it in a new Collection Tube and adding 600 µL of ZymoBIOMICS™ HRC Prep Solution. The filter was centrifuged at 8,000 x g for 3 minutes. The prepared Zymo-Spin™ III-HRC Filter was then transferred into a clean 1.5 mL microcentrifuge tube, and the previously eluted DNA was added to the filter. Centrifugation was performed at exactly 16,000 x g for 3 minutes.

Finally, the eluted DNA was mixed by pipetting, and aliquots were prepared in four separate microcentrifuge tubes, each containing approximately 13 µL of DNA diluted in water. The aliquots were stored as follows: one at -80°C for long-term storage, one at -20°C for photosymbiont analysis, one at -20°C for bacterial analysis, and one at -20°C for short-term use (e.g. DNA quantification and PCRs). Each aliquot was stored in the appropriate freezer and labeled accordingly.

Appendix E

PCR and gel-electrophoreses

For ITS2, the primer pair SymPochITS2F and SymPochlITS2R with the sequences GTGAATTGCAGAACTCCGTG and GCCTCCGCTTACTTATATGCTT, was used and for 16S, the primer pair 515F and 806Rb with the sequences GTGCCAGCMGCCGCGGTAA and GGACTACHVGGGTWTCTAAT. These PCRs and gels served as quality checks to confirm successful amplification of bacterial 16S and Symbiodiniaceae ITS2 regions and were not part of the library preparation process.

The following description is based on the "Quick-Start Protocol Taq DNA Polymerase and Taq PCR Core Kit" (Qiagen, 2016). In addition, the steps for Gel-Electrophoresis are added. The 1x PCR buffer, dNTP mix, and primers were thawed. All components, except for the dNTP mix, were vortexed. Everything was placed on ice. In a microcentrifuge tube, the master mix was prepared by adding the appropriate volumes of nuclease-free water, PCR buffer, dNTP mix, primers, and Taq Polymerase (kept on ice) according to the volumes listed in the pre-prepared table. Thorough mixing was ensured using a pipette. 23 µL (for 16S) or 24 µL (for ITS2) of the master mix was dispensed into each individual PCR tube. 2 µL of template DNA for 16S amplification or 1 µL for ITS2 amplification was added to each PCR tube. For the negative control, 2 µL (16S) or 1 µL (ITS2) of nuclease-free water was added. The thermal cycler was programmed with the following conditions:

For 16S amplification:

- 3 minutes at 94°C
- 10 cycles of 30 seconds at 94°C, 30 seconds of touchdown from 63°C to 58°C, and 40 seconds at 72°C
- 25 cycles of 30 seconds at 94°C, 30 seconds at 58°C, and 40 seconds at 72°C
- A final extension of 10 minutes at 72°C

For ITS2 amplification:

- 3 minutes at 94°C
- 30 cycles of 30 seconds at 94°C, 30 seconds at 53°C, and 40 seconds at 72°C
- A final extension of 10 minutes at 72°C

A gel casting frame large enough to accommodate the number of PCR tubes was selected. Combs were placed in the frame to form wells for loading samples. The appropriate volume of agarose gel was calculated based on the size of the casting frame. For example, for a 100 mL gel, 1.5 g of agarose was weighed out and dissolved in 100 mL of 1x TBE buffer. The TBE buffer was measured accurately using a measuring cylinder. The agarose and buffer were combined in a flask, and a magnetic stir bar was added. The opening of the flask was covered, and the solution was placed on a magnetic stirrer with heating capabilities. The solution was stirred at approximately 300 rpm while being heated to 175°C until the agarose was completely dissolved. Once the solution boiled, the flask was removed from the heater and placed on a cooling magnetic stirrer. Stirring continued at 300 rpm as the solution cooled. Once the agarose solution cooled sufficiently, 4 µL of Midori Green Extra dye was added for every 100 mL of gel. The agarose solution was poured into the prepared casting frame, ensuring that the combs remained in place. The gel was allowed to set at room temperature.

Once the gel had solidified, it was carefully transferred into the electrophoresis tank, and the tank was filled with 1x TBE buffer until the gel was covered. A molecular weight ladder was loaded into the first well of the gel for comparison with the PCR samples. For each PCR sample, 4 µL of the PCR product was mixed with 1 µL of loading buffer. This mixture was then loaded into the wells. The prepared PCR samples were loaded into the appropriate wells of the gel. The electrophoresis system was set to run at 85V for approximately 35 minutes, or until the dye front had migrated sufficiently through the gel. After electrophoresis, the gel was transferred to an imaging system equipped with a camera. Photographs were taken of the gel, capturing both color images and black-and-white reversed images for documentation purposes.

Bibliography

Allemand, D., Ferrier-Pagès, C., Furla, P., Houlbrèque, F., Puverel, S., Reynaud, S., Tambutté, E., Tambutté, S., & Zoccola, D. (2004). Biomineralisation in reef-building corals: From molecular mechanisms to environmental control. *Comptes Rendus Palevol, 3*(6–7), 453–467. https://doi.org/10.1016/j.crpv.2004.07.011

Apprill, A. M., & Gates, R. D. (2007). Recognizing diversity in coral symbiotic dinoflagellate communities. *Molecular Ecology, 16*(6), 1127–1134. https://doi.org/10.1111/j.1365-294X.2006.03214.x

Ban, S. S., Graham, N. A. J., & Connolly, S. R. (2014). Evidence for multiple stressor interactions and effects on coral reefs. *Global Change Biology, 20*(3), 681–697. https://doi.org/10.1111/gcb.12453

Botté, E. S., Cantin, N. E., Mocellin, V. J. L., O'Brien, P. A., Rocker, M. M., Frade, P. R., & Webster, N. S. (2022). Reef location has a greater impact than coral bleaching severity on the microbiome of *Pocillopora acuta*. *Coral Reefs, 41*(1), 63–79. https://doi.org/10.1007/s00338-021-02201-y

Bourne, D. G., Iida, Y., Uthicke, S., & Smith-Keune, C. (2008). Changes in coral associated microbial communities during a bleaching event. *The ISME Journal, 2*(4), 350–363. https://doi.org/10.1038/ismej.2007.112

Bourne, D. G., Morrow, K. M., & Webster, N. S. (2016). Insights into the coral microbiome: Underpinning the health and resilience of reef ecosystems. *Annual Review of Microbiology, 70*, 317–340. https://doi.org/10.1146/annurev-micro-102215-095440

Callahan, B. J., McMurdie, P. J., & Holmes, S. P. (2017). Exact sequence variants should replace operational taxonomic units in marker-gene data analysis. *The ISME Journal, 11*(12), 2639–2643. https://doi.org/10.1038/ismej.2017.119

Cooper, T. F., Berkelmans, R., Ulstrup, K. E., Weeks, S., Radford, B., Jones, A. M., Doyle, J., Canto, M., O'Leary, R. A., & van Oppen, M. J. H. (2011). Environmental factors controlling the distribution of *Symbiodinium* harboured by the coral *Acropora millepora* on the Great Barrier Reef. *PLoS One, 6(10),* e25536. https://doi.org/10.1371/journal.pone.0025536

Cunning, R., Gates, R. D., & Edmunds, P. J. (2017). Using high-throughput sequencing of ITS2 to describe *Symbiodinium* metacommunities in St. John, US Virgin Islands. *PeerJ, 5*, e3472. https://doi.org/10.7717/peerj.3472

Cunning, R., Silverstein, R. N., & Baker, A. C. (2018). Symbiont shuffling linked to differential photochemical dynamics of *Symbiodinium* in three Caribbean reef corals. *Coral Reefs, 37*(1), 145–152. https://doi.org/10.1007/s00338-017-1640-3

Curry, K. D., Wang, Q., Nute, M. G., DeReus, J., Reeves, C. A., & Pop, M. (2022). Emu: Species-level microbial community profiling of full-length 16S rRNA Oxford Nanopore sequencing data. *Nature Methods, 19*(7), 845–853. https://doi.org/10.1038/s41592-022-01520-4

Davis, N. M., Proctor, D. M., Holmes, S. P., Relman, D. A., & Callahan, B. J. (2018). *decontam:* Identifying and removing contaminant DNA from marker-gene and metagenomics data* (Version 1.20.0) [R package]. Bioconductor. https://bioconductor.org/packages/decontam

de Cáceres, M., & Legendre, P. (2022). *indicspecies: Relationship between species and groups of sites* (Version 1.8.0) [R package]. https://cran.r-project.org/package=indicspecies

De Coster, W., & Rademakers, R. (2023). NanoPack2: Population-scale evaluation of long-read sequencing data. *Bioinformatics, 39*(5), btad311. https://doi.org/10.1093/bioinformatics/btad311

Fisher, R., O'Leary, R. A., Low-Choy, S., Mengersen, K., Knowlton, N., Brainard, R. E., & Caley, M. J. (2015). Species richness on coral reefs and the pursuit of convergent global estimates. *Current Biology, 25*(4), 500–505. https://doi.org/10.1016/j.cub.2014.12.022

Florida Fish and Wildlife Conservation Commission. (2012). *Yellow pencil coral* [Photograph]. Flickr. https://www.flickr.com/photos/myfwc/7507846130/

Fox, J., Weisberg, S., & Price, B. (2024). *car: Companion to Applied Regression* (Version 3.1-3) [R package]. CRAN. https://CRAN.R-project.org/package=car

Frade, P. R., Bongaerts, P., Winkelhagen, A. J. S., Tonk, L., & Bak, R. P. M. (2008a). In situ photobiology of

corals over large depth ranges: A multivariate analysis on the roles of environment, host, and algal symbiont. *Limnology and Oceanography, 53*(6), 2711–2723. https://doi.org/10.4319/lo.2008.53.6.2711

Frade, P. R., De Jongh, F., Vermeulen, F., van Bleijswijk, J., & Bak, R. P. M. (2008b). Variation in symbiont distribution between closely related coral species over large depth ranges. *Molecular Ecology, 17*(2), 691–703. https://doi.org/10.1111/j.1365-294X.2007.03612.x

Frade, P. R., Reyes-Nivia, M. C., Faria, J., Kaandorp, J. A., Luttikhuizen, P. C., & Bak, R. P. M. (2010). Semi permeable species boundaries in the coral genus *Madracis*: Introgression in a brooding coral system. *Molecular Phylogenetics and Evolution, 57*(3), 1072–1090. https://doi.org/10.1016/j.ympev.2010.09.010

Frade, P. R., Schwaninger, V., Glasl, B., Sintes, E., Hill, R. W., Simó, R., & Herndl, G. J. (2015). Dimethylsulfoniopropionate in corals and its interrelations with bacterial assemblages in coral surface mucus. *Environmental Chemistry, 13*(2), 252–265. https://doi.org/10.1071/EN15023

Furla, P., Allemand, D., Shick, J. M., Ferrier-Pagès, C., Richier, S., Plantivaux, A., Merle, P.-L., & Tambutté, S. (2005). The symbiotic anthozoan: A physiological chimera between alga and animal. *Integrative and Comparative Biology, 45*(4), 595–604. https://doi.org/10.1093/icb/45.4.595

Gardner, S. G., Leggat, W., & Ainsworth, T. D. (2023). The microbiome of the endosymbiotic Symbiodiniaceae in corals exposed to thermal stress. *Hydrobiologia*, *850*(17), 3685-3704. https://doi.org/10.1007/s10750-023-05221-7

Glasl, B., Herndl, G. J., & Frade, P. R. (2016). The microbiome of coral surface mucus has a key role in mediating holobiont health and survival upon disturbance. *The ISME journal*, *10*(9), 2280–2292. https://doi.org/10.1038/ismej.2016.9

Glasl, B., Webster, N. S., & Bourne, D. G. (2017). Microbial indicators as a diagnostic tool for assessing water quality and climate stress in coral reef ecosystems. *Marine Biology, 164*(91). https://doi.org/10.1007/s00227-017-3097-x

Grottoli, A. G., Dalcin Martins, P., Wilkins, M. J., Johnston, M. D., Warner, M. E., Cai, W. J., Melman, T. F., Hoadley, K. D., Pettay, D. T., Levas, S., & Schoepf, V. (2018). Coral physiology and microbiome dynamics under combined warming and ocean acidification. *PLOS ONE, 13*(1), e0191156. https://doi.org/10.1371/journal.pone.0191156

Hadaidi, G., Röthig, T., Yum, L. K., Ziegler, M., Arif, C., Roder, C., Burt, J. A., & Voolstra, C. R. (2017). Stable mucus-associated bacterial communities in bleached and healthy corals of *Porites lobata* from the Arabian Seas. *Scientific Reports, 7*, 45362. https://doi.org/10.1038/srep45362

Helgoe, J., Davy, S. K., Weis, V. M., & Rodriguez-Lanetty, M. (2024). Triggers, cascades, and endpoints: Connecting the dots of coral bleaching mechanisms. *Biological Reviews, 99*(3), 715–752. https://doi.org/10.1111/brv.13042

Hernandez-Agreda, A., Gates, R. D., & Ainsworth, T. D. (2017). Defining the core microbiome in corals' microbial soup. *Trends in Microbiology, 25*(2), 125–140. https://doi.org/10.1016/j.tim.2016.11.003

Hernandez-Agreda, A., Leggat, W., Bongaerts, P., & Ainsworth, T. D. (2016). The Microbial Signature Provides Insight into the Mechanistic Basis of Coral Success across Reef Habitats. *MBio, 7*(4), 10-1128.https://doi.org/10.1128/mBio.00560-16

Hoegh-Guldberg, O., Pendleton, L., & Kaup, A. (2019). People and the changing nature of coral reefs. *Regional Studies in Marine Science, 30*, 100699. https://doi.org/10.1016/j.rsma.2019.100699

Howe-Kerr, L. I., Bachelot, B., Wright, R. M., Kenkel, C. D., Bay, L. K., & Correa, A. M. S. (2020). Symbiont community diversity is more variable in corals that respond poorly to stress. *Global Change Biology, 26*(4), 2220–2234. https://doi.org/10.1111/gcb.14999

Hu, T., Chitnis, N., Monos, D., & Dinh, A. (2021). Next-generation sequencing technologies: An overview. *Human Immunology, 82*(11), 801–811. https://doi.org/10.1016/j.humimm.2021.02.012

Huggett, M. J., & Apprill, A. (2019). Coral microbiome database: Integration of sequences reveals high diversity and relatedness of coral-associated microbes. *Environmental microbiology reports*, *11*(3), 372–385. https://doi.org/10.1111/1758-2229.12686

Hughes, T. P., Baird, A. H., Bellwood, D. R., Card, M., Connolly, S. R., Folke, C., Grosberg, R., Hoegh

Guldberg, O., Jackson, J. B., Kleypas, J., Lough, J. M., Marshall, P., Nyström, M., Palumbi, S. R., Pandolfi, J. M., Rosen, B., & Roughgarden, J. (2003). Climate change, human impacts, and the resilience of coral reefs. *Science, 301*(5635), 929–933. https://doi.org/10.1126/science.1085046

Hughes, T. P., & Jackson, J. B. C. (1985). Population dynamics and life histories of foliaceous corals. *Ecological Monographs, 55*(2), 141–166. https://www.jstor.org/stable/1942555

Hughes, T. P., Kerry, J. T., Baird, A. H., Connolly, S. R., Dietzel, A., Eakin, C. M., Heron, S. F., Hoey, A. S., Hoogenboom, M. O., Liu, G., McWilliam, M. J., Pears, R. J., Pratchett, M. S., Skirving, W. J., Stella, J. S., & Torda, G. (2018). Global warming transforms coral reef assemblages. *Nature, 556*(7702), 492–496. https://doi.org/10.1038/s41586-018-0041-2

Hume, B. C. C., Smith, E. G., Ziegler, M., Warrington, H. J. M., Burt, J. A., LaJeunesse, T. C., Wiedenmann, J., & Voolstra, C. R. (2019). SymPortal: A novel analytical framework and platform for coral algal symbiont next-generation sequencing ITS2 profiling. *Molecular ecology resources*, *19*(4), 1063–1080. https://doi.org/10.1111/1755-0998.13004

Hume, B. C. C., Ziegler, M., Poulain, J., Pochon, X., Romac, S., Boissin, E., de Vargas, C., Planes, S., Wincker, P., & Voolstra, C. R. (2018). An improved primer set and amplification protocol with increased specificity and sensitivity targeting the *Symbiodinium* ITS2 region. *PeerJ, 6*, e4816. https://doi.org/10.7717/peerj.4816

Hyndman, R. J. (2019). *broom: Convert statistical analysis objects into tidy data frames* (Version 0.5.1) [R package]. CRAN. https://CRAN.R-project.org/package=broom

Jackson, J. B. C. (1977). Competition on Marine Hard Substrata: The Adaptive Significance of Solitary and Colonial Strategies. *The American Naturalist*, *111*(980), 743–767. http://www.jstor.org/stable/2460328

Jeffrey, S. W., & Humphrey, G. F. (1975). New spectrophotometric equations for determining chlorophylls a, b, c_1 and c_2 in higher plants, algae and natural phytoplankton. *Biochemie und Physiologie der Pflanzen (BPP)*, *167*(2), 191–194. https://doi.org/10.1016/S0015-3796(17)30778-3

Kai, S., Matsuo, Y., Nakagawa, S., Kryukov, K., Matsukawa, S., Tanaka, H., Iwai, T., Imanishi, T., & Hirota, K. (2019). Rapid bacterial identification by direct PCR amplification of 16S rRNA genes using the MinION™ nanopore sequencer. *FEBS Open Bio, 9*(3), 548–557. https://doi.org/10.1002/2211-5463.12590

Kayal, E., Roure, B., Philippe, H., Collins, A. G., & Lavrov, D. V. (2013). Cnidarian phylogenetic relationships as revealed by mitogenomics. *BMC evolutionary biology*, *13*, 1-18. https://doi.org/10.1186/1471-2148-13-5

Kerry, J. T., & Bellwood, D. R. (2012). The effect of coral morphology on shelter selection by coral reef fishes. *Coral Reefs, 31*(2), 415–424. https://doi.org/10.1007/s00338-011-0859-7

Knowlton, N., Brainard, R. E., Fisher, R., Moews, M., Plaisance, L., & Caley, M. J. (2010). Coral reef biodiversity. In A. D. McIntyre (Ed.), *Life in the world's oceans: Diversity, distribution, and abundance* (pp. 65–74). Wiley-Blackwell.

Kolde, R. (2019). *pheatmap: Pretty Heatmaps* (Version 1.0.12) [R package]. CRAN. https://CRAN.R-project.org/package=pheatmap

LaJeunesse, T. C., Parkinson, J. E., Gabrielson, P. W., Jeong, H. J., Reimer, J. D., Voolstra, C. R., & Santos, S. R. (2018). Systematic revision of *Symbiodiniaceae* highlights the antiquity and diversity of coral endosymbionts. *Current Biology, 28*(16), 2570–2580. https://doi.org/10.1016/j.cub.2018.07.008

Lawson, C. A., Raina, J.-B., Kahlke, T., Seymour, J. R., & Suggett, D. J. (2017). Defining the core microbiome of the symbiotic dinoflagellate, *Symbiodinium*. *Environmental Microbiology Reports, 10*(1), 7–11. https://doi.org/10.1111/1758-2229.12599

Lee, S. T., Davy, S. K., Tang, S. L., & Kench, P. S. (2016). Mucus Sugar Content Shapes the Bacterial Community Structure in Thermally Stressed Acropora muricata. *Frontiers in microbiology*, *7*, 371. https://doi.org/10.3389/fmicb.2016.00371

Lesser, M. P. (1997). Oxidative stress causes coral bleaching during exposure to elevated temperatures. *Coral Reefs, 16*, 187–192. https://doi.org/10.1007/s003380050073

Littman, R., Willis, B. L., & Bourne, D. G. (2011). Metagenomic analysis of the coral holobiont during a

natural bleaching event on the Great Barrier Reef. *Environmental microbiology reports*, *3*(6), 651–660. https://doi.org/10.1111/j.1758-2229.2010.00234.x

Louca, S., Parfrey, L. W., & Doebeli, M. (2016). Decoupling function and taxonomy in the global ocean microbiome. *Science, 353*(6305), 1272–1277. https://doi.org/10.1126/science.aaf4507

Love, M. I., Huber, W., & Anders, S. (2014). *DESeq2: Differential gene expression analysis based on the negative binomial distribution* (Version 1.48.1) [R package]. Bioconductor. https://bioconductor.org/packages/DESeq2

Lu, H., Giordano, F., & Ning, Z. (2016). Oxford Nanopore MinION sequencing and genome assembly. *Genomics, Proteomics & Bioinformatics, 14*(5), 265–279. https://doi.org/10.1016/j.gpb.2016.05.004

Maher, R. L., Rice, M. M., McMinds, R., Burkepile, D. E., & Vega Thurber, R. (2020). Coral microbiomes demonstrate flexibility and resilience through a reduction in community diversity following a thermal stress event. *Frontiers in Ecology and Evolution, 8*, 555698. https://doi.org/10.3389/fevo.2020.555698

Maire, J., Girvan, S. K., Barkla, S. E., Perez-Gonzalez, A., Suggett, D. J., Blackall, L. L., & van Oppen, M. J. H. (2021). Intracellular bacteria are common and taxonomically diverse in cultured and in hospite algal endosymbionts of coral reefs. *The ISME Journal, 15*(7), 2028–2042. https://doi.org/10.1038/s41396-021-00902-4

Marchioro, G. M., Glasl, B., Engelen, A. H., Serrão, E. A., Bourne, D. G., Webster, N. S., & Frade, P. R. (2020). Microbiome dynamics in the tissue and mucus of acroporid corals differ in relation to host and environmental parameters. *PeerJ, 8*, e9644. https://doi.org/10.7717/peerj.9644

Martinez Arbizu, P. (2020). *pairwiseAdonis: Pairwise multilevel comparison using adonis* (Version 0.4) [R package]. GitHub. https://github.com/pmartinezarbizu/pairwiseAdonis

Matthews, J. L., Bartels, N., Doomun, S. N. E., Davy, S. K., & De Souza, D. P. (2023). Gas chromatography mass spectrometry-based targeted metabolomics of hard coral samples. *Journal of Visualized Experiments, (200)*, e65628. https://doi.org/10.3791/65628

Matthews, J. L., Raina, J. B., Kahlke, T., Seymour, J. R., van Oppen, M. J. H., & Suggett, D. J. (2020). Symbiodiniaceae-bacteria interactions: rethinking metabolite exchange in reef-building corals as multi-partner metabolic networks. *Environmental microbiology*, *22*(5), 1675–1687. https://doi.org/10.1111/1462-2920.14918

Maynard, J., van Hooidonk, R., Eakin, C. M., Puotinen, M., Garren, M., Williams, G., Heron, S. F., Lamb, J. B., Weil, E., & Willis, B. L. (2015). Projections of climate conditions that increase coral disease susceptibility and pathogen abundance and virulence. *Nature Climate Change, 5*, 688–694. https://doi.org/10.1038/nclimate2625

McDevitt-Irwin, J. M., Baum, J. K., Garren, M., & Vega Thurber, R. L. (2017). Responses of coral-associated bacterial communities to local and global stressors. *Frontiers in Marine Science, 4*, 262. https://doi.org/10.3389/fmars.2017.00262

McMurdie, P. J., & Holmes, S. (2013). *phyloseq: An R package for reproducible interactive analysis and graphics of microbiome census data* (Version 1.40.0) [R package]. Bioconductor. https://bioconductor.org/packages/phyloseq

Morata de Ambrosini, V. I., Martín, M. C., & Merín, M. G. (2014). Classification of the bacteria: Traditional. In C. A. Batt & M. L. Tortorello (Eds.), *Encyclopedia of food microbiology* (2nd ed., pp. 169–173). Academic Press. https://doi.org/10.1016/B978-0-12-384730-0.00027-6

Morrow, K. M., Pankey, M. S., & Lesser, M. P. (2022). Community structure of coral microbiomes is dependent on host morphology. *Microbiome, 10*, 113. https://doi.org/10.1186/s40168-022-01308-w

Mouchka, M. E., Hewson, I., & Harvell, C. D. (2010). Coral-associated bacterial assemblages: Current knowledge and the potential for climate-driven impacts. *Integrative and Comparative Biology, 50*(4), 662–674. https://doi.org/10.1093/icb/icq061

Moya, A., Ferrier-Pagès, C., Furla, P., Richier, S., Tambutté, E., Allemand, D., & Tambutté, S. (2008). Calcification and associated physiological parameters during a stress event in the scleractinian

coral *Stylophora pistillata*. *Comparative Biochemistry and Physiology Part A: Molecular & Integrative Physiology, 151*(1), 29–36. https://doi.org/10.1016/j.cbpa.2008.05.009

Muscatine, L. (1990). The role of symbiotic algae in carbon and energy flux in reef corals. *Ecosystems of the world, 25*, 75-87.

Muscatine, L., & Cernichiari, E. (1969). Assimilation of photosynthetic products of zooxanthellae by a reef coral. *The Biological Bulletin, 137*(3), 506–523. https://doi.org/10.2307/1540172

Muscatine, L., & Porter, J. W. (1977). Reef corals: Mutualistic symbioses adapted to nutrient-poor environments. *BioScience, 27*(7), 454–460. https://doi.org/10.2307/1297526

National Oceanic and Atmospheric Administration (NOAA). (n.d.). Aruba, Curacao, and Bonaire 5 km Regional Bleaching Heat Stress Maps and Gauges (Version 3.1). *NOAA Coral Reef Watch*. Retrieved April 25, 2025, from https://coralreefwatch.noaa.gov/product/vs/gauges/abc_islands.php

Neave, M. J., Apprill, A., Ferrier-Pagès, C., & Voolstra, C. R. (2016). Diversity and function of prevalent symbiotic marine bacteria in the genus Endozoicomonas. *Applied microbiology and biotechnology*, *100*(19), 8315–8324. https://doi.org/10.1007/s00253-016-7777-0

Neave, M. J., Michell, C. T., Apprill, A., & Voolstra, C. R. (2017). Endozoicomonas genomes reveal functional adaptation and plasticity in bacterial strains symbiotically associated with diverse marine hosts. *Scientific reports*, *7*, 40579. https://doi.org/10.1038/srep40579

Neuwirth, E. (2014). *RColorBrewer: ColorBrewer palettes* (Version 1.1-2) [R package]. CRAN. https://CRAN.R-project.org/package=RColorBrewer

NOAA Coral Reef Watch. (2025). *Current global bleaching: Status update & data submission*. National Oceanic and Atmospheric Administration. Retrieved April 23, 2025, from https://www.coralreefwatch.noaa.gov/satellite/research/coral_bleaching_report.php

Oakley, C. A., & Davy, S. K. (2018). Cell biology of coral bleaching. In M. van Oppen & J. Lough (Eds.), *Coral Bleaching* (Vol. 233, pp. 189–211). Springer. https://doi.org/10.1007/978-3-319-75393-5_8

O'Brien, P. A., Tan, S., Yang, C., Frade, P. R., Andreakis, N., Smith, H. A., Miller, D. J., Webster, N. S., Zhang, G., & Bourne, D. G. (2020). Diverse coral reef invertebrates exhibit patterns of phylosymbiosis. *The ISME journal*, *14*(9), 2211–2222. https://doi.org/10.1038/s41396-020-0671-x

Oksanen, J., Blanchet, F. G., Friendly, M., Kindt, R., Legendre, P., McGlinn, D., Minchin, P. R., O'Hara, R. B., Simpson, G. L., Solymos, P., Stevens, M. H. H., Szoecs, E., & Wagner, H. (2024). *vegan: Community ecology package* (Version 2.6-3) [R package]. CRAN. https://CRAN.R-project.org/package=vegan

Peixoto, R. S., Rosado, P. M., Leite, D. C., Rosado, A. S., & Bourne, D. G. (2017). Beneficial Microorganisms for Corals (BMC): Proposed Mechanisms for Coral Health and Resilience. *Frontiers in microbiology*, *8*, 341. https://doi.org/10.3389/fmicb.2017.00341

Pochon, X., Putnam, H. M., & Gates, R. D. (2014). Multi-gene analysis of *Symbiodinium* dinoflagellates: A perspective on rarity, symbiosis, and evolution. *PeerJ, 2*, e394. https://doi.org/10.7717/peerj.394

Pogoreutz, C., Rädecker, N., Cárdenas, A., Gärdes, A., Wild, C., & Voolstra, C. R. (2018). Dominance of *Endozoicomonas* bacteria throughout coral bleaching and mortality suggests structural inflexibility of the *Pocillopora verrucosa* microbiome. *Ecology and Evolution, 8*(4), 2240–2252. https://doi.org/10.1002/ece3.3830

Pogoreutz, C., Voolstra, C. R., Rädecker, N., Weis, V., Cardenas, A., & Raina, J. B. (2020). The coral holobiont highlights the dependence of cnidarian animal hosts on their associated microbes. In *Cellular dialogues in the holobiont* (pp. 91-118). CRC Press.

Pollock, F. J., McMinds, R., Smith, S., Bourne, D. G., Willis, B. L., Medina, M., & Thurber, R. V. M. (2018). Coral-associated bacteria demonstrate phylosymbiosis and cophylogeny. *Nature Communications, 9*, 4921. https://doi.org/10.1038/s41467-018-07275-x

Qiagen. (2016). *Quick-start protocol: Taq DNA polymerase and Taq PCR core kit* (Cat. No. HB-0657-002). Qiagen. https://www.qiagen.com/us/resources/download.aspx?id=2cd95ae5-80af-4b4e-a355-8dc5c58b97e5&lang=en

Quigley, K. M., Alvarez Roa, C., Torda, G., Bourne, D. G., & Willis, B. L. (2020). Co dynamics of *Symbiodiniaceae* and bacterial populations during the first year of symbiosis with *Acropora tenuis* juveniles. *MicrobiologyOpen, 9*(2), e959. https://doi.org/10.1002/mbo3.959

Rädecker, N., Pogoreutz, C., Voolstra, C. R., Wiedenmann, J., & Wild, C. (2015). Nitrogen cycling in corals: The key to understanding holobiont functioning? *Trends in Microbiology, 23*(8), 490–497. https://doi.org/10.1016/j.tim.2015.03.008

Raina, J. B., Clode, P. L., Cheong, S., Bougoure, J., Kilburn, M. R., Reeder, A., Forêt, S., Stat, M., & Bourne, D. G. (2016). Subcellular tracking reveals the location of dimethylsulfoniopropionate (DMSP) in microalgae and visualizes its uptake by marine bacteria. *eLife, 5*, e23008. https://doi.org/10.7554/eLife.23008

Reshef, L., Koren, O., Loya, Y., Zilber-Rosenberg, I., & Rosenberg, E. (2006). The coral probiotic hypothesis. *Environmental Microbiology, 8*(12), 2068–2073. https://doi.org/10.1111/j.1462-2920.2006.01148.x

Rhein, M., Rintoul, S. R., Aoki, S., Campos, E., Chambers, D., Feely, R. A., Gulev, S., Johnson, G. C., Josey, S. A., Kostianoy, A., Mauritzen, C., Roemmich, D., Talley, L. D., & Wang, F. (2013). Observations: Ocean. In T. F. Stocker, D. Qin, G.-K. Plattner, M. Tignor, S. K. Allen, J. Boschung, A. Nauels, Y. Xia, V. Bex, & P. M. Midgley (Eds.), *Climate Change 2013: The Physical Science Basis. Contribution of Working Group I to the Fifth Assessment Report of the Intergovernmental Panel on Climate Change* (pp. 255–316). Cambridge University Press. https://doi.org/10.1017/CBO9781107415324.010

Roberts, C. M., McClean, C. J., Veron, J. E., Hawkins, J. P., Allen, G. R., McAllister, D. E., Mittermeier, C. G., Schueler, F. W., Spalding, M., Wells, F., Vynne, C., & Werner, T. B. (2002). Marine biodiversity hotspots and conservation priorities for tropical reefs. *Science, 295*(5558), 1280–1284. https://doi.org/10.1126/science.1067728

Ros, M., Suggett, D. J., Edmondson, J., Grimaldi, A. G., & Warner, M. E. (2021). Symbiont shuffling across environmental gradients aligns with changes in carbon uptake and translocation in the reef-building coral *Pocillopora acuta*. *Coral Reefs, 40*, 595–607. https://doi.org/10.1007/s00338-021-02066-1

Silverstein, R. N., Cunning, R., & Baker, A. C. (2015). Change in algal symbiont communities after bleaching, not prior heat exposure, increases heat tolerance of reef corals. *Global Change Biology, 21*(1), 236–249. https://doi.org/10.1111/gcb.12706

Simpson, G. L. (2023). *ggvegan: 'ggplot2' Plots for the 'vegan' Package* (Version 0.1.999) [R package]. GitHub. https://github.com/gavinsimpson/ggvegan

Slowikowski, K. (2021). *ggrepel: Repulsive text and label geoms for ggplot2* (Version 0.9.6) [R package]. CRAN. https://CRAN.R-project.org/package=ggrepel

Stat, M., & Gates, R. D. (2011). Clade D *Symbiodinium* in scleractinian corals: A "nugget" of hope, a selfish opportunist, an ominous sign, or all of the above? *Journal of Marine Biology, 2011*, 730715. https://doi.org/10.1155/2011/730715

Suggett, D. J., & Smith, D. J. (2019). Coral bleaching patterns are the outcome of complex biological and environmental networking. *Global Change Biology, 26*(1), 68–79. https://doi.org/10.1111/gcb.14871

Tagliafico, A., Baker, P., Kelaher, B., Ellis, S., & Harrison, D. (2022). The effects of shade and light on corals in the context of coral bleaching and shading technologies. *Frontiers in Marine Science, 9*, 919382. https://doi.org/10.3389/fmars.2022.919382

Thompson, J. R., Rivera, H. E., Closek, C. J., & Medina, M. (2015). Microbes in the coral holobiont: Partners through evolution, development, and ecological interactions. *Frontiers in Cellular and Infection Microbiology, 4*, Article 176. https://doi.org/10.3389/fcimb.2014.00176

Thornhill, D. J., LaJeunesse, T. C., Kemp, D. W., Fitt, W. K., & Schmidt, G. W. (2005). Multi year, seasonal genotypic surveys of coral–algal symbioses reveal prevalent stability or post-bleaching reversion. *Marine Biology, 148*(4), 711–722. https://doi.org/10.1007/s00227-005-0114-2

Thurber, R. V., Willner-Hall, D., Rodriguez-Mueller, B., Desnues, C., Edwards, R. A., Angly, F., Dinsdale, E., Kelly, L., & Rohwer, F. (2009). Metagenomic analysis of stressed coral holobionts. *Environmental Microbiology, 11*, 2148–2163. https://doi.org/10.1111/j.1462-2920.2009.01935.x

van der Loos, L. M., D'hondt, S., Willems, A., & De Clerck, O. (2021). Characterizing algal microbiomes using long-read nanopore sequencing. *Algal Research, 59*, 102456. https://doi.org/10.1016/j.algal.2021.102456

van de Water, J. A. J. M., Chaib De Mares, M., Dixon, G. B., Raina, J.-B., Willis, B. L., Bourne, D. G., & van Oppen, M. J. H. (2018). Antimicrobial and stress responses to increased temperature and bacterial pathogen challenge in the holobiont of a reef-building coral. *Molecular Ecology, 27*(4), 1065–1080. https://doi.org/10.1111/mec.14489

van Oppen, M. J. H., Oliver, J. K., Putnam, H. M., & Gates, R. D. (2015). Building coral reef resilience through assisted evolution. *Proceedings of the National Academy of Sciences of the United States of America, 112*(8), 2307–2313. https://doi.org/10.1073/pnas.1422301112

Vanwonterghem, I., & Webster, N. S. (2020). Coral Reef Microorganisms in a Changing Climate. *iScience*, *23*(4), 100972. https://doi.org/10.1016/j.isci.2020.100972

Venn, A. A., Wilson, M. A., Trapido-Rosenthal, H. G., Keely, B. J., & Douglas, A. E. (2006). The impact of coral bleaching on the pigment profile of the symbiotic alga, *Symbiodinium*. *Plant, Cell & Environment, 29*(12), 2133–2142. https://doi.org/10.1111/j.1365-3040.2006.001587.x

Voolstra, C. R., Raina, J.-B., Dörr, M., Cárdenas, A., Pogoreutz, C., Silveira, C. B., Mohamed, A. R., Bourne, D. G., Luo, H., Amin, S. A., & Peixoto, R. S. (2024). The coral microbiome in sickness, in health and in a changing world. *Nature Reviews Microbiology, 22*(8), 460–475. https://doi.org/10.1038/s41579-024-01015-3

Voolstra, C. R., Ziegler, M. (2020). Adapting with microbial help: Microbiome flexibility facilitates rapid responses to environmental change. *BioEssays, 42*(7), e2000004. https://doi.org/10.1002/bies.202000004

Wang, X., Zoccola, D., Liew, Y. J., Tambutté, E., Cui, G., Allemand, D., Tambutté, S., & Aranda, M. (2021). The evolution of calcification in reef-building corals. *Molecular Biology and Evolution, 38*(9), 3543–3555. https://doi.org/10.1093/molbev/msab103

Warner, M. E., Fitt, W. K., & Schmidt, G. W. (1999). Damage to photosystem II in symbiotic dinoflagellates: A determinant of coral bleaching. *Proceedings of the National Academy of Sciences, 96*(14), 8007–8012. https://doi.org/10.1073/pnas.96.14.8007

Wickham, H. (2023a). *tidyr: Tidy messy data* (Version 1.3.0) [R package]. CRAN. https://CRAN.R-project.org/package=tidyr

Wickham, H. (2025). *ggplot2:* Create elegant data visualisations using the grammar of graphics* (Version 3.5.5) [R package]. CRAN. https://CRAN.R-project.org/package=ggplot2

Wickham, H. (2023b). *tidyverse: Easily Install and Load the 'Tidyverse'* (Version 2.0.0) [R package]. CRAN. https://CRAN.R-project.org/package=tidyverse

Wickham, H., François, R., Henry, L., & Müller, K. (2023c). *dplyr: A grammar of data manipulation* (Version 1.1.3) [R package]. CRAN. https://CRAN.R-project.org/package=dplyr

Ziegler, M., Eguíluz, V. M., Duarte, C. M., & Voolstra, C. R. (2018). Rare symbionts may contribute to the resilience of coral–algal assemblages. *The ISME Journal, 12*(1), 161–172. https://doi.org/10.1038/ismej.2017.151

Ziegler, M., Grupstra, C. G. B., Barreto, M. M., Eaton, M., BaOmar, J., Zubier, K., Al-Sofyani, A., Turki, A. J., Ormond, R., & Voolstra, C. R. (2019). Coral bacterial community structure responds to environmental change in a host-specific manner. *Nature Communications, 10*, 3092. https://doi.org/10.1038/s41467-019-10969-5

Ziegler, M., Seneca, F. O., Yum, L. K., Palumbi, S. R., & Voolstra, C. R. (2017). Bacterial community dynamics are linked to patterns of coral heat tolerance. *Nature Communications, 8*, 14213. https://doi.org/10.1038/ncomms14213

Zymo Research. (2023). *ZymoBIOMICS™ DNA Miniprep Kit: Instruction manual* (Ver.1.5.4). https://files.zymoresearch.com/protocols/_d4300t_d4300_d4304_zymobiomics_dna_miniprep_kit.pdf